

Fraunhofer-Institut für Angewandte Polymerforschung IAP

---

**Synthesis of side-chain polystyrenes for all organic solution processed  
OLEDs**

**Dissertation  
zur Erlangung des akademischen Grades  
"doctor rerum naturalium"  
(Dr. rer. nat.)  
in der Wissenschaftsdisziplin „Polymerchemie“**

**eingereicht an der  
Mathematisch-Naturwissenschaftlichen Fakultät  
der Universität Potsdam**

**von  
Alejandro José Lorente Sánchez**

geboren am 19.06.1989

**Potsdam, Januar 2017**

---

This work is licensed under a Creative Commons License:  
Attribution 4.0 International  
To view a copy of this license visit  
<http://creativecommons.org/licenses/by/4.0/>

*"It takes a revolution,  
to make a solution"*

Robert Nesta "Bob" Marley

Published online at the  
Institutional Repository of the University of Potsdam:  
URN [urn:nbn:de:kobv:517-opus4-398006](http://nbn-resolving.de/urn:nbn:de:kobv:517-opus4-398006)  
<http://nbn-resolving.de/urn:nbn:de:kobv:517-opus4-398006>

---

## Abstract

In the present work side-chain polystyrenes were synthesized and characterized, in order to be applied in multilayer OLEDs fabricated by solution process techniques. Manufacture of optoelectronic devices by solution process techniques is meant to decrease significantly fabrication cost and allow large scale production of such devices.

This dissertation focusses in three series, enveloped in two material classes. The two classes differ to each other in the type of charge transport exhibited, either ambipolar transport or electron transport. All materials were applied in all-organic solution processed green Ir-based devices.

In the first part, a series of ambipolar host materials were developed to transport both charge types, holes and electrons, and be applied especially as matrix for green Ir-based emitters. It was possible to increase devices efficacy by modulating the predominant charge transport type. This was achieved by modification of molecules electron transport part with more electron-deficient heterocycles or by extending the delocalization of the LUMO. Efficiencies up to 28.9 cd/A were observed for all-organic solution-process three layer devices.

In the second part, suitability of triarylboranes and tetraphenylsilanes as electron transport materials was studied. High triplet energies were obtained, up to 2.95 eV, by rational combination of both molecular structures. Although the combination of both elements had a low effect in materials electron transport properties, high efficiencies around 24 cd/A were obtained for the series in all-organic solution-processed two layer devices.

In the last part, benzene and pyridine were chosen as the series electron-transport motif. By controlling the relative pyridine content (RPC) solubility into methanol was induced for polystyrenes with bulky side-chains. Materials with  $RPC \geq 0.5$  could be deposited orthogonally from solution without harming underlying layers. From the best of our knowledge, this is the first time such materials are applied in this architecture showing moderate efficiencies around 10 cd/A in all-organic solution processed OLEDs.

Overall, the outcome of these studies will actively contribute to the current research on materials for all-solution processed OLEDs.

---

## Acknowledgments

I would like to thank Priv.-Doz. Dr. habil. Silvia Janietz and Dr. habil. Hartmut Krüger for the opportunity to work in their group, for the supervision, the trust and consideration during the entire PhD.

Specially thanks to Dr. Patrick Pingel for the fabrication of devices and the help with interpretation and discussion of the results, and Dr. Despina Triantou for teaching me how to work with cyclovoltammetry techniques.

Thanks to Dr. Georgios Liaptsis and Dr. Arunas Miasojedovas for the joint work and low-temperature phosphorescence measurements.

Thanks to Fraunhofer Institute for Advanced Polymer Research for the financial support, the great installations and interdisciplinary work environment.

Thanks to all the members of the Polymers and Electronics department of these three years. In particular, Martin Blümke and Dr. Felix Limberg for discussions, suggestions and advices. Also thanks to Dr. Miriam Biedermann for her advice and language corrections.

Thanks to the lab members, Franziska Wieland and Eileen Katholing for their patience, comprehension and taking care of many issues of the daily chemist routine. In addition to Diana Zimmermann, Diana Mang, Jonas Schröder, Tatjana Egorov-Brening and Björn Gruber.

Thanks to the great people I meet during these years in Berlin and their friendship. Hector Gavilán and Anna Vila, Kevin Knuth, Alessandro Maiorano, Nora, Mauro Quaresima, Antonello Moschini, Sarah Hinkeldey and Isi Röstel you were a great support.

Thanks to my friends from Valencia Natxo Martinez, Alex Sanchez, Paco Bosch and Pili Martínez, Raúl Gotor and Katherine Chulvi, Reservoir, Jordi A. Cuello, Martina Delbianco and all people that support me at any time.

And overall, thanks to my family from Almansa and Alustante, and my parents and sister Rosario, Alejandro, and Julia for your endless support.

---

## List of abbreviations

A	absorption
acac	acetylacetonate
AIBN	azobis(isobutyronitril)
a.u.	arbitrary units
B3PyMPM	4,6-bis(3,5-di(pyridin-3-yl)phenyl)-2-methylpyrimidine
BMes <sub>2</sub>	dimesitylborane
<i>n</i> -BuLi	<i>n</i> -butyllithium
<i>t</i> -BuOK	potassium <i>tert</i> -butoxide
<i>t</i> -BuONa	sodium <i>tert</i> -butoxide
CBP	4,4'-Di(9H-carbazol-9-yl)-1,1'-biphenyl
mCP	1,3-di(9H-carbazol-9-yl)benzene
mCPy	2,6-di(9H-carbazol-9-yl)pyridine
CV	cyclic voltammetry
DFT	density functional theory
DMF	<i>N,N</i> -dimethylformamide
DP	degree of polymerization
DSC	differential scanning calorimetry
E <sub>g</sub>	optical band gap
E <sub>T</sub>	triplet energy
E <sub>ox</sub>	oxidation potential

---

$E_{\text{red}}$	reduction potential
EL	electroluminescence
EML	emissive layer
EQE	external quantum efficiency
ETL	electron transport layer
ETM	electron transport material
ET	electron transport
exo	exothermic
F	fluorescence
HOMO	highest occupied molecular orbital
HT	hole transport
HTL	hole transport layer
IQE	internal quantum efficiency
ISC	intersystem crossing
ITO	indium-tin oxide
LED	light emitting diode
Liq	lithium quinolate
LUMO	lowest unoccupied molecular orbital
$M_n$	number average molar mass
$M_{\text{monomer}}$	monomer molecular mass
$M_w$	mass average molar mass

---

MePPh <sub>3</sub> Br	methyltriphenylphosphonium bromide
OLED	organic light emitting diode
OSC	organic semiconductor
PEDOT:PSS	poly(3,4-ethylenedioxythiophene) polystyrene sulfonate
P( <i>t</i> -Bu) <sub>3</sub>	tri- <i>tert</i> -butylphosphine
PD	polydispersity index
PL	photoluminescence
PESA	photoelectron spectroscopy in air
piq	1-phenylisoquinoline
ppy	2-phenylpyridine
Pd <sub>2</sub> (dba) <sub>3</sub>	Tris(dibenzylideneacetone)dipalladium(0)
Pd(dppf)Cl <sub>2</sub> · CH <sub>2</sub> Cl <sub>2</sub>	[1,1'-Bis(diphenylphosphino)ferrocene]dichloropalladium(II), complex with dichloromethane
RPC	relative pyridine content
RSIC	reverse intersystem crossing
TADF	thermally activated delayed fluorescence
TAPC	4,4'-(cyclohexane-1,1-diyl)bis(N,N-di- <i>p</i> -tolylaniline)
TCTA	4,4',4''-tris(N-carbazolyl)triphenylamine
<i>m</i> -TDATA	4,4',4''-Tris[(3-methylphenyl)phenylamino]-triphenylamine
THF	tetrahydrofuran
TMA	trimethylamine
TPBi	1,3,5-Tris(1-phenyl-1H-benzo[d]imidazol-2-yl)benzene

---

TTA	triplet-triplet annihilation
mTP	<i>meta</i> -tertphenyl
TPTA	triphenyltriazine
T <sub>g</sub>	glass transition temperature
<i>p</i> -TsOH	<i>p</i> -toluenesulfonic acid
UV	ultraviolet
Vis	visible
XL-HTL	cross-linkable hole transport layer
VR	vibrational relaxation
26DCzPPy	2,6-bis(3-(9H-carbazol-9-yl)phenyl)pyridine
3TPYMB	tris(2,4,6-trimethyl-3-(pyridin-3-yl)phenyl)borane
4CbzIPN	(4 <i>s</i> ,6 <i>s</i> )-2,4,5,6-tetra(9H-carbazol-9-yl)isophthalonitrile



---

## Declaration of approval

I hereby declare that I have not submitted the thesis at any other university and that I prepared it out by myself only with the help of the indicated means.

---

Place, Date

---

Alejandro José Lorente Sánchez

---

## Table of Contents

<b>1. Introduction .....</b>	<b>1</b>
1.1 OLED principles.....	4
1.1.1 OLED operation .....	4
1.1.2 Light emission and emitter classes.....	7
1.2 Multilayer OLED devices.....	12
1.2.1 Hole transport materials .....	13
1.2.2 Electron transport materials .....	14
1.2.3 Host-guest systems and host materials.....	15
1.3 Fabrication of OLEDs .....	18
1.3.1 Thermal cross-linking strategies for multilayer solution processing .....	19
1.3.2 Orthogonal strategies for multilayer solution processing.....	20
1.4 Side-chain polymers in OLEDs.....	21
1.5 Aim of the thesis.....	24
<b>2. Ambipolar polymer matrix for multilayer solution processed OLEDs.....</b>	<b>26</b>
2.1 Materials design and synthesis .....	28
2.2 Characterization.....	31
2.2.1 GPC and DSC.....	31
2.2.2 Theoretical calculations.....	32
2.2.3 Optical properties.....	33
2.2.4 Molecular orbitals .....	36
2.2.5 Solution processed multilayer OLEDs.....	38
2.3 Conclusion .....	41

---

<b>3. Electron transport materials based on dimesitylborane and tetraphenylsilane .....</b>	<b>42</b>
3.1 Synthesis.....	44
3.2 Characterization .....	48
3.2.1 GPC and DSC.....	48
3.2.2 Theoretical calculations .....	50
3.2.3 Optical properties.....	51
3.2.4 Electrochemical properties.....	53
3.2.5 Solution processed multilayer OLEDs .....	55
3.3 Conclusions.....	58
<b>4. Orthogonal solution processable electron transport layers .....</b>	<b>60</b>
4.1 Choice of materials.....	62
4.2 Synthesis.....	63
4.3 Characterization .....	64
4.3.1 Solubility .....	64
4.3.2 GPC and DSC.....	66
4.3.3 Theoretical caluculations.....	67
4.3.4 Optical properties.....	68
4.3.5 Electrochemical properties.....	70
4.3.6 Solution processed devices .....	72
4.4 Conclusions.....	74
<b>5. Summary.....</b>	<b>75</b>
<b>6. Outlook.....</b>	<b>79</b>
<b>7. Experimental.....</b>	<b>80</b>

7.1	Methods.....	80
7.1.1	Characterization .....	80
7.1.2	Device fabrication and characterization .....	82
7.2	Synthesis.....	84
7.2.1	Materials.....	84
7.2.2	1,3-Dibromo-5-vinylbenzene (2) .....	84
7.2.3	9,9'-(5-Vinyl-1,3-phenylene)bis(9H-carbazole) (3).....	85
7.2.4	3-Bromo-9-(6-fluoropyridin-2-yl)-9H-carbazole (5) .....	85
7.2.5	9-(6-(9H-carbazol-9-yl)pyridin-2-yl)-3-bromo-9H-carbazole (6) .....	86
7.2.6	9-(6-(9H-carbazol-9-yl)pyridin-2-yl)-3-vinyl-9H-carbazole (7).....	86
7.2.7	2,6-Bis(3-(9H-carbazol-9-yl)phenyl)-nicotinaldehyde (9).....	87
7.2.8	9,9'-((3-Vinylpyridine-2,6-diyl)bis(3,1-phenylene))bis(9H-carbazole) (10) .....	88
7.2.9	9,9'-((6-Chloro-1,3,5-triazine-2,4-diyl)bis(3,1-phenylene))bis(9H-carbazole) (12b) .....	89
7.2.10	9,9'-((6-(3-Vinylphenyl)-1,3,5-triazine-2,4-diyl)bis(9H-carbazole) (13a) .....	89
7.2.11	9,9'-((6-(3-Vinylphenyl)-1,3,5-triazine-2,4-diyl)bis(3,1-phenylene))bis(9H-carbazole) (13b).....	90
7.2.12	Poly[9,9'-(5-vinyl-1,3-phenylene)bis(9H-carbazole)] (P1) .....	90
7.2.13	Poly(9-(6-(9H-carbazol-9-yl)pyridin-2-yl)-3-vinyl-9H-carbazole) (P2).....	91
7.2.14	Poly[9,9'-((3-vinylpyridine-2,6-diyl)bis(3,1-phenylene))bis(9H-carbazole)] (P3)....	92
7.2.15	Poly[9,9'-((6-(3-vinylphenyl)-1,3,5-triazine-2,4-diyl)bis(9H-carbazole)] (P4).....	92
7.2.16	Poly[9,9'-((6-(3-vinylphenyl)-1,3,5-triazine-2,4-diyl)bis(3,1-phenylene))bis(9H-carbazole)] (P5) .....	93
7.2.17	General technique I: 4-(dimesitylboranyl)-benzaldehyde (19) .....	94
7.2.18	4-(Triphenylsilyl)benzaldehyde (15) .....	94
7.2.19	4-((4-Bromophenyl)diphenylsilyl)benzaldehyde (23a).....	95
7.2.20	4-(Bis(4-bromophenyl)(phenyl)silyl)benzaldehyde (23b) .....	95

7.2.21	General technique II: (4-(1,3-dioxan-2-yl)phenyl)(4-bromophenyl)diphenylsilane (24a)	96
7.2.22	(4-(1,3-Dioxan-2-yl)phenyl)bis(4-bromophenyl)(phenyl)silane (24b)	97
7.2.23	General Technique III: (4-bromophenyl)-dimesitylborane (18)	97
7.2.24	(4-Bromophenyl)(4-(dimesitylboranyl)phenyl)diphenylsilane (21)	98
7.2.25	(4-(1,3-Dioxan-2-yl)phenyl)(4-(dimesitylboranyl)phenyl)diphenylsilane (25a)	98
7.2.26	(4-(1,3-Dioxan-2-yl)phenyl)bis(4-(dimesitylboranyl)phenyl)(phenyl)silane (25b)	99
7.2.27	General Technique IV: 4-((4-(dimesitylboranyl)phenyl)diphenylsilyl)-benzaldehyde (26a)	100
7.2.28	4-(Bis(4-(dimesitylboranyl)phenyl)(phenyl)-silyl)benzaldehyde (26b)	100
7.2.29	General Technique V: dimesityl(4-vinylphenyl)borane (20)	101
7.2.30	Triphenyl(4-vinylphenyl)silane (16)	101
7.2.31	(4-(Dimesitylboranyl)phenyl)diphenyl(4-vinylphenyl)silane (27a)	102
7.2.32	Bis(4-(dimesitylboranyl)phenyl)(phenyl)(4-vinylphenyl)silane (27b)	103
7.2.33	(4-(Dimesitylboranyl)phenyl)diphenyl(4'-vinyl-[1,1'-biphenyl]-4-yl)silane (22)	103
7.2.34	General technique VI: Poly(triphenyl(4-vinylphenyl)silane) (P6)	104
7.2.35	Poly(dimesityl(4-vinylphenyl)borane) (P7)	105
7.2.36	Poly[(4-(dimesitylboranyl)phenyl)diphenyl(4-vinylphenyl)silane] (P8)	105
7.2.37	Poly[(4-(dimesitylboranyl)phenyl)diphenyl(4'-vinyl-[1,1'-biphenyl]-4-yl)silane] (P9)	106
7.2.38	Poly[bis(4-(dimesitylboranyl)phenyl)(phenyl)(4-vinylphenyl)silane] (P10)	106
7.2.39	2,2'-(5-Vinyl-1,3-phenylene)bis(4,4,5,5-tetramethyl-1,3,2-dioxaborolane) (28)	108
7.2.40	5'-Vinyl-1,1':3',1''-terphenyl (29a)	108
7.2.41	3,3'-(5-Vinyl-1,3-phenylene)dipyridine (29b)	109
7.2.42	3,3'-(5'-Vinyl-[1,1':3',1''-terphenyl]-4,4''-diyl)dipyridine (29c)	109
7.2.43	3,3'-(5'-Vinyl-[1,1':3',1''-terphenyl]-3,3''-diyl)dipyridine (29d)	110

---

7.2.44	3,3',3'',3'''-(5'-Vinyl-[1,1':3',1''-terphenyl]-3,3'',5,5''-tetrayl)tetrapyrindine (29e).....	111
7.2.45	Poly(5'-vinyl-1,1':3',1''-terphenyl) (P11a).....	111
7.2.46	Poly(3,3'-(5-vinyl-1,3-phenylene)dipyridine) (P11b).....	112
7.2.47	Poly(3,3'-(5'-vinyl-[1,1':3',1''-terphenyl]-4,4''-diyl)dipyridine) (P11c) .....	112
7.2.48	Poly(3,3'-(5'-vinyl-[1,1':3',1''-terphenyl]-3,3''-diyl)dipyridine) (P11d).....	113
7.2.49	Poly(3,3',3'',3'''-(5'-vinyl-[1,1':3',1''-terphenyl]-3,3'',5,5''-tetrayl)tetrapyrindine) (P11e)	113
<b>8.</b>	<b>Literature .....</b>	<b>115</b>
	<b>List of publications .....</b>	<b>129</b>
	<b>Curriculum vitae .....</b>	<b>131</b>

# 1. Introduction

Artificial light sources play a major role in nowadays society. We found them in almost every aspect of our daily life. These sources transform electrical energy into light and are based on different physical principles (e.g. incandescence, fluorescence or electroluminescence). According to the International Lighting Agency (ILA), worldwide, grid-based electric lighting consumes 19% of total global electricity production.<sup>1</sup> Therefore, utilization and development of light sources as efficient as possible and well adapted for its purpose is of importance to drive society and industry to a more sustainable economic growth.

The first invention which transforms electrical energy into light was the incandescent bulb, developed independently by Swan and Edison in the nineteenth century.<sup>2</sup> The operation principle is based on a wire filament heated by passing an electrical current through it, until it glows with visible light. This technology, which has been extensively used during the twentieth century, converts less than 5% of the energy (ca. 15 lm/W) into light, while the remaining 95% is lost as heat. Later on, development of the fluorescent tube at the beginning of the twentieth century introduced a significant improvement in efficacy. In this case, an electric current excites mercury vapour which generates ultraviolet radiation and causes a phosphor coating of the lamp inner wall to radiate visible light. The luminous efficacy ranges within 60-80 lm/W;<sup>3</sup> however, the utilization of mercury vapours renders highly toxic waste after service life.

A revolutionary progress in artificial lighting was achieved by the utilization of electroluminescence (EL) as light generation principle. This phenomenon was discovered in 1907 by H. J. Round resulting of radiative recombination of electrons and holes in a silicon carbide crystal.<sup>4</sup> Based on this principle, light emitting diodes (LED) were developed during the 1960s and reach his highest recognition in 2014, when the Nobel Prize of physics was awarded to Nakamura, Akasaki and Amano for the development of high-brightness blue LED.<sup>5</sup> This technology is currently among the most efficient light sources with efficiencies over 80 lm/W.<sup>3</sup> Since LEDs are point light sources and emit targeted light, they are very suitable for applications in shop, street or automotive lighting. The higher efficiency of LEDs minimizes the

loss of energy as heat, and therefore they are also perfectly suited as a general lighting technology.

Nevertheless, artificial light sources are so extended nowadays that more specialized products, which allow generation of light in innovative ways and open new design boundaries are highly demanded. Organic light emitting diodes (OLEDs, Figure 1), which are also based on electroluminescence as light generation principle, merged in the last decades as an attractive new way of generating light. Unlike LEDs, OLEDs utilize organic semiconductor thin layers instead of point-shaped single crystals to generate light.<sup>6</sup> Therefore, they can be fabricated into flexible large-area and low-weight substrates.<sup>7</sup> Mobile telephones, TV screens, light-panels for indoor illumination or signage are among the current applications that OLED reached in the recent years.<sup>8</sup>

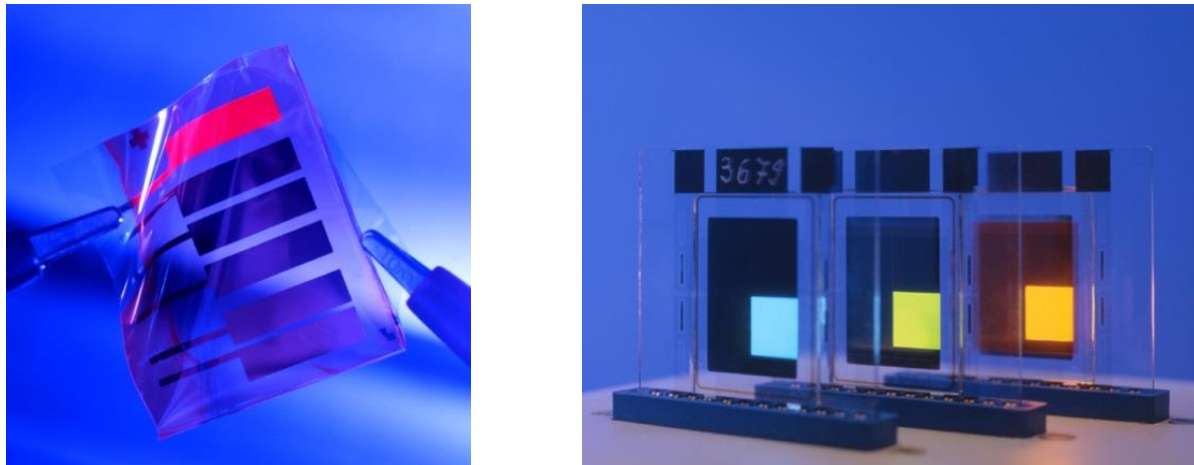


**Figure 1.** OLED in flexible (left) and rigid (right) substrates developed in Fraunhofer Institute for Applied Polymer Research.

OLED research reached a first milestone in 1987 when Tang and VanSlyke presented an OLED with an efficiency of 1.5 lm/W.<sup>9</sup> This device consisted of two organic layers sandwiched between two electrodes. The technique for fabrication used was thermal vapour deposition, which provided a strategy for further understanding and developing highly efficient OLEDs.



A second milestone was reached a few years later by Burroughes et al., who fabricated a single layer OLED by spin-coating a soluble sulphonium poly(*p*-phenylene vinylene) precursor onto an ITO substrate and evaporating a top contact of aluminum.<sup>10</sup> Although spin-coating is not economically viable technique due to the misuse of product, this device lighted the possibility and importance to further development of solution process techniques like printing. Such techniques are expected to decrease significantly the fabrication cost and allow OLEDs large scale fabrication.

Since then an extraordinary amount of organic molecules, polymers, metal complexes have been created in order to make OLEDs an economical, efficient, environmental respectfully and versatile light source.

## 1.1 OLED principles

In this section the basic processes required to understand the different aspects of OLEDs that lead to light generation are described.

### 1.1.1 OLED operation

For ease of comprehension the basic function of a single layer OLED consisting of an emissive layer sandwiched between two electrodes (Figure 2) will be used as example to describe the different processes that take part during OLED operation.

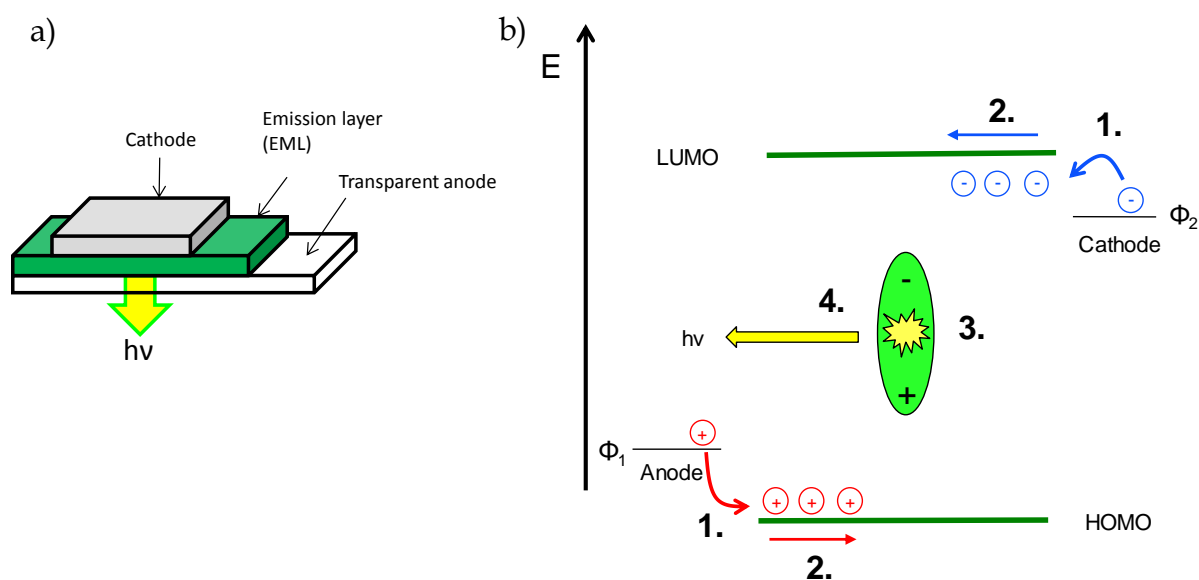


**Figure 2.** a) Single layer OLED. b) Basic steps during OLED operation. Injection of charges in organic materials (1), transport of the charge carriers (2), formation of excitons (3) and light emission (4).

#### Charge injection (1)

The first process occurring when a voltage is applied to the electrodes of an OLED is the injection of charges into the organic materials. This process can be depicted as the formation of radical cations or anions in the metal-organic interface. In the case of hole injection, the anode oxidizes the organic material subtracting a negative charge (electron) from its highest occupied molecular orbital (HOMO) and a positive charge (hole) is generated. Electron injection,

inversely, occurs when the cathode reduces the organic material by addition of a negative charge to its lowest unoccupied molecular orbital (LUMO). The efficiency of charge injection is determined by the energy difference between the Fermi-surface level of the electrode material and the frontier molecular orbitals (HOMO for holes and LUMO for electrons) of the organic material. A decrease in this difference, improves charge injection efficiency by decreasing the energy barrier and, hence, the efficiency of the device.<sup>11</sup> Although the exact description of the process is rather complicated, it has been studied by several models including thermionic emission<sup>12</sup> or charge tunneling.<sup>13</sup>

Several materials can be used as anode. One of the widest materials used is indium-tin-oxide (ITO),<sup>14</sup> due to its electrical conductivity, high work function and optical transparency as a thin layer. It is normally deposited onto glass substrates by vacuum deposition, and it has a work function ( $\phi$ ) reported to vary from 4.2 up to 4.8 eV depending on the pre-treatment applied before device fabrication.<sup>15</sup> This wide range can result in increased energy barriers for hole injection into the organic layers which can limit the materials choice. To circumvent this problem, additional interlayers between the anode and the organic materials such as poly(3,4-ethylenedioxythiophene)-poly(styrenesulfonate), also known as PEDOT:PSS, are often used on top of ITO.<sup>16</sup>

Alkaline earth metals with relatively low work function are very suitable for application as cathode materials. However, due to their high chemical reactivity rapid deterioration of the cathode in the ambient medium occurs. To protect the active metal from the adverse effects of oxygen and moisture, two-layered cathodes are used, in which an active, low- $\phi$  metal, such as Ba, Ca, or Mg, adjacent to the organic layer is coated with a corrosion-resistive layer of aluminium or silver. Such electrodes become stable to ambient-air effects while keeping the high injection capacity intact.<sup>11</sup>

## **Charge transport (2)**

Following charge injection, the next process that takes place during OLED operation is charge transport through the device. Generally, due to the method of deposition, organic semiconductor (OSC) materials used in OLEDs can be described as amorphous (i.e. structurally

disordered) molecular films.<sup>17</sup> The band structure of organic thin film semiconductors is determined by the molecular orbitals of the molecules composing the film. The random variation of the electronic polarization of the molecule neighbourhood leads to a Gaussian distribution of the density of states.<sup>18</sup> Electrons can hop between LUMO levels of neighbouring molecules, and analogously holes can hop between HOMO levels of neighbouring molecules. This process, also described as a cascade of redox reactions within neighbouring molecules,<sup>19</sup> is driven by the external electrical field resulting in a net flux of charges in both directions of the organic material.

### **Exciton formation (3) and light emission (4)**

The third step depicted in Figure 2b corresponds to the formation of excitons, which occurs when two opposite charges are close enough and recombine due to columbic interaction in the organic semiconductor. Unlike formation of excited states upon optical absorption, which preserves spin and thus only creates singlet excitons, electrical excitation leads to the formation of both singlet and triplet states.

Electrons and holes are independently injected into the organic semiconductor HOMO and LUMO levels, respectively, and have an intrinsically associated spin number ( $s_n = \pm \frac{1}{2}$ ). When recombination occurs, if the spins are antiparallel the resulting total spin quantum number is  $S = 0$ . In case that the spins are parallel, the resulting total spin quantum number is  $S = 1$ . Consequently, the multiplicities of the angular momentum states ( $M_s, -S \leq M_s \leq S$ ) is  $M_s = 0$  for  $S = 0$ , and  $M_s = -1, 0, 1$  for  $S = 1$ , which corresponds to one singlet state and three triplet states, respectively (Figure 3). Therefore, since formation of the described excitons is equally probable, the recombination of charge carriers in OLEDs creates a larger number of triplet (75% of all excitons formed) than singlet excitons (25% of all excitons formed), although recently studies on spin statistics suggest some variations in the singlet-to-triplet ratios occur.<sup>20</sup>

The final step during OLED operation is exciton relaxation by radiative pathways. The different aspects of this process are introduced in the next section.

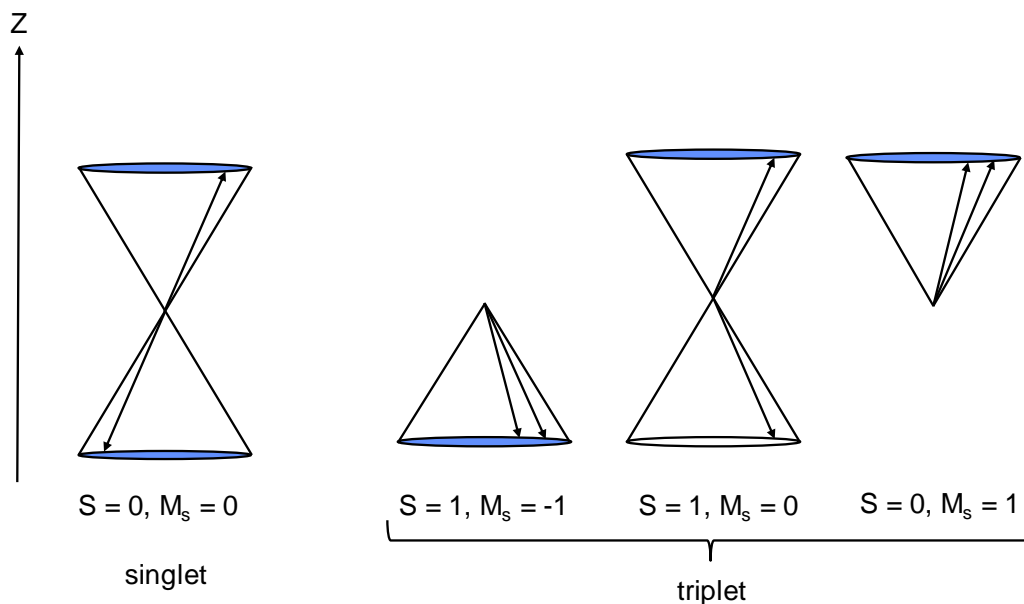


**Figure 3.** Singlet and triplet state as a vector diagram illustrating the relative orientations of the two electron spins for the singlet and triplet state.<sup>21</sup>

### 1.1.2 Light emission and emitter classes

Upon formation of excitons under electric current four different excited states are formed, 1 singlet state and 3 triplet states. The nature of the electroluminescence generated from this excited states, either as of fluorescence or phosphorescence (Figure 4), vary depending on the properties of the material where the excitons decay occur.

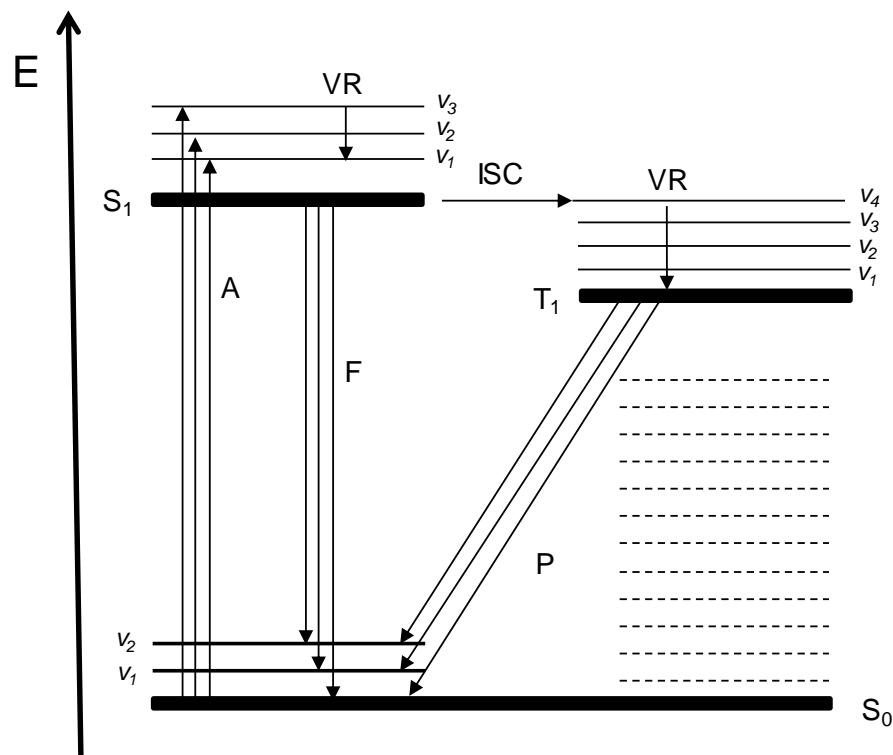


**Figure 4.** Jablonski energy diagram where absorption (A), fluorescence (F), phosphorescence (P), intersystem crossing (ISC) and vibrational relaxation (VR) processes are represented.

### Singlet emitters

Conjugated polymers such as Poly[2-methoxy-5-(2-ethylhexyloxy)-1,4-phenylenevinylene] (MEH-PPV) or small like molecules 4-(dicyanomethylene)-2-methyl-6-[(4-dimethylaninostyryl)-4-H-pyran] (DCM) and 9-(trifluoromethyl)-2,3,6,7,9,10-hexahydro-1H,5H,11H-pyrano[2,3-f]pyrido[3,2,1-ij]quinolin-11-one (C540A) have been used since the early research in OLEDs as emitting fluorescent materials (Figure 5).<sup>22-24</sup> It is well known that in this class of compounds the only spin-allowed transition for excitons is from the singlet excited state ( $S_1$ ) to the singlet ground state ( $S_0$ ), also known as fluorescence (Figure 4). As discussed previously, the formation of excitons under electrical excitation generates 25% of singlet and 75% of triplet excitons. In the case of singlet emitters, 75% of the excitons formed cannot undergo radiative relaxation and they are dissipated as heat by non-radiative processes. Internal quantum efficiency (IQE)<sup>25</sup> is therefore limited to 25%, being fabrication of highly efficient OLEDs theoretically restricted.

Nevertheless, the use of these materials in combination with other emitter classes can lead to long device lifetimes in white OLEDs.<sup>26</sup>

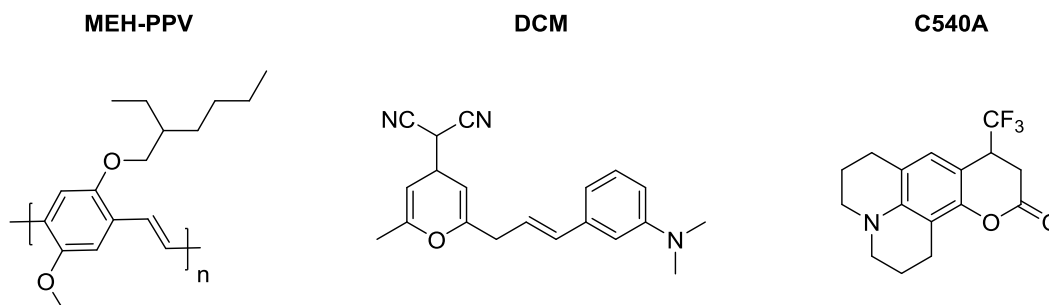


**Figure 5.** Fluorescent materials employed as singlet emitters in OLEDs. Poly[2-methoxy-5-(2-ethylhexyloxy)-1,4-phenylenevinylene] (MEH-PPV), 4-(dicyanomethylene)-2-methyl-6-[(4-dimethylanilino)styryl]-4H-pyran] (DCM), 9-(trifluoromethyl)-2,3,6,7,9,10-hexahydro-1H,5H,11H-pyrano[2,3-f]pyrido[3,2,1-ij]quinolin-11-one (C540A).

### Triplet emitters

Transformation of all electrical energy supplied to OLEDs into light is crucial to fabricate highly efficient devices. Since singlet emitters have a theoretical limitation to convert 75% of the energy into light, Baldo et al. proposed a new class of organometallic complexes as emitting materials.<sup>27</sup> Their strategy is based on the incorporation of heavy metals into the aromatic organic frameworks to increase spin-orbit interactions. In this case, transition from the lowest triplet state ( $T_1$ ) to the ground state ( $S_0$ ) (e.g. phosphorescence, Figure 4) is allowed by the effect of spin-orbit coupling (SOC).<sup>28</sup> Furthermore, intersystem crossing (ISC) rate from the first excited singlet state ( $S_1$ ) to the triplet state ( $T_1$ ) is highly increased, which allows the conversion of singlet excitons into triplet excitons. These two effects combined result in theoretical IQEs<sup>25</sup> up to 100%.

Triplet emitters derived from Tris[2-phenylpyridinato-C<sub>2</sub>,N]iridium(III) ( $\text{Ir}(\text{ppy})_3$ ) are among the widest used in OLED applications (Figure 6).  $\text{Ir}(\text{ppy})_3$ -based OLEDs show green electroluminescence emission. Modification of the metal environment allows covering the entire visible spectrum. For example, changing the ligands structure can lead to red emission like in

the case of tris[1-phenylisoquinolino- $C^{2,N}$ ]iridium(III) ( $\text{Ir}(\text{piq})_3$ ), while substitution of phenylpyridine by other ligands can lead to blue emission as observed for Bis[2-(4,6-difluorophenyl)pyridinato- $C^{2,N}$ ](picolinato)iridium(III) ( $\text{FIrpic}$ ).<sup>29,30</sup>

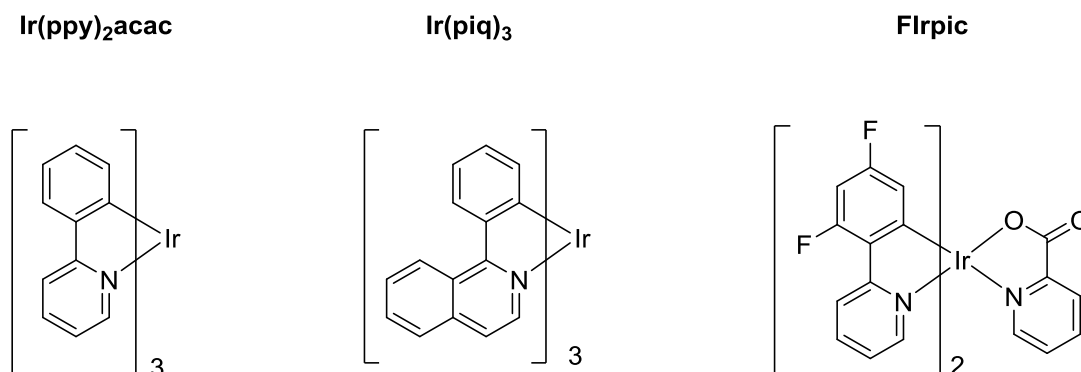


**Figure 6.** Iridium based emitters.  $\text{Ir}(\text{ppy})_3$  (green),  $\text{Ir}(\text{piq})_3$  (red),  $\text{FIrpic}$  (blue).

### Thermally activated delayed fluorescence (TADF) emitters

Mechanisms that allow the emission of 100% of the excitons, such as in phosphorescent emitters, are required to achieve high efficient OLEDs. However, iridium and platinum are rare metals, expensive and dependent on limited global sources, which limits the potential high scale manufacture of efficient OLEDs.<sup>31</sup> An alternative to these materials is based on TADF. This process can occur when the materials exhibit a small energy difference between  $S_1$  and  $T_1$  (i.e. in the order of  $k_B T$ , Figure 7), which establishes a thermal equilibrium between the two states. In this case, two distinct unimolecular mechanisms occur. On one side, singlet excitons (25%) relax almost immediately by prompt fluorescence.<sup>32</sup> On the other side, triplet excitons (75%) can be back transferred to  $S_1$  via reverse intersystem crossing (RISC) and decay radiatively from  $S_1$  by delayed fluorescence.<sup>33</sup> Therefore, 100% IQE is theoretically possible.



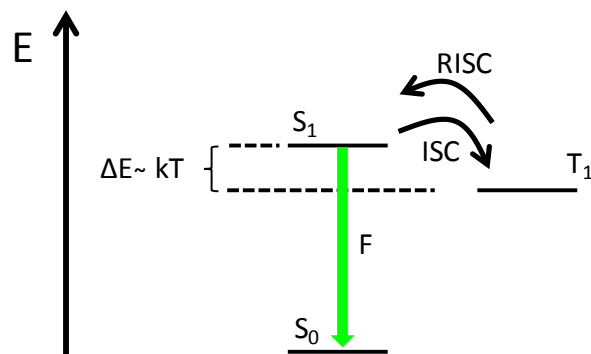


**Figure 7.** TADF process. ISC and RISC are activated at room temperature due to the energy difference between  $T_1$  and  $S_1$ , allowing all excitons to relax radiatively by fluorescence (F).

Although this process is known since the early 1960s, first applications in OLEDs were attempted in 2009,<sup>34</sup> and a first milestone was reached when Adachi et al. reported devices with high external quantum efficiencies (EQEs).<sup>25,35</sup> To obtain such very small  $\Delta E_{ST}$  between  $S_1$  and  $T_1$  excited states, partially separated donor and acceptor moieties in the same molecule were used such as in (4s,6s)-2,4,5,6-tetra(9H-carbazol-9-yl)isophthalonitrile (4CzIPN). Yersin et al. also showed efficient TADF emitters with heteroleptic copper (I) complexes presenting current efficiencies in OLEDs as high as 71 cd/A at 100 cd/cm<sup>2</sup> brightness (Figure 8).<sup>36</sup> In both cases efficient emitters have been developed free of expensive metals, while continuous research is being done to improve lifetimes of devices based on these materials.

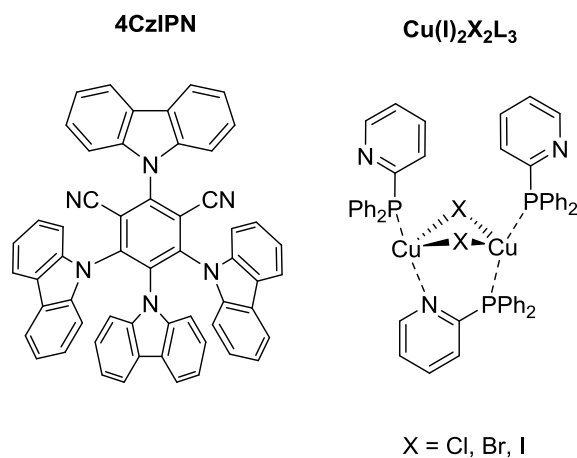


**Figure 8.** 4CzIPN and halide-bridged di-nuclear Cu (I) complexes used as TADF emitters.

## 1.2 Multilayer OLED devices

Single layer OLEDs, as described in Section 1.1.1, show low efficiencies and require high driving voltages to produce light.<sup>37</sup> The main reasons for such drawbacks are:

- High energy barriers for charge injection into the emissive organic layer from the electrodes
- Unbalanced transport of holes and electrons through the organic layers until charge recombination occurs
- Exciton quenching in case that the recombination takes place close to the electrodes
- Flow of charges through the organic layer without recombining

To overcome these problems a more complex device structure consisting of several layers has been widely established.<sup>9,38,39</sup> Multilayer OLEDs (Figure 9) sandwich an emissive layer (EML) in between a hole and electron transport layer (HTL and ETL, respectively). The incorporation of such additional layers serves to reduce the injection barriers through the device, improve the recombination of charges and confine the excitons in the EML.<sup>40</sup> To fulfil those functions the materials used as hole or electron transport layers have to meet the following characteristics:<sup>41</sup>

- Deep HOMO level ( $< -6.3$  eV) for the electron transport layer and high LUMO level ( $> -2.4$  eV) for hole transport layers. This will prevent the charges to go through the device without recombination due to a large energy barrier between the EML and the electrode
- Triplet energy higher than that of the emitter to avoid exciton quenching by the charge transport layers, due to energy transfer or diffusion of the excitons
- Balanced carrier mobility to favour generation of excitons in the EML

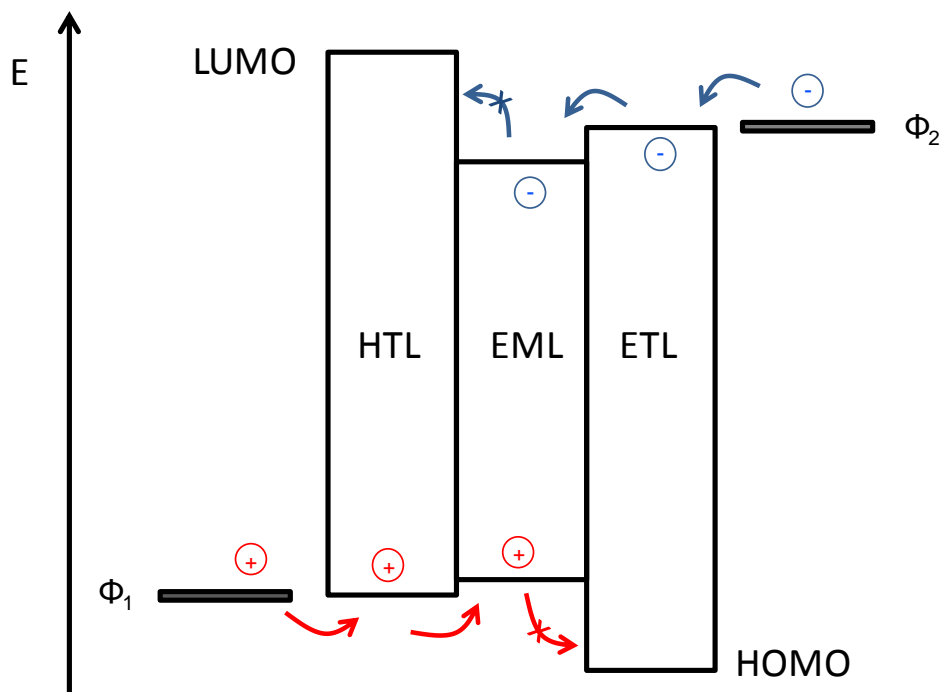


**Figure 9.** General multilayer OLED energy diagram. High LUMO level of the HTL blocks negative charges to reach the anode and deep HOMO level of the ETL blocks positive charges to reach the cathode.

### 1.2.1 Hole transport materials

The current main chemical structures that are suitable to transport holes successfully are phenylamine-based, because stabilization of the positive charges is favoured principally by resonance effects. Concretely, triphenylamine derivatives are the typical structures used as good hole transport materials (Figure 10).<sup>42</sup> Structures bearing this motif show high triplet energy and high hole mobility due to the delocalization of the free electron pair of the nitrogen.<sup>43</sup>

A good example of efficient hole transport molecules is 4,4',4''-tris(N-carbazolyl)triphenylamine (TCTA). This dendritic structure with three carbazole groups in the periphery of a triphenylamine shows a triplet energy of 2.76 eV and HOMO/LUMO values of -5.7/-2.4.<sup>44</sup> These values feature the required properties for good hole injection, electron blocking and exciton blocking. 4,4'-

(cyclohexane-1,1-diyl)bis(N,N-di-p-tolylaniline) (TAPC) shows also suitable energy levels for hole injection and electron blocking (HOMO/LUMO: -5.5/-2.0 eV), due to the disrupted conjugation by the cyclohexane ring it also shows a high triplet energy ( $E_T = 2.87$  eV),<sup>45</sup> while the hole mobility is as high as  $1 \times 10^{-3} \text{ cm}^2 \text{ V}^{-1} \text{ s}^{-1}$ .<sup>46</sup>

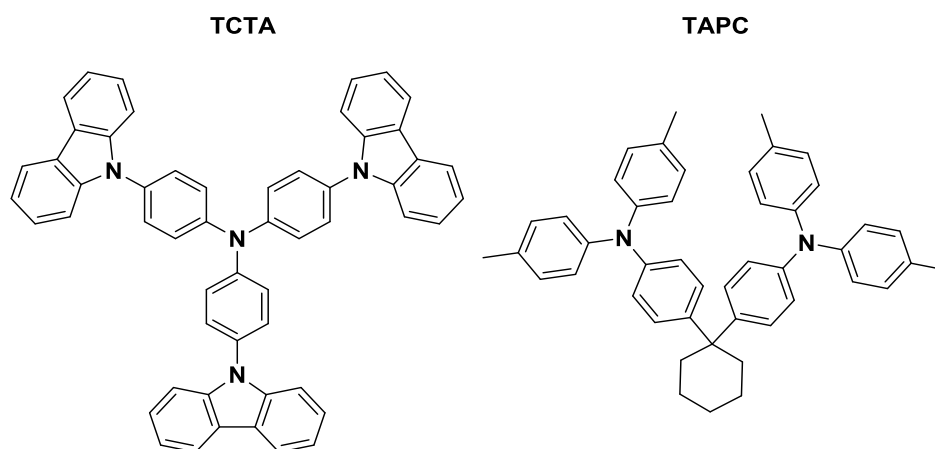


**Figure 10.** Hole transport structures based on triphenylamine structures.

### 1.2.2 Electron transport materials

Application of electron transport materials separated from the emissive layer were introduced into OLEDs by Adachi et al.<sup>38,39</sup> Materials suitable for electron transport are based on electropositive atoms and/or electron deficient heterocycles, which are able to stabilize negative charges by delocalization within the aromatic ring. A wide library of materials has been developed in the recent years with many different molecular motifs.<sup>41,47-49</sup> Phenylbenzimidazoles, triazines, pyrimidines or pyridines are among the structures that feature the requirements for effective electron transport.

1,3,5-Tris(1-phenyl-1H-benzo[d]imidazol-2-yl)benzene (TPBi), shown in Figure 11, is a widely used electron transport material and hole blocking material. The HOMO between -6.2 and -6.7 eV can effectively block holes from reaching the cathode and the LUMO at -2.8 eV is in a good range to decrease the energy barrier between the cathode and the emissive layer.<sup>50</sup> Other structures such as tris(2,4,6-trimethyl-3-(pyridin-3-yl)phenyl)borane (3TPYMB)<sup>51</sup> or 4,6-bis(3,5-

di(pyridin-3-yl)phenyl)-2-methylpyrimidine (B3PyMPM),<sup>52</sup> combine exciton and hole blocking properties while also show high electron mobility to provide sufficient flux of electrons into the emissive layer.

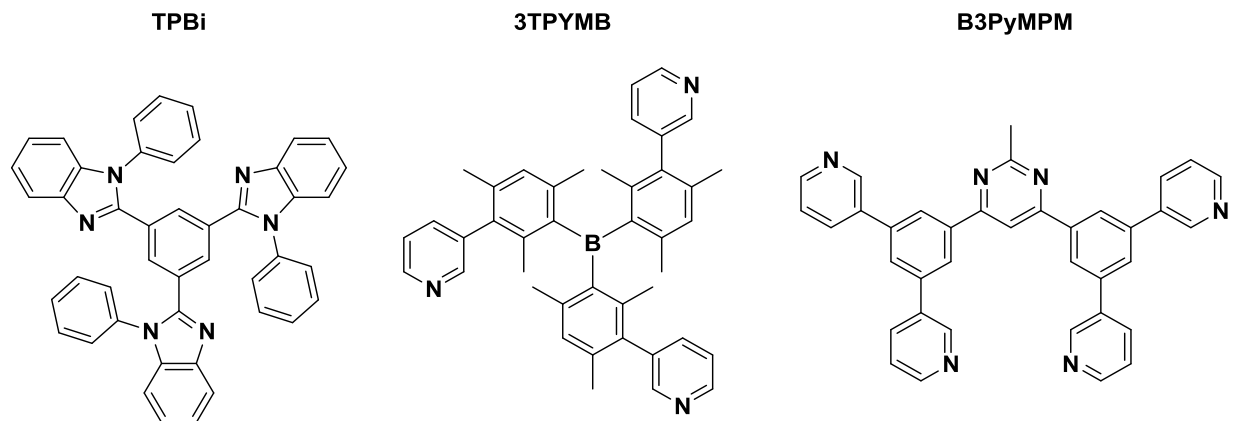


**Figure 11.** Some well-known electron transport small molecules used in small molecule-based devices.

### 1.2.3 Host-guest systems and host materials

Although phosphorescent and TADF emitters are useful to achieve high efficiencies, these materials are not normally applied as one component layer in OLEDs. Typically, they are applied as blends with a second material or “host” (at concentrations below 20%wt for the emitter). These systems are also known as host-guest systems and are used to prevent of self-quenching processes such as triplet-triplet annihilation (TTA).<sup>53,54</sup> In those systems, formation of excitons can occur either in the host or in the emitter (guest). While the excitons formed in the emitter can simply decay radiatively, the excitons formed in the host undergo by energy transfer reactions to the guest by either Förster or Dexter mechanism before decay radiatively.<sup>55</sup>

To obtain efficient energy transfer reactions from the host to the emitter, it is crucial that the triplet state of the host is higher in energy than the emitter (Figure 12a). Otherwise, the triplet excitons formed have to overcome an energy barrier to be transferred from the host to the emitter (Figure 12b), or can be back-transferred to the host from the emitter (Figure 12c), decaying radiationless and resulting in low IQEs.<sup>56</sup>

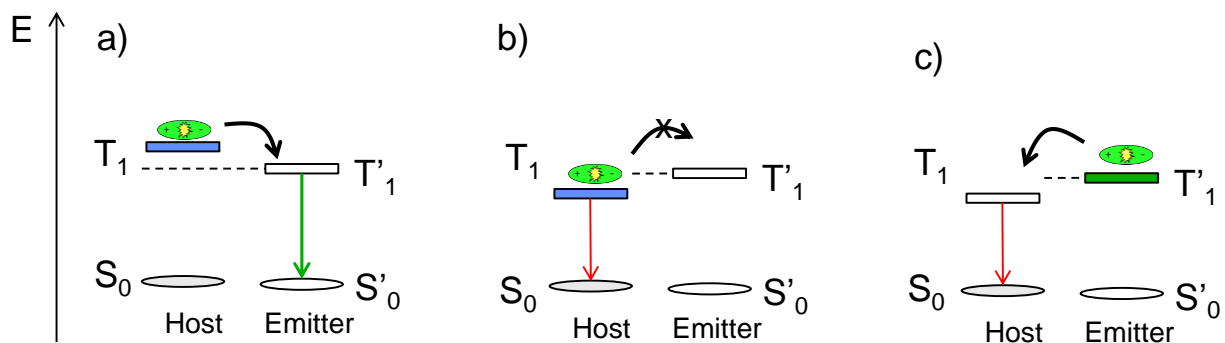


**Figure 12.** Higher triplet energies of the host than the emitter lead to efficient energy transfer (a) and radiative relaxation (green). Low triplet energies result in an energy barrier for energy transfer (b) or back-energy transfer (c) to the host, and therefore radiatonless relaxation (red) of the excitons.

There have been many kinds of materials applied as host for phosphorescent emitters (**Error! Reference source not found.**). On one side, tetraphenylsilane derivatives like 1,3-bis(triphenylsilyl)benzene (UGH3), which possess high triplet energies, can confine excitons effectively.

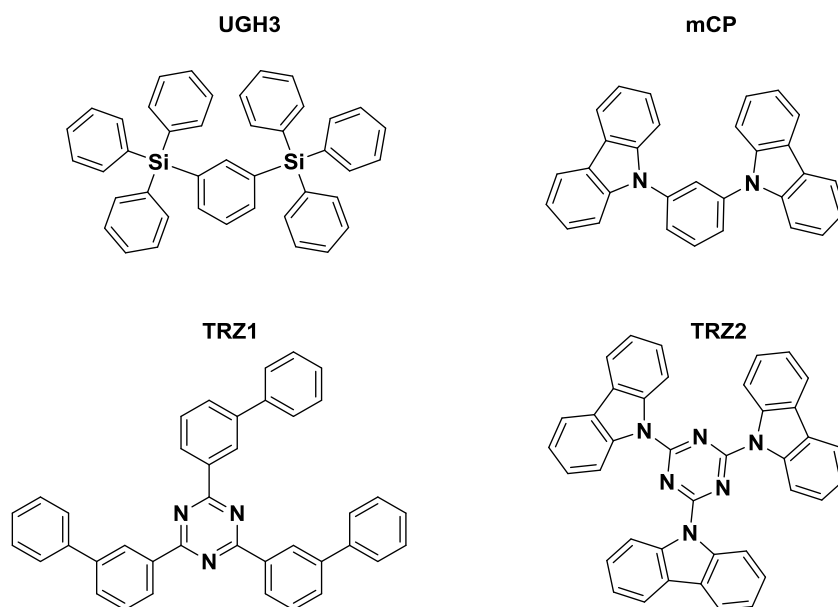


**Figure 13.** Ultrahigh energy gap (UGH3) host, unipolar hole- (mCP), electron-transport (TRZ1) host materials and ambipolar host material (TRZ2).

However, due to the small  $\pi$ -conjugated system, they show poor charge transport properties resulting in higher driving voltages.<sup>57,58</sup> On the other side, unipolar materials like 1,3-di(9H-carbazol-9-yl)benzene (mCP) or 2,4,6-tri([1,1'-biphenyl]-3-yl)-1,3,5-triazine (TRZ1) that are able to transport mainly one type of charge, either holes or electrons, can be also employed with decreased driving voltages.<sup>59,60</sup> However, when these materials are used the recombination area where the excitons are formed is located in the surrounding of the interface of the EML and the HTL or ETL, depending on the nature of the host (Figure 14, HT-host and ET-host). The recombination zone in this case is rather narrow and can lead to increase of quenching effects such as TTA.<sup>53,54</sup>

The later approach used are those host materials which combine in the same molecular structure the three after mentioned properties (high triplet energy, hole- and electron-transport). This is possible to achieve by combining electron-rich (e.g. carbazole) and electron-poor (e.g. triazine) moieties in narrowly delocalized  $\pi$ -system like in 2,4,6-tri(9H-carbazol-9-yl)-1,3,5-triazine (TRZ2).<sup>61</sup> For these materials the recombination zone is wider and quenching effects such as TTA or exciton migration minimized (Figure 14, ambipolar host).

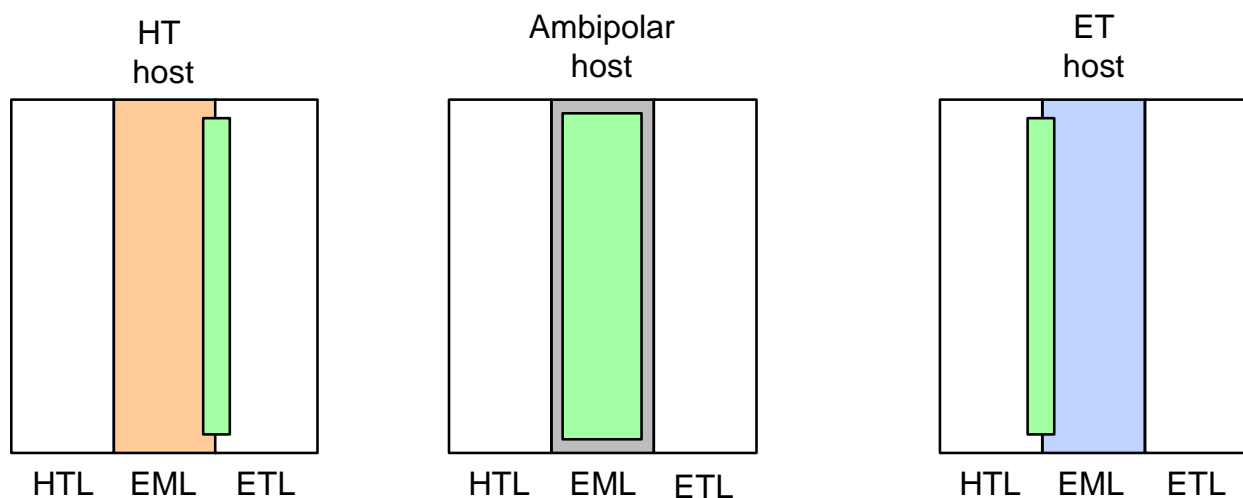


**Figure 14.** Schematic representation of the recombination zone (green) when unipolar (HT or ET hosts) or ambipolar hosts are used.<sup>62</sup>

### 1.3 Fabrication of OLEDs

Two main strategies are used for fabrication of multilayer OLED devices, vacuum and solution techniques. On the one hand, vacuum process of small molecules, achieved by evaporating the material under high vacuum (Figure 15a), can be used to deposit organic materials starting from ITO anode. This technique showed the highest efficiencies to date in OLEDs.<sup>63</sup> This is mainly due to the possibility of constructing well-defined complex multilayer structures (e.g. by controlling the deposition rate). Furthermore, small molecules allow for a high degree of purification by recrystallization or sublimation, which is additionally applied prior to the deposition of the materials.<sup>64</sup> However, this technique shows some major disadvantages for mass production and large area applications (e.g. lighting), due to the high operation cost of the vacuum deposition chambers. Additionally, during deposition the majority of the valuable organic material is widespread over the deposition chamber, being the materials use yield around 20%. It is also relatively time-consuming due to required time to reach high vacuum previous to materials sublimation ( $\approx 10^{-6}$  mBar).<sup>65</sup>

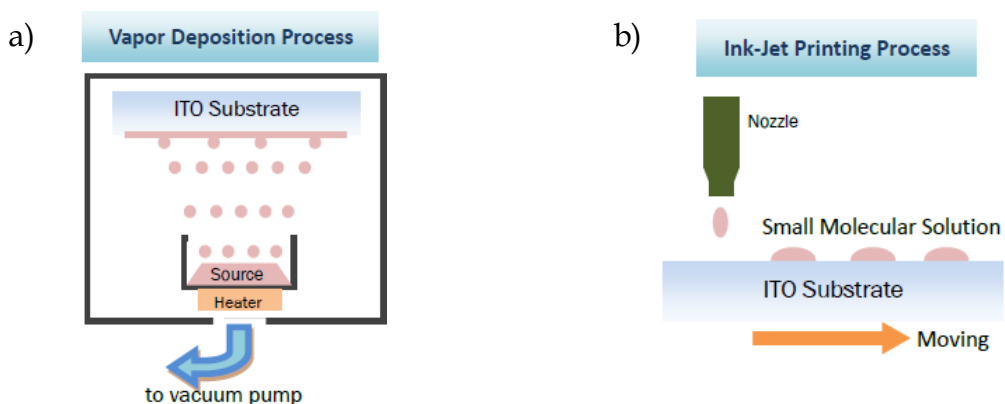


**Figure 15.** Examples of vacuum (a) and solution patterning (b) techniques.

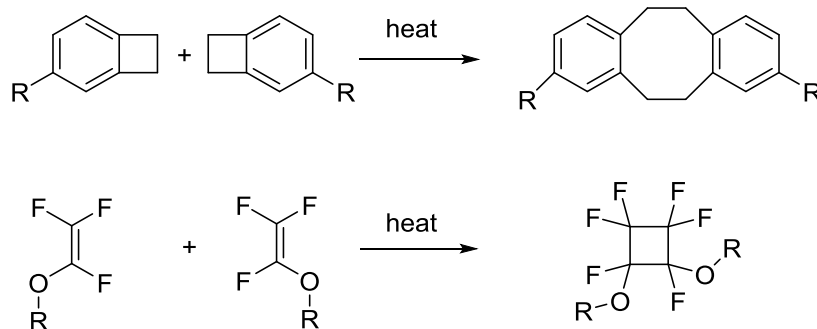


On the other hand, solution process, of either small molecules or polymers, merged as an economically alternative to vacuum deposition. In this case, the organic layers are deposited from organic inks by printing techniques such as roll-to-roll,<sup>66</sup> screen printing,<sup>67</sup> dye diffusion,<sup>68</sup> dip-coating,<sup>69</sup> slot-die or ink-jet (Figure 15b).<sup>70</sup> These techniques improve significantly the materials usage and simplify the fabrication process. However, they still have to overcome some drawbacks such as device lifetimes and degree of materials purity. Concerning device assembly another major drawback to be overcome is re-dissolution or harm of previously deposited layers by the solvent used to deposit the upcoming layer. This occurs when materials show similar solubility in the processing solvent and results in defects or destruction of the previous deposited layers, generating undefined multilayer structures. There exist two main approaches to overcome this problem, crosslinking and orthogonal processing, which are described in the next sections.

### 1.3.1 Thermal cross-linking strategies for multilayer solution processing

This approach consists in the cross-linking of the layers after deposition.<sup>71</sup> Crosslinking can be realized with molecules incorporating additional functionalities. When a thermal<sup>72</sup> or photochemical<sup>73</sup> treatment is applied a reaction takes place in the film and covalent linkages are formed between the polymer chains. This cross-linkage leads to insolubility of the film and a next solution can be applied without affecting the properties of the previous deposited layer.

The chosen cross-linking mechanism has to be efficient. Low activation energy and fast reaction rate of the functional groups is required to reduce possible side-reactions during the process. It is also preferred that the cross-linking reaction does not need any chemical initiator or generate any by-products to ensure the long-term stability of the devices. Some of the chemical structures that can fulfil these requirements are phenylcyclobutenes<sup>74</sup> or trifluorovinyltethers (Scheme 1).<sup>71</sup> Nevertheless, high curing temperatures are often required to obtain full crosslink. These temperatures can affect negatively previous deposited organic layers when this strategy is applied for fabrication of multilayer devices.



**Scheme 1.** Products formed after thermal crosslink of cyclobutenes and trifluorovinylethers.

### 1.3.2 Orthogonal strategies for multilayer solution processing

Fabrication of multilayer structures by orthogonal strategies is based on the insolubility of the underlying layer in the solvent used to deposit the upcoming layer. Although finding such combination of solvents and materials is rather challenging, orthogonal processing allows for rapid processing without application of high curing temperatures required for cross-linking. A common example of orthogonal processing is the application of PEDOT:PSS from aqueous solutions, which is insoluble towards organic solvents,<sup>16</sup> or the deposition of alcohol soluble materials onto materials only soluble in aromatic solvents.<sup>75-77</sup> Nevertheless, this strategy can be difficult to apply because it is not always possible to dissolve materials providing high efficiencies into a combination of solvents which allow orthogonal processing.

## 1.4 Side-chain polymers in OLEDs

Two main kinds of materials are generally used in OLED applications, small molecules and polymers. The use of small molecules has been widely established in the last years.<sup>63</sup> They can be highly purified (e.g. train sublimation purification) and, when applied by vacuum processing techniques, fabrication of multilayer structures is easily achievable. This allows for fabrication of devices showing high device lifetimes and high efficiencies.<sup>78,79</sup> However, when applied from solution, de-wetting or inhomogeneous film formation are often observed. Additionally, when operating at high temperatures (i.e. over the glass transition temperature), crystallization,<sup>80</sup> morphology defects,<sup>81</sup> or phase separation<sup>82</sup> can occur. These drawbacks are mainly related to their low molecular weights. Therefore, in order to have suitable materials for solution process, it is required to increase the molecular weight of the molecules. This can be done by two main approaches.

On one side, increased molecular weights can be obtained designing new small molecules, for instance by dimerization of known structures, resulting in higher molecular weights and defined glass transition temperatures.<sup>83</sup> However, modification of such molecules has to be designed carefully not to alter their optoelectronic properties. On the other hand, an alternative to increase the molecular weight is the incorporation of small molecules as side-chains into electronically inert polymer backbones, for instance polystyrene.<sup>82,84</sup> This approach provides a straight way to increase the molecular weights of small molecules and improve the morphological and thermal stability while affecting slightly the optoelectronic properties of the side-chains.

In this context, our group has been exploring this approach and providing side-chain polystyrenes applicable in solution processed OLEDs (Figure 16 and Figure 17).

Thesen et al.<sup>85</sup> designed a series of polystyrene bearing as side-chain triphenylamines derivatives adapted from well-known small molecules such as 4,4',4''-Tris[(3-methylphenyl)phenylamino]-triphenylamine (m-TDATA) or TCTA. These polymers show glass transition temperatures of 141 and 246 °C, respectively, ensuring high thermal and morphological stability during operation. The materials were applied as hole transport layers in all-solution processed OLEDs with efficiencies up to 35 cd/A at brightness of 100 cd/m<sup>2</sup>.

Debaux et al.<sup>50</sup> and Salert et al.<sup>86</sup> applied a similar strategy to adapt small molecule electron-transport materials into solution processable polymers. A series of TPBi- and triphenyltriazine (TPTA)-based polystyrenes were respectively presented. Besides the improvement of their  $T_g$ s, devices containing poly-triphenyltriazine as ETL showed promising device lifetimes.

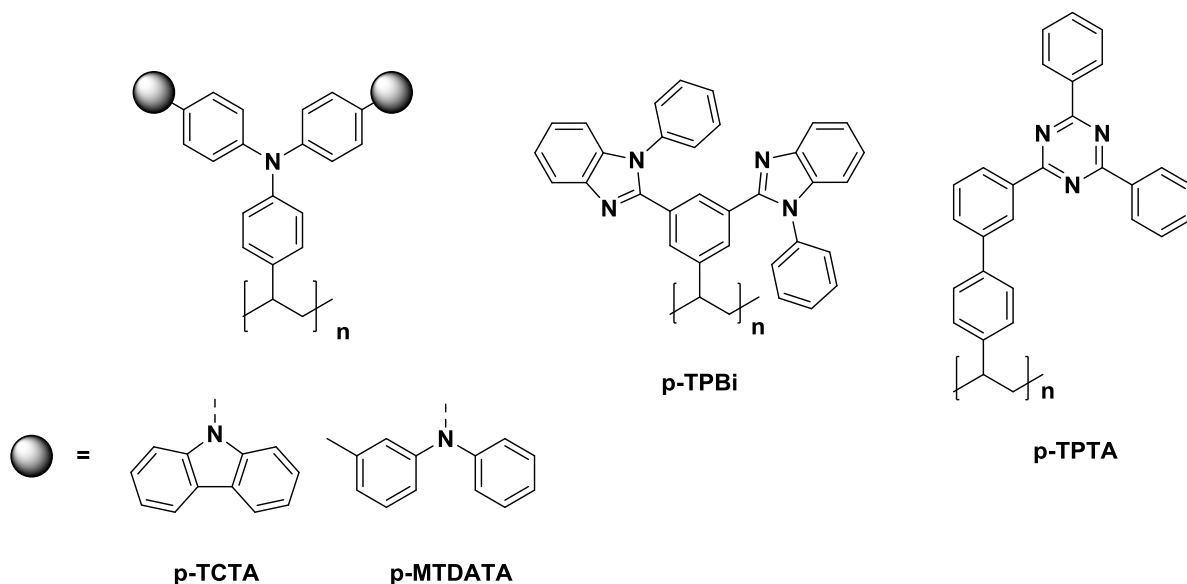


**Figure 16.** Polymeric HTLs (p-TCTA and p-MTDATA) and polymeric ETLs (p-TPBi and p-TPTA) developed previously in our group.<sup>50,85,86</sup>

Furthermore, the development of styrene-like monomers allows for ease fabrication of copolymers. Synthesis of copolymers is of high interest, since it provides a straightforward strategy to develop an infinite range of materials combining other functionalities. For example, Thesen et al. incorporated into polymers Ir-based phosphorescent emitters to prevent phase separation (Figure 17a).<sup>87</sup> Additionally, they also incorporate electron and hole transport monomers to provide polymers with ambipolar transport properties. Lately, Limberg et al. combined monomers bearing cross-linkable units with TCTA-based monomers to fabricate copolymers by free-radical polymerization (Figure 17b).<sup>88,89</sup> These copolymers were deposited from solution and after thermal treatment (170°C, 40 min), a second layer could be applied from solution without harming the cross-linked one.

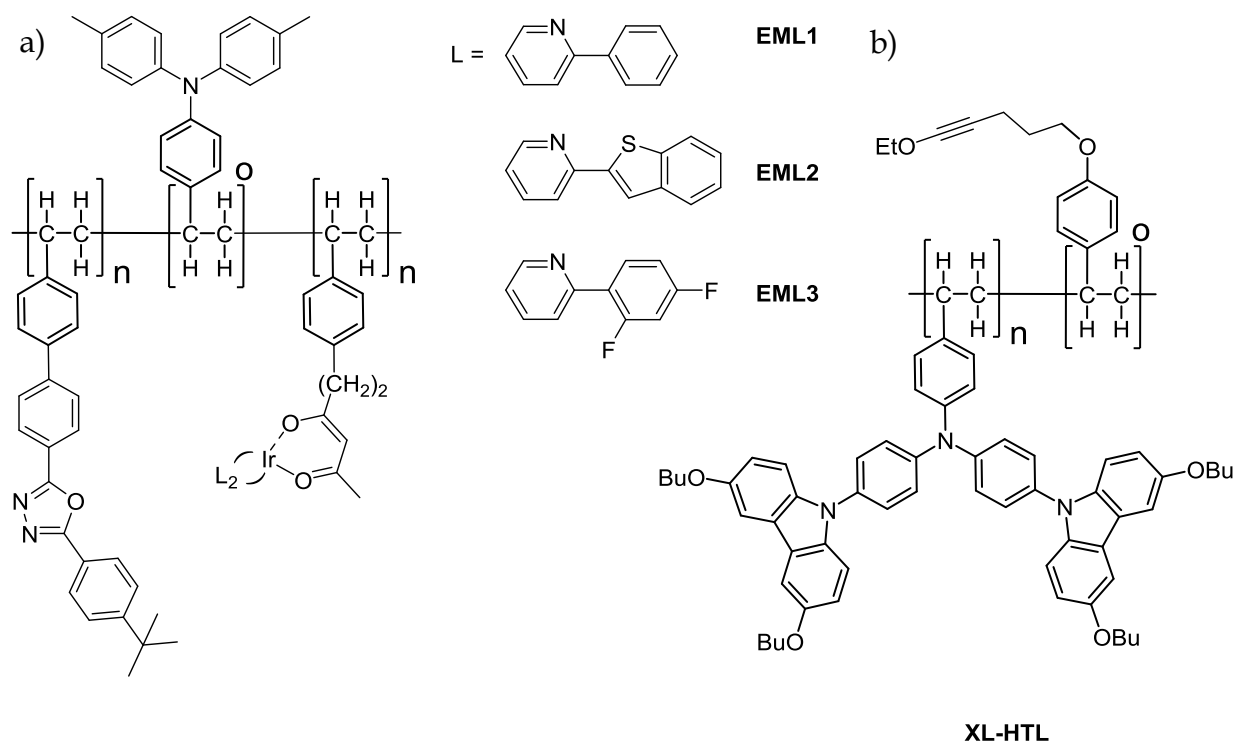


**Figure 17.** (a) Single layer emissive layers (EML1-3) and (b) cross-linkable HTL (XL-HTL) developed in our group.<sup>87,88</sup>

In summary, our previous work highlights the potential and suitability of polymers in this field. Concretely, polystyrene shows a high versatility to turn vacuum-processed small molecules into solution-processed materials for any of OLEDs active layers (HTL, EML or ETL) due to its high thermal and chemical stability.

## **1.5 Aim of the thesis**

The aim of this thesis is the development of side-chain polystyrenes applicable as charge transport layers in multilayer all-organic solution processed OLEDs.

In the recent years, new classes of small molecules are constantly being discovered to be used as more efficient transport layers. Generally, the straightest way to evaluate their suitability is to apply them in to vacuum processed devices. Unfortunately, the application of these small molecules from solution is not always considered or feasible due to some problems, such as recrystallization or de-wetting. However, in the pursuit of large area applications and lowering fabrication costs, efficient charge transport materials that can be applied from organic solutions are still highly demanded.

The main strategy employed in this work to develop solution processable materials is to modify slightly the structure of these efficient and previously studied small molecules, and incorporate them as side-chains into polystyrene backbones. Increasing significantly the molecular weight most of the drawbacks of small molecules can be overcome. This strategy has been demonstrated previously to provide solution-process materials for OLEDs with high performances.

Modification of the small molecules into monomers is achieved by functionalization with a single aromatic terminal alkene in some part of the molecule. The general techniques used for this purpose are Wittig olefination or Suzuki C-C coupling. Subsequent free-radical polymerization is expected to provide polystyrenes with high molecular weights and high glass transitions as well as good filming properties. Due to the non-conjugated nature of polystyrene backbone, the optoelectronic properties of the small molecules incorporated as side-chain are expected not to be significantly affected.

Among the different layers forming an OLED we concretely focused in developing solution-process charge transport materials for emissive and electron transport layers.

The first series of materials (Chapter 2) is thought to serve as ambipolar host for the emissive layer of phosphorescent OLEDs. In order to be applied in such form, the materials must have sufficient high triplet energy and feature both, electron and hole, transport. Generally, sufficient

high triplet energies ( $\geq 2.7$  eV) can be achieved limiting the conjugation to biphenyl units through the side-chain. To achieve hole transport properties carbazole groups have been shown to be excellent for OLED applications. Electron transport properties can be incorporated by electron-deficient heterocycles such as pyridines or triazines.

The second group of materials (Chapter 3) we aim to study are arylborane derivatives in combination with a tetraphenylsilane core. Recently, arylboranes have been gaining interest as materials for optoelectronic applications. They exhibit an electronic configuration analogue to a  $sp^2$  carbocation in their neutral state, which could stabilize effectively negative charges, providing suitable electron transport properties in OLEDs. Several arylborane units can be incorporated to the periphery of the tetraphenylsilane core, in the pursuit of increasing charge transport properties while retaining polymers high triplet energy

The last group of materials (Chapter 4) focus on the development of an orthogonal processable electron transport layer. Orthogonal processing profits of organic materials different solubility to deposit successive layers, without affecting previous deposited ones. For instance, a material which is insoluble into alcohols allows deposition of a second material soluble into alcohols on top in a defined fashion. A potential molecular motif that can provide this property is phenylpyridine, due to the favourable hydrogen bond interactions of pyridine. Additionally, phenylpyridine based small molecules are among the best electron transport materials developed to date. Nevertheless, these high efficiencies are always achieved for vacuum processed devices. Adaption of such molecules to their solution counterparts can provide interesting results for further development of solution process materials.

## 2. Ambipolar polymer matrix for multilayer solution processed OLEDs

Multilayer OLEDs consist of several layers with different functions. A common device architecture comprehends three organic layers consisting of a HTL an EML and an ETL, separately.<sup>38,39</sup> Previous work in our group, addressed the fabrication of multilayer solution processed OLEDs by developing HTLs based on TCTA derivatives, which could be crosslinked.<sup>88,89</sup> This is a pre-requisite to successfully deposit subsequently several organic layers from solution. The following step after establishing a suitable cross-linkable HTL is the development of a solution processable emissive layer.

Since the discovery of triplet emitters that allow the theoretical emission of all excitons formed,<sup>90</sup> the emissive layer is normally composed of a phosphorescent emitter dispersed into a host.<sup>91</sup> This is required to avoid quenching effects such as triplet-triplet annihilation (TTA).<sup>54</sup> The materials used to serve as host need to realize several functions. They must be able to transport both, positive and negative charges which should then recombine radiatively on the emitter. Moreover, the transport of such carriers in the EML should be balanced for an effective exciton generation in the EML and prevent the build-up of space charges in the devices. Furthermore, suitable host materials for phosphorescent OLEDs need to have a high triplet energy, i.e., higher than the emitters triplet energy ( $> 2.6$  eV for green emission, for instance), in order to exclude energy transfer from the emitters' relatively long-lived triplet excitons to the host. The latter requirements are somewhat in conflict, because the transport of charges is generally enhanced upon extension of the  $\pi$ -conjugated system,<sup>92</sup> while a high triplet energy is obtained when the  $\pi$ -conjugation is reduced.<sup>93</sup> This trade-off is a key aspect upon the synthesis of suitable host materials.

In Figure 18, we outlined a strategic route for the optimization of ambipolar host materials based on various known strategies previously used in development of charge transport materials.<sup>93,94</sup> 4,4'-Di(9H-carbazol-9-yl)-1,1'-biphenyl (CBP) has been used as host material for phosphorescent emitters; however, it has low triplet energy due to the wide delocalization of the triplet state through the molecule.<sup>95</sup> A general strategy to increase the triplet energy is to



decrease the conjugation through the molecule, giving 1,3-bis(*N*-carbazolyl)benzene (mCP) as a high triplet host material. Although mCP has a high triplet energy, their ability to transport electrons is poor, and behaves mainly as a hole transport material.<sup>93</sup> To recover ambipolar transport characteristics electron deficient heterocycles such as pyridine can be incorporated in the molecule like in 2,6-di(9H-carbazol-9-yl)pyridine (mCPy).<sup>96</sup> If the conjugation extension is confined, high triplet energy can be maintained while electron transport is enhanced. Further increase of the electron transport character can be introduced by extending the delocalization of the LUMO. This is achieved by insertion of additional phenyl rings between the electron donor and electron acceptor moieties. Furthermore, if the connectivity of such structures is kept in *meta*-positions internal charge transfer reactions can be avoided, and sufficient triplet energies obtained as in the case of 2,6-bis(3-(9H-carbazol-9-yl)phenyl)pyridine (26DczPPy).<sup>94</sup>

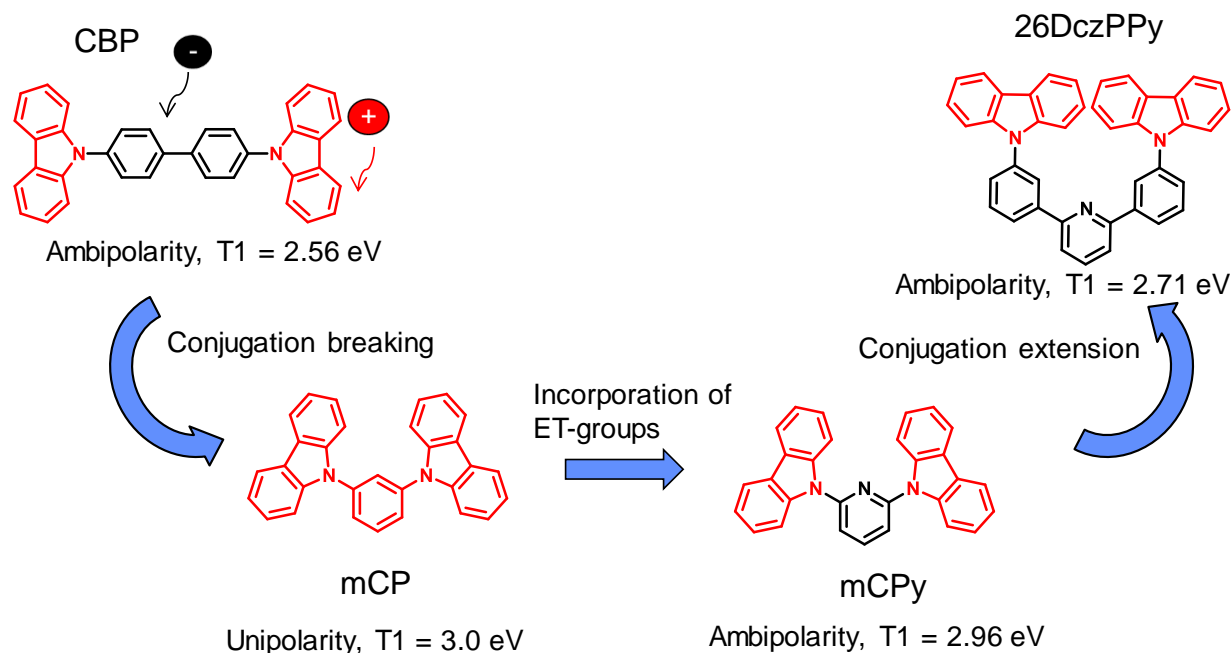


**Figure 18.** Optimization of CBP host material towards high-triplet host with ambipolar transport properties.<sup>93,94</sup>

In this chapter we applied our side-chain approach to some of this known small molecular structures, aiming the improvement of their thermal and morphological stability, as well as their applicability from solutions.

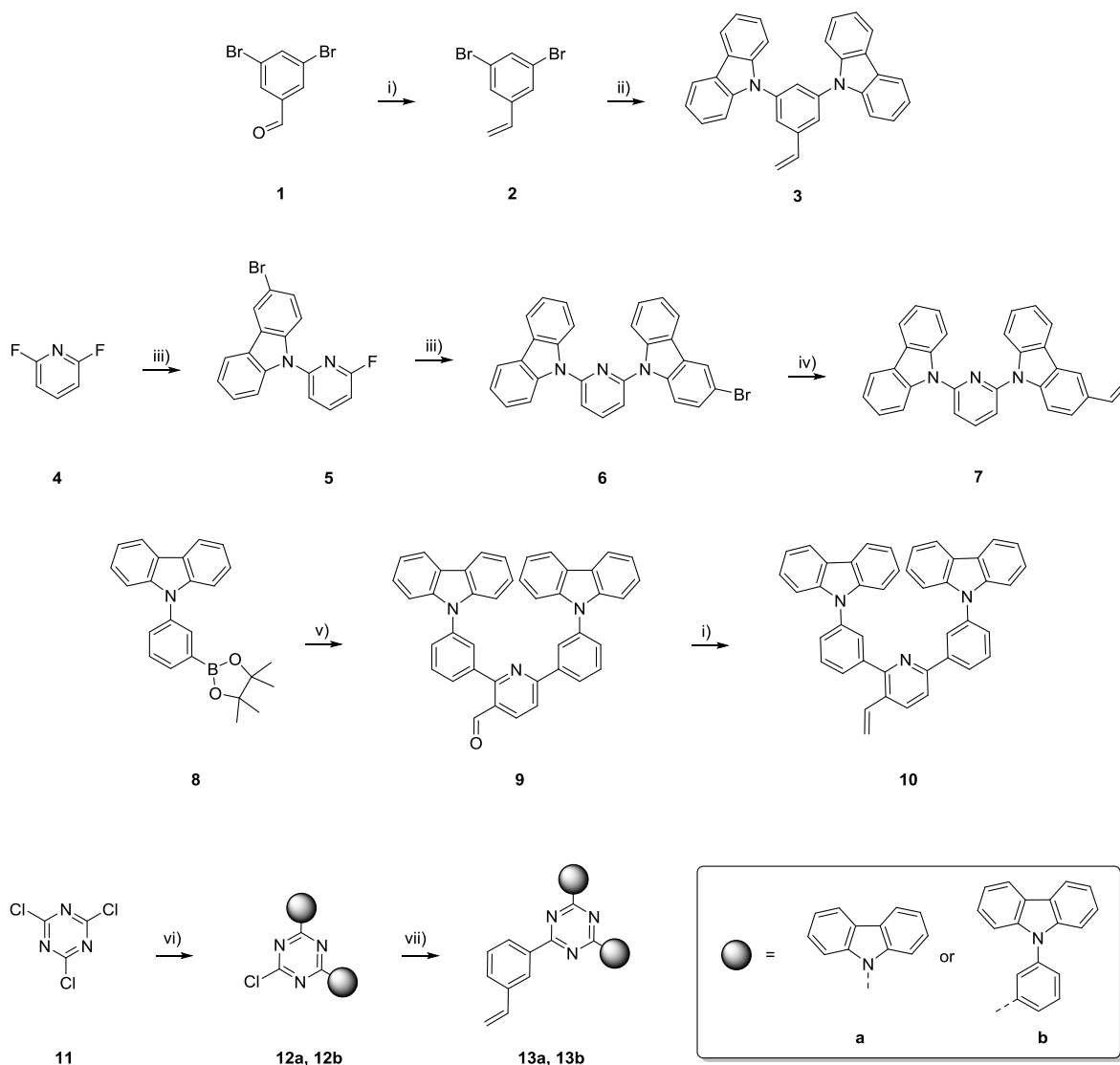
## 2.1 Materials design and synthesis

The monomers' synthetic steps are depicted in Scheme 2. The alkene function can be introduced at different positions, depending on the synthetic feasibility. It is expected that, after polymerization, the side-chain arrangement of the functional semiconducting unit has a negligible effect on the optoelectronic properties as compared to its molecular counterpart. Besides, due to the reactivity of the alkene function and its synthetic precursors, different synthetic routes were required to yield the monomers.

In order to obtain polymeric host materials with ambipolar character, we modify the chemical structure of mCP side-group following the strategy depicted in Figure 18. As a result, monomers **3**, **7**, **10** were developed. A second group of monomers is developed by replacing the central pyridine unit of poly-mCPy by a different electron-deficient monomer unit like phenyltriazine (monomer **13a**). Due to this strategy, the electron transport can be enhanced further, as has been shown for related molecular compounds.<sup>97</sup> Extra phenyl units are introduced between the carbazole and the triazine cores in monomer **13b**.<sup>98</sup> Phenyl-heterocycle and phenyl-carbazole connections are chosen to be in *meta*-positions as this disrupts the conjugation between electron-rich and electron-poor parts of the molecule.

Monomer **3** was synthesized by a two-step route. Firstly, the alkene function was introduced in 3,5-dibromoaldehyde **1** by a Wittig reaction to give **2**. Afterwards, a Buchwald-Hartwig C-N coupling reaction was used to introduce the carbazole motifs. Monomer **7** was synthesized using aromatic nucleophilic substitution of 2,6-difluoropyridine **4**. The mono-substitution was achieved by controlling the equivalents of carbazole added in each step. The styrene function was introduced afterwards using conventional Suzuki coupling. Monomer **10** was synthesized by coupling 9-(3-(4,4,5,5-tetramethyl-1,3,2-dioxaborolan-2-yl)phenyl)-9H-carbazole **8** to 2,6-dibromonicotinaldehyde by Suzuki-coupling. The aldehyde functionality is compatible with the reaction mechanism if potassium carbonate is used as base. Finally, the alkene group was introduced by a Wittig reaction using MePPh<sub>3</sub>Br and *t*-BuOK as base. Monomers **13a** and **13b**

were synthesized following a similar route. Firstly, cyanuric chloride was di-substituted either with carbazole (**12a**) or 3-bromophenylcarbazole (**12b**) controlling the equivalents added. Subsequently, Suzuki-coupling using 3-vinylphenylboronic acid results in good yields for the introduction of the alkene function.



**Scheme 2.** Monomers synthesis. *Reagents and conditions:* i)  $\text{MePPh}_3\text{Br}$ ,  $t\text{-BuOK}$ , THF, 0.5 h, 0 °C, **2** 65 %, **10** 79 %. ii) **2**, carbazole,  $\text{P}(t\text{-Bu})_3$ ,  $t\text{-BuONa}$ ,  $\text{Pd}_2(\text{dba})_3$ , toluene, 110 °C, 4 h, **3** 26 %. iii)  $\text{NaH}$ , 3-bromocarbazole (**5**) or carbazole (**6**), THF, 80 °C, 6 h, **5** 72 %, **6** 80 %. iv) Potassium vinyltrifluoroborate,  $\text{Pd}(\text{PPh}_3)_4$ ,  $\text{Na}_2\text{CO}_3$ , THF: $\text{H}_2\text{O}$  (9:1), 110°C, 20 h, **7** 75 %. v) 2,6-dibromobenzaldehyde,  $\text{Pd}(\text{PPh}_3)_4$ ,  $\text{K}_2\text{CO}_3$ , toluene: EtOH: $\text{H}_2\text{O}$  (2:1:1) 110 °C, 20 h, **9** 91 %. vi)  $n\text{-BuLi}$ , carbazole (**a**) or 3-bromophenylcarbazole (**b**), THF, -78 °C to r.t., 4 h, **12b** 19 %. vii) 3-vinylphenylboronic acid,  $\text{Pd}(\text{PPh}_3)_4$ ,  $\text{Cs}_2\text{CO}_3$  toluene: $\text{H}_2\text{O}$  (2:1:1), 100 °C, 20 h, **13a** 52 %, **13b** 53 %.

Polymers **P1-P5** (Figure 19) were synthesized by free radical polymerization of **3**, **7**, **10**, **13a** and **13b**, respectively. The reaction was conducted in a nitrogen atmosphere glove box system using 2 mol% AIBN as radical initiator at 50 °C for 3 days. The polymers were firstly precipitated into methanol and, when required, demonomerized into ethyl acetate/heptane or ethyl acetate/methanol mixtures. All the materials show good solubility in aromatic solvents such as toluene or chlorobenzene, as well as in halogenated solvents (e.g., chloroform and dichloromethane). The good solubility and film forming properties of the polymers allowed for characterization and possible application into solution processed OLEDs.

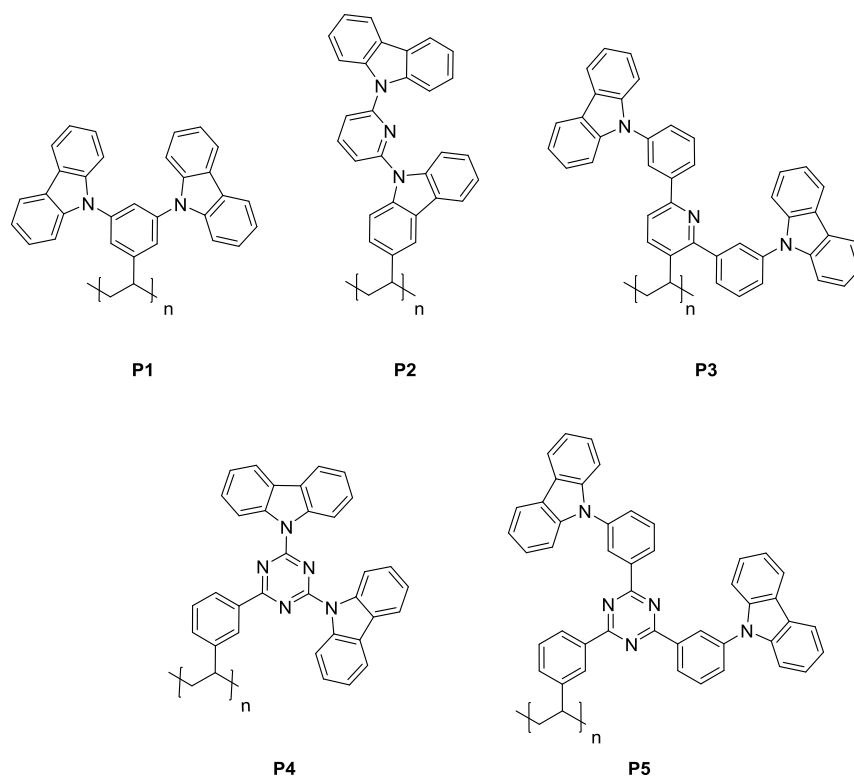


**Figure 19.** Yields and structures of polymers **P1** (62%), **P2** (68%), **P3** (69%), **P4** (80%) and **P5** (71%).

## 2.2 Characterization

### 2.2.1 GPC and DSC

Gel permeation chromatography (GPC) was used to characterize the polymers' molecular weights in tetrahydrofuran using polystyrene as a standard. The weight-average molecular weights of **P2-P5** were determined to be in the range from 30.8 to 123.5 kg mol<sup>-1</sup> with a polydispersity index (PD) ranging from 2.21 to 3.42. For **P1** an average molecular weight of 88.5 kg mol<sup>-1</sup> and a PD of 9.88 were determined. The higher PD value for this polymer is due to a bimodal distribution observed. The origin of this bimodal distribution may occur from a chain transfer reaction; however, this process was not studied in detail. The degrees of polymerization (DPs) are in the range from 20 to 88. Although DP for polymers **P1**, **P3** and **P4** are relatively low, previous studies in our group show that DP over 15 are large enough to prevent recrystallization.<sup>88</sup>

**Table 1.** Overview on analytical data of polymers **P1-P5**

Polymer	M <sub>n</sub> (kg mol <sup>-1</sup> ) <sup>a</sup>	M <sub>w</sub> (kg mol <sup>-1</sup> ) <sup>a</sup>	PD <sup>a</sup>	T <sub>g</sub> (°C) <sup>b</sup>	DP
P1	9.0	88.5	9.88	n. d. <sup>c</sup>	20
P2	38.4	123.5	3.21	211	88
P3	13.9	30.8	2.21	244	23
P4	11.8	35.0	2.96	275	22
P5	21.2	72.6	3.42	229	31

<sup>a</sup> Determined from GPC. <sup>b</sup> Determined from DSC measurements. <sup>c</sup> Not detectable.

Differential scanning calorimetry (DSC) measurements were performed to determine the thermal behaviour and the glass transition temperatures (T<sub>g</sub>) of the series (Table 1, Figure 20). For polymer **P1** no T<sub>g</sub> was detected in a range from 25 °C to 350 °C; probably due to the high PD, which hinders the observation of a clear transition during the DSC-scans. **P2** with the carbazole units connected directly to the pyridine shows with 211 °C the lowest T<sub>g</sub>. The introduction of phenyltriazine instead of pyridine in **P4** results in a T<sub>g</sub> increase up to 275 °C.

This is caused due to the different connectivity of the side-chain to the polymer backbone. For polymers **P3** and **P5**, with additional *meta*-phenyl bridges,  $T_g$  of 244 °C and 229 °C were observed respectively. This slight difference is related to the additional phenyl ring in the **P5** structure which enhances flexibility when compared with **P4**. Since the detected glass transitions are all well above 200 °C it is expected that the polymers are ideal for forming morphologically stable emission layers.

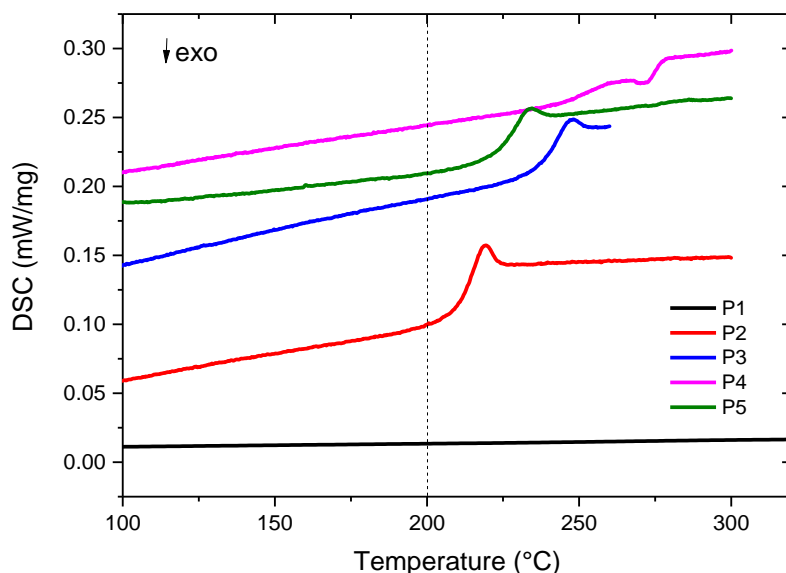


**Figure 20.** Differential-scanning calorimetry scans for polymers **P1-P5**. The 2<sup>nd</sup> heating cycles are displayed.

### 2.2.2 Theoretical calculations

Quantum chemical calculations were performed on the side-chain units of **P1-P5** at the B3LYP/6-31G\* level in order to examine the relationship between the chemical structure and the location of the HOMO and LUMO within the series. According to DFT calculation results shown in Figure 21, the HOMO orbitals of the series are located at the electron-donating carbazole moiety. For the LUMO orbitals, the replacement of phenyl (**P1**) by *N*-heterocycles (**P2**, **P4**) results in a shift of the LUMO position from the carbazole to the electron-poor core units. Introduction of an additional phenyl unit between the carbazole and the *N*-heterocycles (**P3**, **P5**)

in *meta*-position retains the delocalization of the HOMO within the carbazole, and of the LUMO within the phenylpyridine or phenyltriazine moieties. The calculations are in good agreement with previous studies on similar compounds.<sup>93,95,97,99</sup>

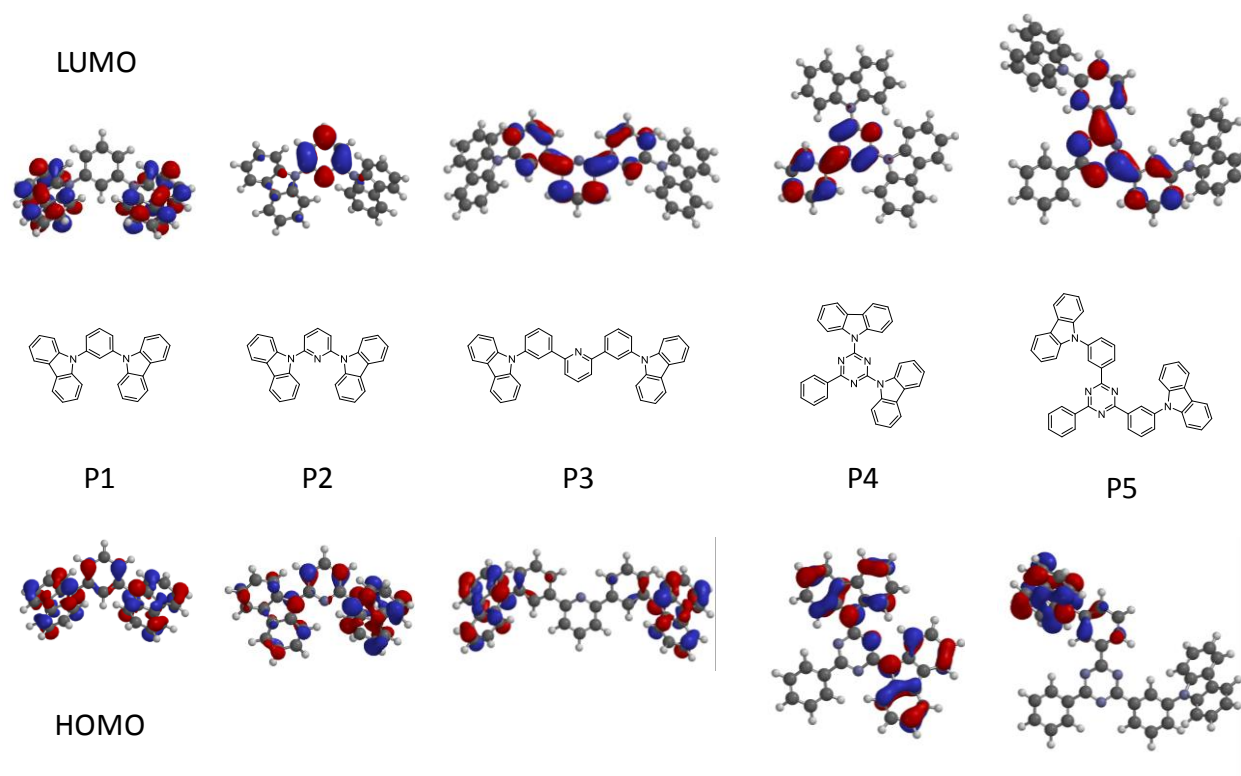


**Figure 21.** Calculated spatial distributions of the LUMO (top) and HOMO (bottom) of the corresponding **P1-P5** side-chains employing B3LYP/6-31G\* theoretical level.

### 2.2.3 Optical properties

The absorption, PL emission, and low temperature PL emission spectra of the polymers are shown in Figure 22. Table 2 summarizes the optical transitions extracted from the spectra. Absorption bands around 280 and 330 nm can be observed through the whole series. These peaks can be attributed to  $n-\pi^*$  and  $\pi-\pi^*$  transitions of the carbazole chromophore. Bands at about 210, 240 and 260 nm can be attributed to  $\pi-\pi^*$  and  $n-\pi^*$  transitions of phenyl.<sup>100,101</sup> The optical energy band gaps ( $E_g$ ) of polymers **P1-P5**, determined from the onset of UV/Vis spectra of solid films, range from 3.41 to 3.49 eV.

The PL emission maximum peaks ( $\lambda_{em}$ ) of the host polymers **P1-P5** are in the range from 381 to 456 nm. Replacement of pyridine (**P2**) by phenyl-triazine (**P4**) results in a strong bathochromic shift due to the higher electron affinity of the triazine core. Introduction of additional phenyl within carbazole and the *N*-heterocycles (**P3** and **P5**) results as well in a strong bathochromic shift due to the conjugation extension when compared with **P2** and **P4**.

**Table 2.** Photophysical properties of polymers **P1-P5**

Polymer	$\lambda_{max, abs}$ (nm) <sup>a</sup>	$\lambda_{em}$ (nm) <sup>a</sup>	$E_g$ (eV) <sup>b</sup>	$E_T$ (eV) <sup>c</sup>	$E_T$ (eV) <sup>d</sup>
P1	207, 244, 297, 326, 341	415	3.49	2.97	3.00 <sup>93</sup>
P2	206, 243, 344	295, 381	3.44	2.97	2.93 <sup>102</sup>
P3	207, 242, 328, 343	296, 415	3.43	2.73	2.71 <sup>100</sup>
P4	206, 313, 328	229, 280, 436	3.41	n. d. <sup>e</sup>	2.94 <sup>97</sup>
P5	209, 284, 328, 341	244, 266, 456	3.47	n. d. <sup>e</sup>	2.52 <sup>98</sup>

<sup>a</sup> Measured as thin film on quartz substrate. <sup>b</sup> Calculated from the onset of the absorption. <sup>c</sup> Determined from the emission spectra at 77 K. <sup>d</sup> Small molecule triplet energies. <sup>e</sup> Not detectable.

The triplet state was estimated from low temperature PL emission spectra at 77 K in 2-methyltetrahydrofuran. Besides fluorescence, an additional low energy tail with a well resolved vibrational structure is observed (marked with a ‘\*’ in Figure 22) which is related to the phosphorescence of the sample. Read-out of the triplet energy was done from the highest energy peak (the 0-0 transition of the phosphorescence). For **P1** and **P2**, which only differ in the choice of the central aromatic ring (phenyl **P1**, or pyridine **P2**), the triplet energies are very similar (2.97 eV). In the case of polymer **P3**, where the introduction of a *meta*-phenyl bridge



results in extension of conjugation in the side-chain, a decrease in the triplet energy is observed (2.73 eV) as expected. Note that the triplet energy of the side-chain polymers correspond closely to the triplet energies of the related molecular structures (see Table 2). For polymers **P4** and **P5** no apparent 0-0 transitions can be discriminated from the low temperature PL data. We expect, however, based on the corresponding published molecular data, that the triplet energy of **P4** is around 2.9 eV. The triplet energy of **P5** is expected to be much lower (ca. 2.5 eV for the molecular derivative) due to the extended LUMO. **P5** may be unsuitable for the use as host material, for instance in green emitting phosphorescent OLEDs such as TEG001 with a triplet energy around 2.6 eV.<sup>86,103</sup>

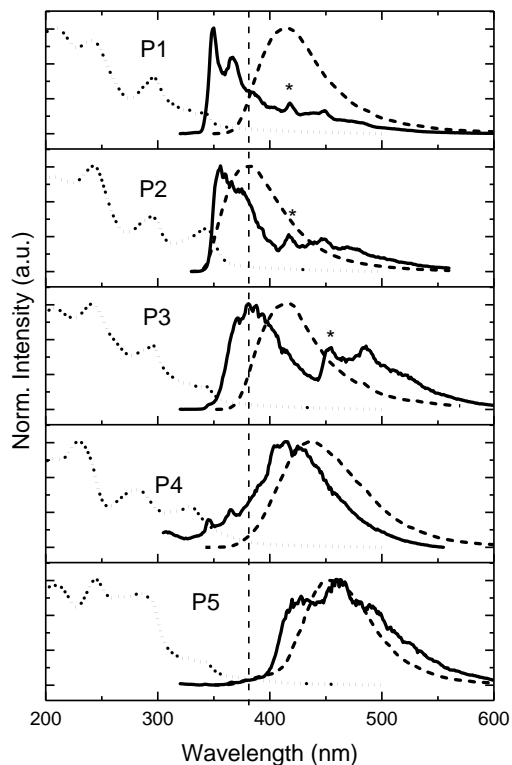


**Figure 22.** UV/vis (dot), emission (dash) and emission at 77 K (solid) spectra for polymers **P1-P5**. \* Read out of triplet energy (peak).

## 2.2.4 Molecular orbitals

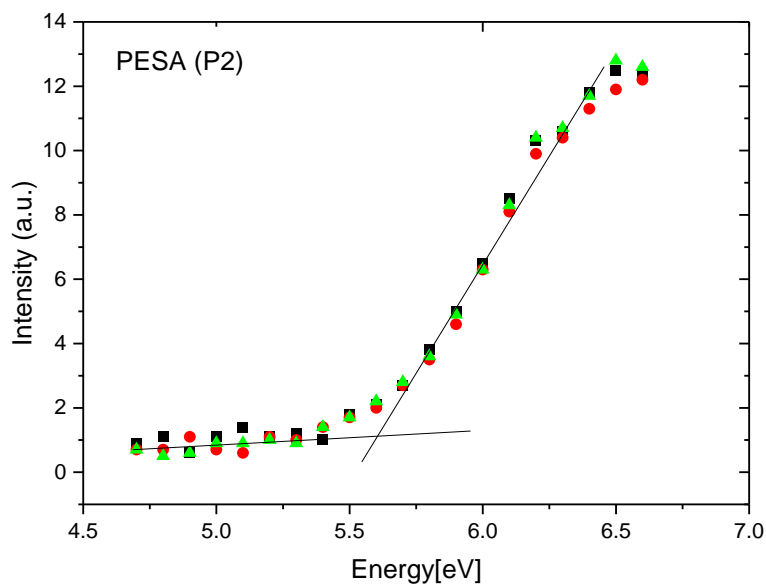
Cyclic voltammetry (CV) and photoelectron spectroscopy in air (PESA) were used to estimate the HOMO energies of polymers **P1-P5**. The corresponding values are compiled in Table 3 and an exemplary PESA measurement and cyclovoltammogram are shown in Figure 23. Good correlation is observed within the two methods, with a maximum deviation of 0.3 eV for **P8**. According to CV, HOMO levels are in the range of -5.9 to -5.7 eV. LUMO levels were estimated by CV. Ambipolar polymer **P2** has a LUMO level of -2.6 eV. The introduction of an additional phenyl ring between the pyridine and the carbazole units (**P3**) result in a stabilization of the LUMO level up to -2.7 eV. This can be related to a higher delocalization of the LUMO in the phenyl bridges. When the central pyridine ring (**P2**) was substituted by a phenyltriazine (**P4**), the LUMO level was estimated to be -2.8 eV. This can be attributed to the higher electron affinity of the triazine core. Similarly, as for polymer **P3**, the introduction of an additional phenyl ring between the carbazole and the triazine units in polymer **P5** results in a further stabilization up to -2.9 eV. No correlation was observed when comparing hole-only transport polymer **P1** with the rest of the series. This might be due to a completely different distribution of the LUMO in the side-chain which is mainly located at the carbazole units instead of at the central aromatic ring (Figure 21).

**Table 3.** Electrochemical properties of polymers **P1-P5**

Polymer	$E_{\text{ox}}$ (V) <sup>a</sup>	HOMO (eV) <sup>b</sup>	HOMO (eV) <sup>c</sup>	$E_{\text{red}}$ (V) <sup>a</sup>	LUMO (eV) <sup>b</sup>
P1	1.4	-5.8	-5.9	-1.6	-2.8
P2	1.4	-5.8	-5.6	-1.8	-2.6
P3	1.3	-5.7	-6.0	-1.7	-2.7
P4	1.5	-5.9	-6.0	-1.6	-2.8
P5	1.4	-5.8	-5.8	-1.5	-2.9

<sup>a</sup>Determined by cyclovoltammetry. <sup>b</sup>Cyclovoltammetry on-set potential against ferrocene standard. <sup>c</sup>From PESA.

a)



b)

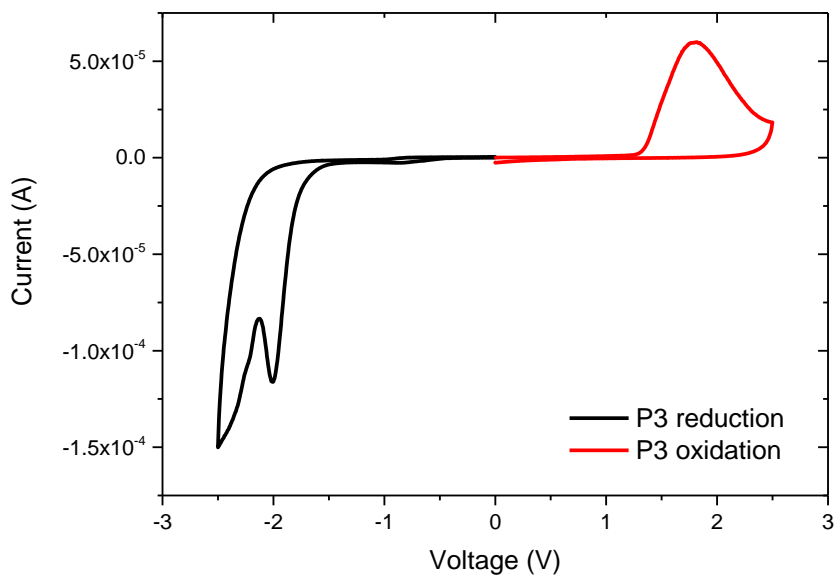


**Figure 23.** a) Exemplary PESA measurement from polymer **P2**. The HOMO value is calculated directly from the onset of the curve. b) Exemplary cyclic voltammogram of polymer **P3**. The oxidation and reduction potential were taken from the onset of the corresponding peak.

### 2.2.5 Solution processed multilayer OLEDs

In order to investigate the potential of the host polymer series for optoelectronic devices, **P1-P5** were used in the emission layer of green OLEDs. These devices consist of a solution processed sequence of PEDOT:PSS, hole transport (HTL), emission, and electron transport layers (ETL), see the diagram in Figure 24a. Upon device fabrication, we use both crosslinking and orthogonal solution approaches in order to avoid the dissolution of the underlying layers. The HTL consists of a side-chain functionalized hole transporting polymer, poly-(3,6-(BuO)<sub>4</sub>TCTA),<sup>88</sup> which has been equipped with cross-linker units. After deposition by spin-coating, the HTL has been thermally cured at 185 °C for 5 min in inert atmosphere. On top of the crosslinked HTL, the emission layer has been spin-coated from chlorobenzene solutions of a blend of the host polymer **P1-P5** and the green phosphorescent emitter TEG001<sup>86,103</sup> (14:86 weight ratio of emitter:polymer). This layer has been annealed at 180 °C for 30 min in order to remove the residual solvent. The ETL layer has been prepared from an isopropanol solution of an electron transporting fluorene-based copolymer. Except the ITO anode and the evaporated Ba/Ag cathode, these multilayer devices are fully solution processed.

**Table 4.** Physical parameters of the OLEDs with polymers **P1-P5** as host material

Polymer	Current on-set voltage (V) <sup>a</sup>	Luminance on-set voltage (V) <sup>b</sup>	Max. current efficacy (cd/A) <sup>c</sup>
P1	4.0	6.3	1.6 (70 cd/m <sup>2</sup> )
P2	4.0	5.7	6.3 (40 cd/m <sup>2</sup> )
P3	3.0	3.6	17.3 (120 cd/m <sup>2</sup> )
P4	2.6	3.0	28.9 (180 cd/m <sup>2</sup> )
P5	2.2	2.5	16.2 (210 cd/m <sup>2</sup> )

<sup>a</sup> At 10<sup>-2</sup> mA/cm<sup>2</sup>, forward sweep. <sup>b</sup> At 10 cd/m<sup>2</sup>, forward sweep. <sup>c</sup> According luminance is denoted in brackets.

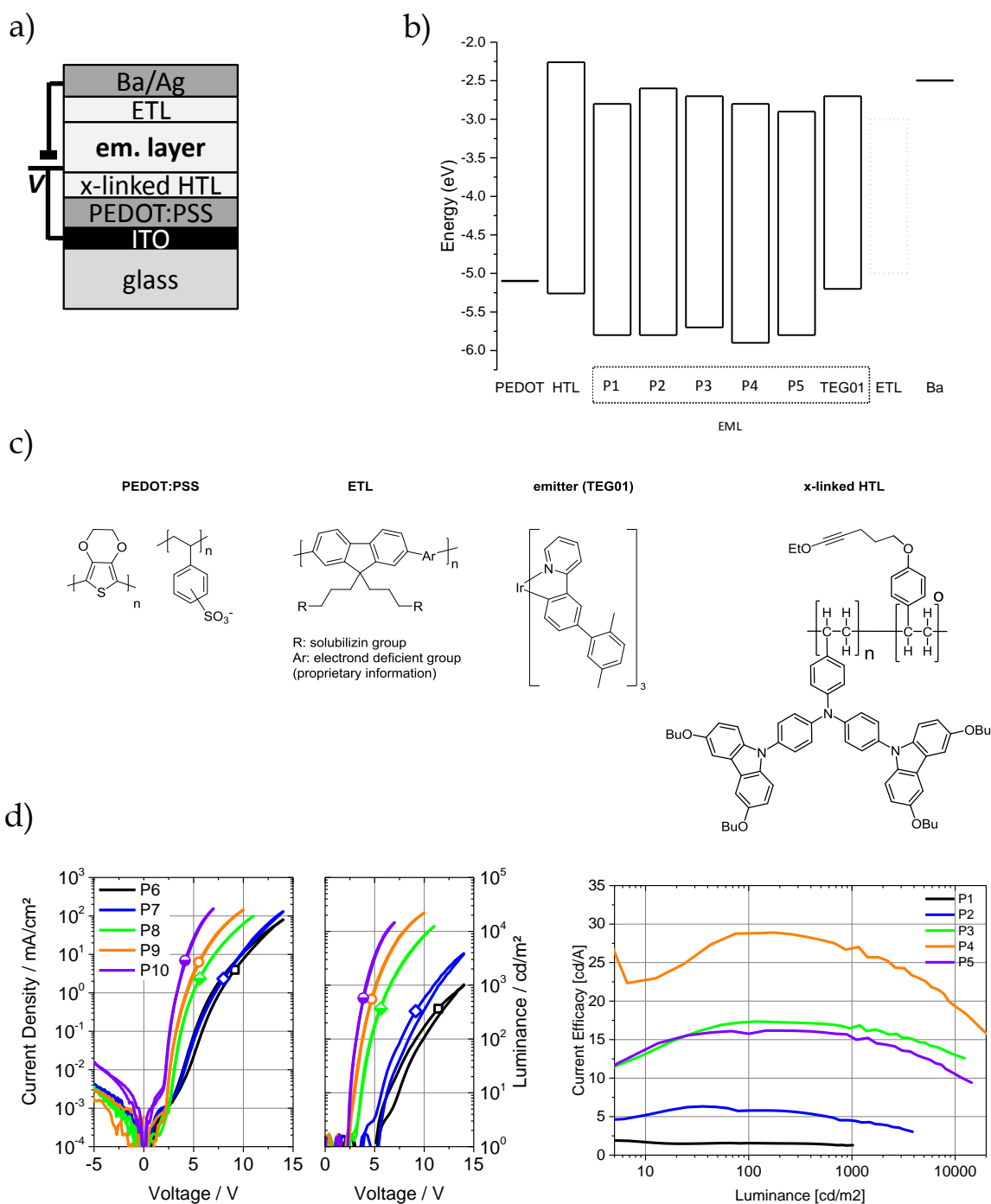


**Figure 24.** a) Device structure consisting of a glass substrate, ITO anode, PEDOT:PSS, crosslinked HTL, emissive layer, ETL and Ag/Ba cathode. b) Energy diagram of the different compounds molecular orbitals. The emissive layer is composed of one polymer and emitter TEG01 for each device. Energy levels and structure of ETL were proprietary from Sirigen Inc. c) chemical structures of materials used additionally in device fabrication. d) Current density and luminance characteristics of multilayer OLEDs with **P1-P5** as host material.

Figure 24d shows the current density-voltage and luminance-voltage characteristics of representative OLED samples. Due to the excellent film forming properties of the materials used, the OLEDs exhibit prominent diode behaviour with very low leakage currents at negative voltages. There is the clear trend that both the current and luminance on-sets shift towards lower voltages from **P1** to **P5** (see also Table 4). As compared to the energy levels of the polymers, this trend does not correlate with the electrochemical parameters reported in Table 3 since the estimated LUMO values for the series do not differ drastically. Therefore, we attribute the lower on-set voltages to modified charge transport properties.

The device with **P1** as host material has the highest on-set voltage throughout the polymer series. Based on the predominant hole transporting character of mCP,<sup>104</sup> we assume that the current in our **P1**-based OLEDs is mainly determined by the charge transport of holes. Moreover, it has been reported that the emitter TEG001 has a hole transporting character as well.<sup>86,103</sup> Accordingly, the unbalanced charge transport in **P1**-based devices leads to a very low current efficacy of only 1.6 cd/A, see Table 4.

A slightly lower luminance on-set voltage and a 4-fold increased current efficacy are exhibited by devices with host polymer **P2**. Further strong on-set voltage lowering and an increase of the current efficacy to 17.3 cd/A are observed for **P3**. As has been outlined above, the functional moieties of these polymers include electron-deficient centres (pyridine) which lead to a delocalization of the LUMO onto the pyridine ring of **P2** and onto the diphenylpyridine unit of **P3** respectively, enhancing electron transport of the hosts. Concurrently, the electron transport is enhanced as compared to **P1**, which leads to a more balanced transport of holes and electrons in the emission layer. It was speculated that the significant larger current efficacy of **P3**-based OLEDs is particularly due to the extended delocalization of the LUMO onto the pyridine and the neighbouring phenyl rings. This should enhance the electron transport, as has been suggested for the molecular derivative of **P3**.<sup>61</sup>

OLEDs with host polymer **P4** or **P5**, having a triazine core instead of pyridine, outperform **P1-P3**. Very low on-set voltages of 2.2 and 2.6 V and considerable current increases are seen, which indicates good charge transport in these layers. The triazine unit has been proven to exhibit very good electron transporting properties in related electron transporting side-chain polystyrenes.<sup>86</sup> Comparing **P4**- and **P5**-based devices, we observe lower on-set voltages for **P5**,

which is probably due to the delocalization of the LUMO across the diphenyltriazine unit<sup>97</sup> and accordingly better electron transport. However, the current efficacy of **P5**-based OLEDs (16.2 cd/A) is lower than that of the **P4**-based devices (28.9 cd/A). Most probably, this is related to the rather low triplet energy of **P5** (2.52 eV for the molecular derivative, see Table 4), which is in the range of the triplet energy of the emitter and possibly leads to quenching of the emitter's phosphorescence.

## 2.3 Conclusion

A series of polymer host materials based on carbazole and aryls like benzene, pyridine and 1,3,5-triazine was synthesized. The moieties were incorporated as side-chains onto polystyrene backbones. Due to this side-chain approach, the polymers combine both the defined optical properties of the conjugated side-chain units as well as the processability and typical morphological stability of polymers. We have observed that the charge transport properties of the host polymers and the performance of the corresponding OLEDs depend crucially on the choice of the electron transporting core unit. While hole-only transport is observed for a polymer with a phenyl core unit (**P1**), ambipolar character was imposed by replacing the phenyl with the more electron-deficient heterocycles pyridine or triazine (**P2-P5**). This led to a delocalization of the LUMO onto the core unit and an improved electron transport. The corresponding OLEDs feature lower luminance on-set voltages and higher efficacies, which is directly related to a more balanced electron and hole transport in the emission layer. Further increase of the ambipolar character of the polymers was achieved by extending the delocalization of the LUMO due to the incorporation of phenyl units at the central pyridine or triazine. This led to OLED current efficacies of up to 28.9 cd/A, and very low luminance on-set voltages down to 3.0 V (**P4**). However, the extension of the LUMO delocalization does concomitantly lead to a decrease of the triplet energy. It was noticed that this is an issue for the triazine-based host polymer **P5**, reducing the current efficacy of the corresponding OLED.

In conclusion, the side-chain approach and the particular combinations of hole transporting carbazole and electron transporting pyridine or triazine units are promising for the further development of ambipolar host materials for multilayer and solution processed OLED devices.

### 3. Electron transport materials based on dimesitylborane and tetraphenylsilane

During the last years, a large number of molecules have been developed to act as electron transport materials in OLEDs.<sup>47</sup> Nevertheless, these materials were mainly designed to be applied in vacuum-process devices.<sup>48</sup> As explained previously in the introduction, high efficiency in all-organic solution processed OLEDs is a milestone still to reach to fabricate OLEDs economically, in industrial scale and with adequate device lifetimes. Therefore, development or adaption of small molecular ETMs into solution processable counterparts is still of high interest.

Electron transport materials need to hold the following optoelectronic properties to be applied as efficient ETLs in phosphorescent OLEDs:<sup>41</sup>

- Suitable LUMO levels to decrease energy barriers between cathode and EML
- Deep HOMO level ( $< -6.3$  eV) to prevent electrons to go through the device without recombination
- Triplet energy higher than that of the emitter (e.g.  $> 2.6$  eV for green emission), to avoid exciton quenching by energy transfer to the ETL, or diffusion of the excitons in the ETL
- Balanced carrier mobility to favour generation of excitons in the EML

Rationally designed electron-deficient *N*-heterocycles (e.g. pyridines or triazines) can fulfil most of these requirements effectively.<sup>40</sup> Stabilization of negative charges is possible by resonance in the aromatic ring and relatively high triplet energy materials ( $\approx 2.7$  eV) can be achieved by keeping the connections within aromatic rings in *meta*-position.<sup>94</sup> Nevertheless, a different class of materials incorporating other electropositive atoms such as boron or phosphor have emerged as interesting new electron transport materials, improving some of their properties such as triplet energy.<sup>51,105</sup>

Concretely, triarylboron derivatives have gain recently much interest in optoelectronic applications due to its chemical singularity.<sup>106</sup> Boron derivatives are isoelectronic and isostructural with a positively charged carbocation and its vacant  $p_{\pi}$  orbital can be conjugated



with  $\pi$ -systems leading to significant delocalization. Additionally, boron compounds show high affinity for electrons (Lewis acidity). However, this affinity also turns them often into unstable molecules. To increase their stability, blocking of the inductively activated positions and the empty  $p_{\pi}$  orbital with bulky substituents (e.g., trianthryl or mesitylene, Figure 25) is required. In particular, it has been demonstrated that two mesityl groups were sufficient to provide an unusual degree of stability and therefore turning dimesitylboranes ( $\text{BMes}_2$ ) an applicable motive for optoelectronic applications.<sup>107</sup>

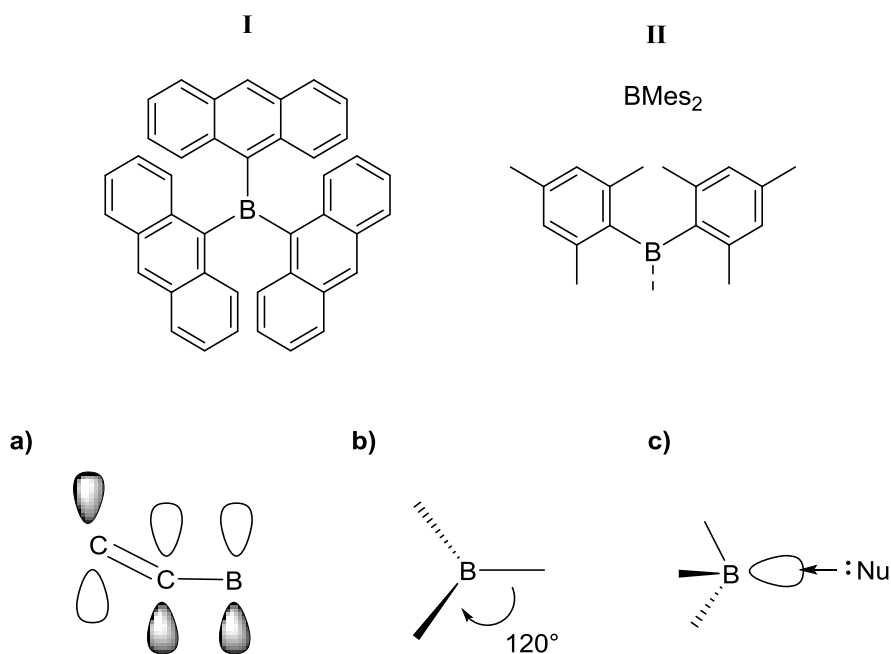


**Figure 25.** Top: tri(anthracen-9-yl)borane (I) and borondimesitylene (II,  $\text{BMes}_2$ ) chemical structures. Bottom: Three fundamental features of boron based materials: a)  $p$ - $\pi^*$  conjugation, b) trigonal planar geometry, c) Lewis acidity.<sup>106</sup>

Besides the after mentioned optoelectronic properties required for ETMs, high thermal and morphological stability as thin films is essential for the lifetime of a device.<sup>80</sup> Tetraphenylsilanes are a class of molecules that have a stable glassy state due to the rigid tetrahedral approach providing homogeneous amorphous thin films.<sup>108</sup> Their synthesis and further functionalization is easily accessible due to the core high chemical stability. Furthermore, the central  $\text{sp}^3$  silicon atom provides high triplet energy for their derivatives, turning this motive a suitable central core, easily modifiable, for developing solution processable ETMs.<sup>58</sup>

As a part of this work, we aim the synthesis and characterization of a series of ETMs containing borondimesitylene and tetraphenylsilane motifs. The materials were incorporated into polystyrenes using the side-chain approach to ensure good solution processability. We characterize them in terms of optoelectronic properties and performance in all-solution processed phosphorescent green OLEDs.

### **3.1 Synthesis**

The polymer series was designed to evaluate the effects of different combination from both molecular structures (triarylborane and tetraphenylsilane) in the electronic and optical properties of the resulting ETMs (Figure 26). Polymer **P6** contains only the tetraphenylsilane group besides the alkene function and was synthesized for comparison with the rest of the series. Similarly, polymer **P7** incorporates the triarylborane solely in order to evaluate the electron transport properties of this group. In the case of polymer **P9**, the tetraphenylsilane and triarylborane are combined in the same molecular structure, while the alkene function is incorporated at a biphenyl in pursuit of straightforward synthetic route. The resulting biphenyl structure is expected to limit the triplet energy of the materials around 2.7 eV, therefore polymer **P8** was synthesized avoiding any phenyl-phenyl linkage, expecting higher triplet energy than for polymer **P9**. The last polymer of the series **P10** is a modification of **P8**, in which an additional triarylborane unit is incorporated. The purpose of such modification is to observe if some LUMO delocalization can occur through the silicon atom, and if it could have a positive effect in charge transport properties of the resulting polymer.

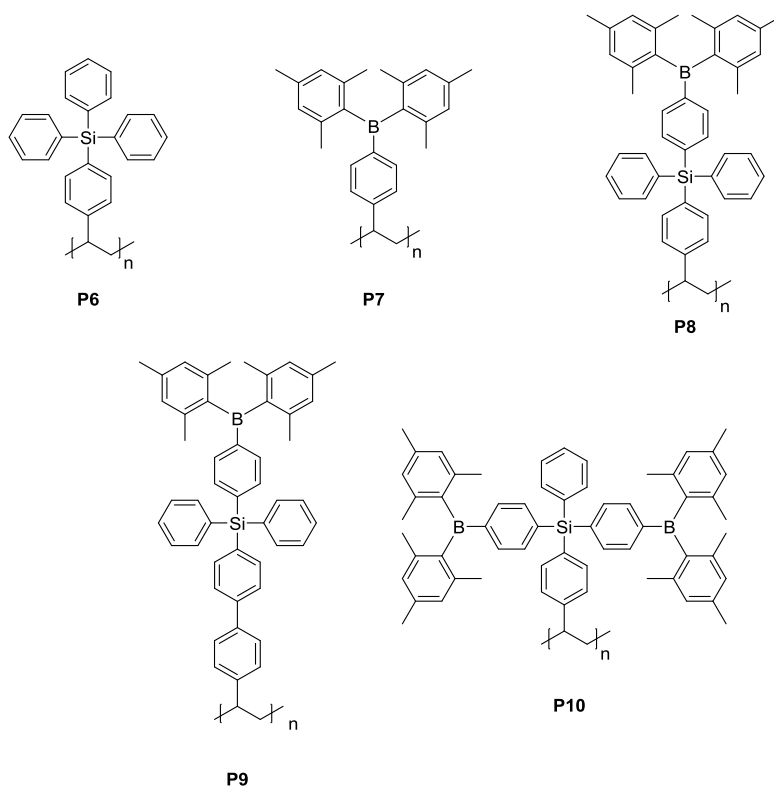
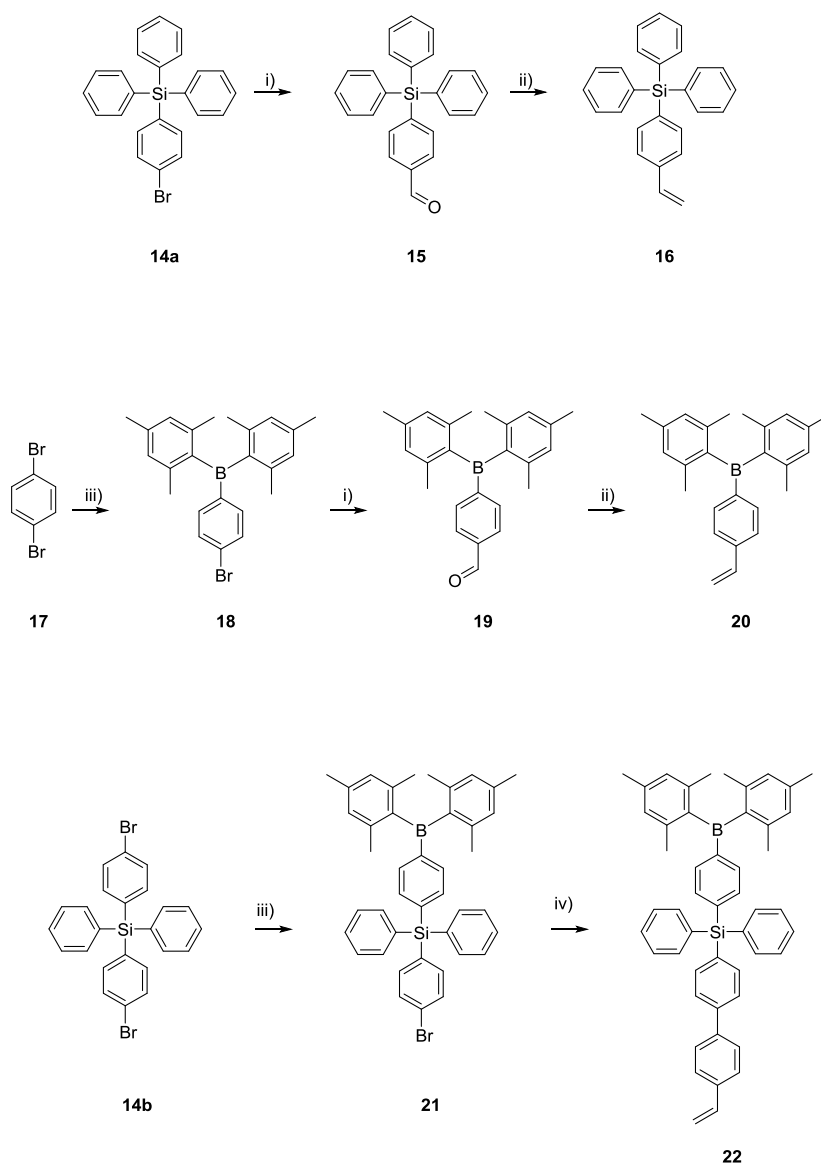


**Figure 26.** Yields and structures of polymers **P6** (63%), **P7** (79%), **P8** (73%), **P9** (37%), **P10** (51%).

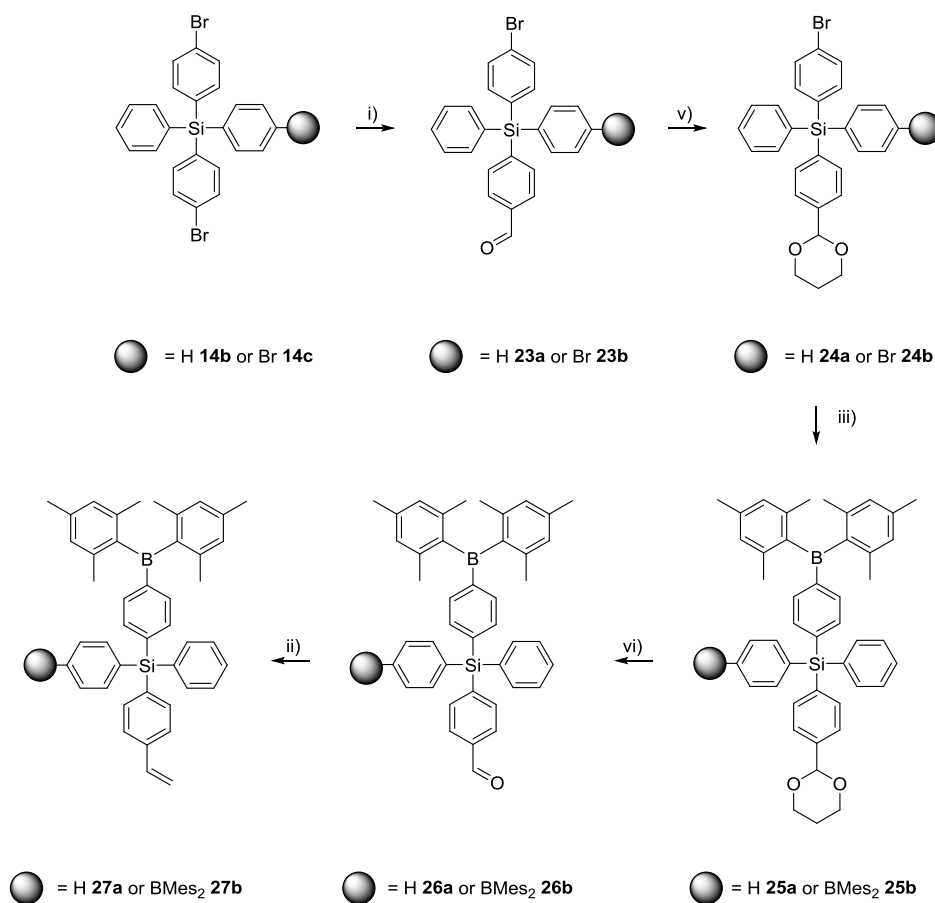
In order to synthesize styrene-based monomers two different functions have to be introduced in the side-chain core. On one side, the arylborane motif and on the other side the aromatic alkene function. Symmetry of bromo-functionalized tetraphenylsilanes can be selectively broken by controlling the equivalents of organolithium salt added. The synthesis routes of the monomers are depicted in Scheme 3 and Scheme 4. Monomer **16** was synthesized in a two-step route. Firstly, lithiation of (4-bromophenyl)triphenylsilane **14a**, followed by addition of DMF and subsequent quenching with acidic conditions gives the corresponding aldehyde **15**. The second step consisted in a Wittig reaction using methyltriphenylphosphonium bromide (MePPh<sub>3</sub>Br) with *t*-BuOK as base. Monomer **20**, was synthesized in a three-step route, starting from 1,4-dibromobenzene. Mono-substitution with dimesitylborane (BMe<sub>2</sub>) was selectively controlled by adding one equivalent of *n*-butyllithium to give **18**. Subsequently, **18** was transformed into the corresponding aldehyde **19** by lithiation and quenching with DMF in acidic media. Finally, the same Wittig reaction protocol used for **15** gave monomer **20**. Monomer **22** was synthesized

in a two-step route starting from bis(4-bromophenyl)diphenylsilane **14b**. Mono-substitution with BMe<sub>2</sub> in a similar way as in **18** gave intermediate **21**. Styrene was coupled under Suzuki conditions using 4-vinylphenylboronic acid in low yields, which might suggest decomposition or hydrolyzation of the BMe<sub>2</sub> group.



**Scheme 3.** i) 1. *n*-BuLi, -78 °C, 1h; 2. DMF, r.t., 4 h; 3. HCl, r.t., 0.5 h, **15** (81%), **19** (71%). ii) MePPh<sub>3</sub>Br, *t*-BuOK, THF, 1 h, 0°C, **16** (60%), **20** (37%). iii) 1. *n*-BuLi, -78 °C, THF, 1 h; 2. BMe<sub>2</sub>F, 50°C, 2 h, **18** (63%), **21** (76%). iv) 4-Vinylphenylboronic acid, Pd(PPh<sub>3</sub>)<sub>4</sub>, Na<sub>2</sub>CO<sub>3</sub> THF:H<sub>2</sub>O (5:3), 100 °C, 4 h, **22** (22%).

Monomers **27a** and **27b** (Scheme 4) were also attempted to be synthesized by coupling potassium vinyltetrafluoroborate to **21** under Suzuki conditions. However, as previously noted, many undesired products were formed. Additionally, this approach was declined due to the similar polarity of the educts and products resulting in a complex purification process. An alternative route was used to yield the monomers **27a-b**. The corresponding bromophenylsilane (**14b** or **14c**) was transformed into the aldehydes (**23a** or **23b**) by lithiation and by addition of DMF. The aldehyde was then protected with 1,3-propanediol under acidic conditions, previous to the introduction of the borondimesitylene moiety by lithiation. Deprotection in aqueous media was followed by Wittig reaction to give the desired monomers.



**Scheme 4.** i) 1. *n*-BuLi, -78 °C, 1h; 2. DMF, r.t., 4 h; 3. HCl, r.t., 0.5 h, **23a** (88%), **23b** (65%). ii) MePPh<sub>3</sub>Br, *t*-BuOK, THF, 1 h, 0°C, **27a** (71%), **27b** (88%). iii) 1. *n*-BuLi, -78 °C, THF, 1 h; 2. BMe<sub>2</sub>F, 50°C, 2 h, **25a** (67%) **25b** (77%). v) *p*-TsOH, 1,3-propanediol, toluene, 150°C, 20 h, **24a** (57%), **24b** (70%) vi) *p*-TsOH, H<sub>2</sub>O:THF, 100 °C, 20 h, **26a** (60%), **26b** (56%).

Polymers **P6-P10** (Figure 26) were synthesized by free radical polymerization from moderate (**P9**, 37%) to good yields (**P7**, 79%). The reaction was conducted in a nitrogen atmosphere glove box system using AIBN as radical initiator at 50 °C for 3 days. The polymers were firstly precipitated into methanol and, when required, demonomerized into methanol or ethyl acetate/methanol mixtures. All the materials show good solubility in aromatic solvents such as toluene or chlorobenzene, as well as in halogenated solvents (e.g., chloroform or dichloromethane). The good solubility and film forming properties of the polymers allow for characterization and potential application as electron transport material into solution processed OLEDs.

## 3.2 Characterization

### 3.2.1 GPC and DSC

Gel permeation chromatography (GPC) was used to characterize polymers' molecular weights in tetrahydrofuran using polystyrene as standard. Number average molar mass ( $M_n$ ) of the series was determined to be in the range from 13.3 to 32.7 kg mol<sup>-1</sup> with a polydispersity index (PD) ranging from 1.56 (**P10**) to 4.13 (**P7**). The higher PD observed for **P7** is due to the bimodal distribution observed in the elogram, which could be related to chain transfer reactions during polymerization. Nevertheless, this process was not further investigated. The degree of polymerization (DP) ranges from 15 for **P10** to 53 for **P7**. The lower DP observed for **P10** is most likely related to the bulkiness of the side-chains.

Differential scanning calorimetry (DSC) measurements were performed to determine the thermal behaviour and  $T_g$ s of the series (Table 5, Figure 27). On one side, reference compound **P6** shows a  $T_g$  of 200 °C. Similarly, reference compound **P7** exhibits a glass transition of 202 °C. On the other side, the combination of the side-chain structures of polymers **P6** and **P7** simultaneously in polymer **P8** side-chain results in a  $T_g$  of 187 °C. This decrease is most probably caused by its lower DP, since the  $T_g$  is dependent of the molecular weight at low values, as described by Flory-Fox equation. For polymer **P9**, with a biphenyl structure as a connector to the polymer backbone, a glass transition of 214 °C is observed. This higher glass transition is most likely due to an increase in the rigidity of the side-chain when compared to

the other polymers. For polymer **P10** no clear  $T_g$  was observed in the range from 25 to 300 °C, which can be related to the low DP, hindering observation of a clear transition during DSC heating cycles. Detected  $T_g$ s are over 180 °C ensuring high thermal and morphological stability of the materials as thin films.

**Table 5.** Overview on analytical data of polymers **P6-P10**

Polymer	$M_n$ (kg mol <sup>-1</sup> ) <sup>a</sup>	$M_w$ (kg mol <sup>-1</sup> ) <sup>a</sup>	PD <sup>a</sup>	$T_g$ (°C) <sup>b</sup>	DP <sup>d</sup>
P6	16.3	40.2	2.47	200	44
P7	18.7	77.2	4.13	202	53
P8	15.6	46.3	2.96	187	25
P9	32.7	60.0	1.84	214	47
P10	13.3	20.8	1.56	n.d. <sup>c</sup>	15

<sup>a</sup>Determined from GPC. <sup>b</sup>Determined from DSC measurements. <sup>c</sup>not detected.

<sup>d</sup>DP =  $M_n/M_{\text{monomer}}$

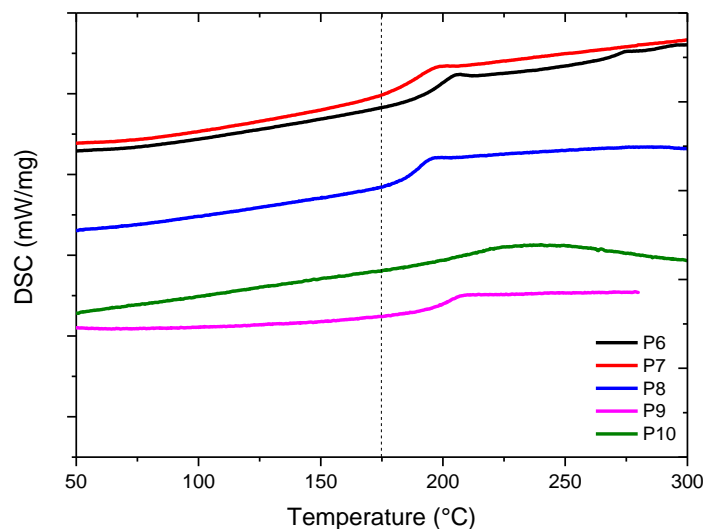


**Figure 27.** Differential-scanning calorimetry scans for polymers **P6-P10**. The 2<sup>nd</sup> heating cycles are displayed.

### 3.2.2 Theoretical calculations

Quantum chemical calculations were performed on the side-chain units of **P6-P10** at the B3LYP/6-31G\* level in order to highlight the relationship between the chemical structure and the location of the HOMO and LUMO within the series (Figure 28). According to DFT calculation results shown in Figure 28, reference compound **P6**, consisting of a tetraphenylsilane core attached to the polymer backbone exhibits a distribution of the LUMO through all the phenyl rings. For reference compound **P7**, LUMO is as well distributed through all aromatic rings of the triarylborane structure. Polymer **P8**, which combines both structures have LUMO and HOMO located in the triarylborane structure. Polymer **P9** with a biphenyl bridge between the polymer backbone and the side-chain locates the HOMO in the biphenyl motif, while the LUMO is distributed in the arylborane unit. For polymer **P10** HOMO is distributed along one triarylborane unit, while the LUMO is partially located within both triarylborane units. These observations might suggest that the disruption in the conjugation by the  $sp^3$  Si atom is not so effective when multiple arylborane units are attached to the tetraphenylsilane core allowing some extension of the conjugation through the C-Si-C bond, which could result in enhanced electron mobility and higher efficacy.<sup>109</sup>



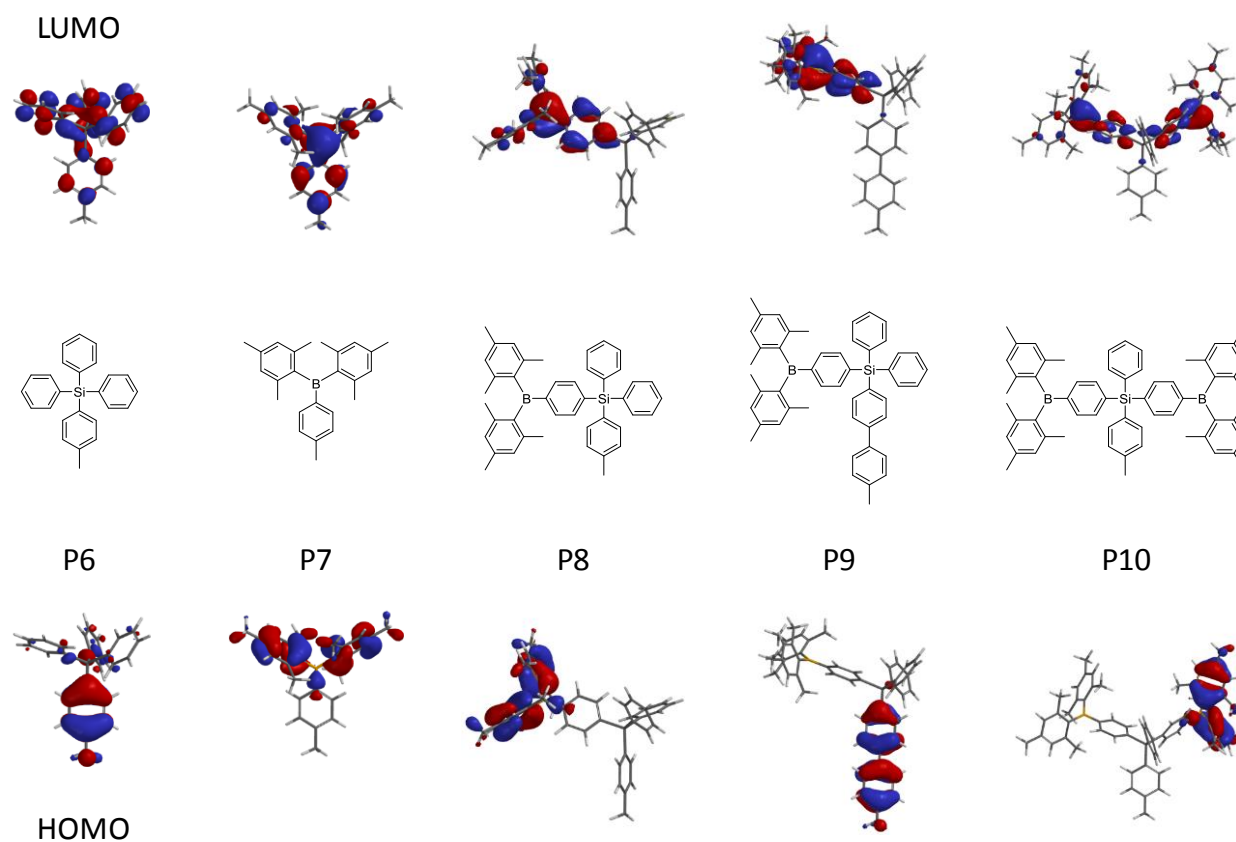


**Figure 28.** Calculated spatial distributions of the LUMO (top) and HOMO (bottom) of the corresponding **P6-P10** side-chains employing B3LYP/6-31G\* theoretical level.

### 3.2.3 Optical properties

The normalized optical absorption, photoluminescence (PL) and low temperature PL emission spectra of the series are shown in Figure 29. Table 6 summarizes the optical transitions extracted from the spectra. Absorption bands at around 270 and 330 nm can be observed for polymers **P7-P10**. This bands are directly related to  $n-\pi^*$  and  $\pi-\pi^*$  transitions of the arylborane moiety since they are not present for **P6**. An additional shoulder can be observed at around 230 nm which can be attributed to a  $n-\pi^*$  transition of phenyl. The optical bandgaps ( $E_g$ ) were determined from the onset of UV/vis spectra of solid films. For reference polymer **P6**, an  $E_g$  of 4.32 eV was measured, as expected from literature.<sup>58</sup> Polymers **P7-P10** show a bandgaps in the range from 3.52 to 3.40 eV.

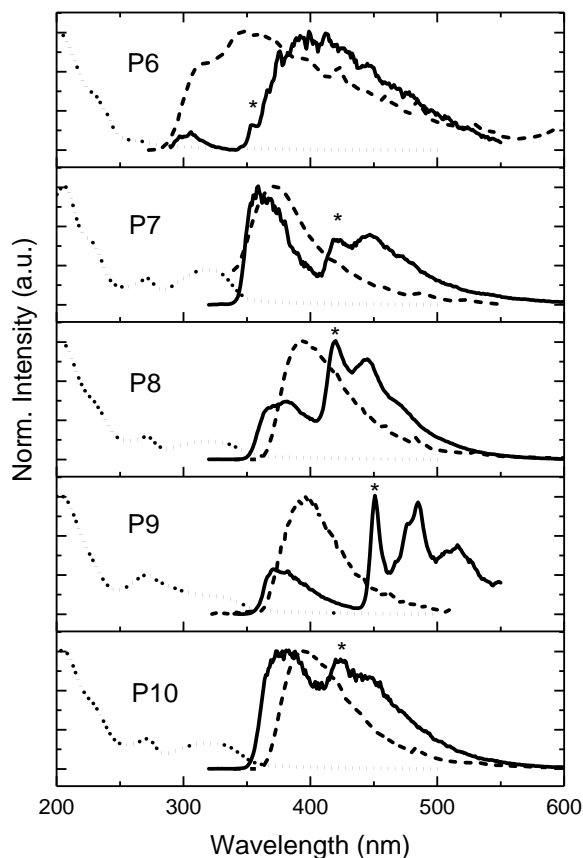


**Figure 29.** Normalized UV/vis (dot), emission (dash) and emission at 77 K (solid) for polymers **P6-P10**. \* Read out of triplet energy (peak).

The PL emission spectra were measured upon excitation at the respective  $\lambda_{\text{max}}$ . PL emission maximum ( $\lambda_{\text{em}}$ ) of reference compound **P7** is 372 nm. For polymers **P8-P10** a bathochromic shift is observed when tetraphenylsilane and  $\text{BMe}_2$  units are combined. This can be related to the higher electronegativity of silicon and slight delocalization through the silicon-carbon bond.

The triplet state was estimated from low-temperature PL emission spectra at 77 K in 2-methyltetrahydrofuran. Besides fluorescence, an additional low-energy tail with a well resolved vibrational structure is observed (marked with a '\*' in Figure 29) which is related to the phosphorescence of the sample. Read-out of the triplet energy was done from the highest energy peak (the 0-0 transition of the phosphorescence). Polymer **P6** has a high triplet energy of 3.30 eV as expected for this class of compounds.<sup>110</sup> Polymers **P7**, **P8** and **P10** show almost

identical triplet energy at around 2.9 eV. This similar value is determined by the localization of the triplet state in the triarylborane moiety. In the case of **P9**, the presence of a biphenyl results in a decrease in of the triplet energy, which has been observed in many other systems containing such unit.<sup>100</sup> Overall, the materials show high triplet energies to avoid charge transfer from excitons to the ETMs.

**Table 6.** Photophysical properties of polymers **P6-P10**

Polymer	$\lambda_{\text{max, abs}}$ (nm) <sup>a</sup>	$\lambda_{\text{em}}$ (nm) <sup>a</sup>	$E_{\text{g}}$ (eV) <sup>b</sup>	$E_{\text{T}}$ (eV) <sup>c</sup>
P6	232	347	4.32	3.30
P7	230, 271, 322	372	3.52	2.94
P8	231, 270, 326	394	3.45	2.95
P9	271, 334	396	3.40	2.75
P10	229, 272, 237	396	3.44	2.93

<sup>a</sup> Measured as thin film on quartz substrate. <sup>b</sup> Calculated from the onset of the absorption. <sup>c</sup> Determined from the emission spectra at 77 K.

### 3.2.4 Electrochemical properties

HOMO and LUMO energy level values were estimated from cyclic voltammetry (CV) studies with thin films on a glassy carbon electrode. An exemplary cyclic voltammogram of **P7** is shown in Figure 30. The corresponding values are compiled in Table 7. For reference compound **P6** no  $E_{\text{ox/red}}$  peaks were detected during the scans within the measuring range due to the high band gap of this kind of compounds.<sup>110</sup> HOMO levels of polymers **P7-P10** are in the range from -7.1 to -7.0 eV, suggesting good hole-blocking property. LUMO level of **P7** is estimated to be -2.7 eV. Polymers **P8-P10** show lower LUMOs in the range from -2.8 to -2.9 eV. In the case of **P7**, the triarylborane structure is connected directly to a  $sp^3$  carbon of the polymer backbone, while for the side-chain structures of **P8-P10** it is connected to a silicon atom. This slight difference in the can be related to the higher electronegativity of carbon than silicon resulting in a stabilization of LUMO level.

**Table 7.** Electrochemical properties of polymers **P6-P10**

Polymer	$E_{\text{ox, peak}}$ (V) <sup>a</sup>	HOMO (eV) <sup>b</sup>	$E_{\text{red, peak}}$ (V) <sup>a</sup>	LUMO (eV) <sup>b</sup>
P6	n.d.	n.d.	n.d.	n.d.
P7	2.3	-7.1	-2.1	-2.7
P8	2.2	-7.0	-1.9	-2.9
P9	2.3	-7.1	-2.1	-2.8
P10	2.2	-7.0	-2.0	-2.8

<sup>a</sup>Determined by cyclic voltammetry. <sup>b</sup>Cyclic voltammetry on-set potential against ferrocene standard.

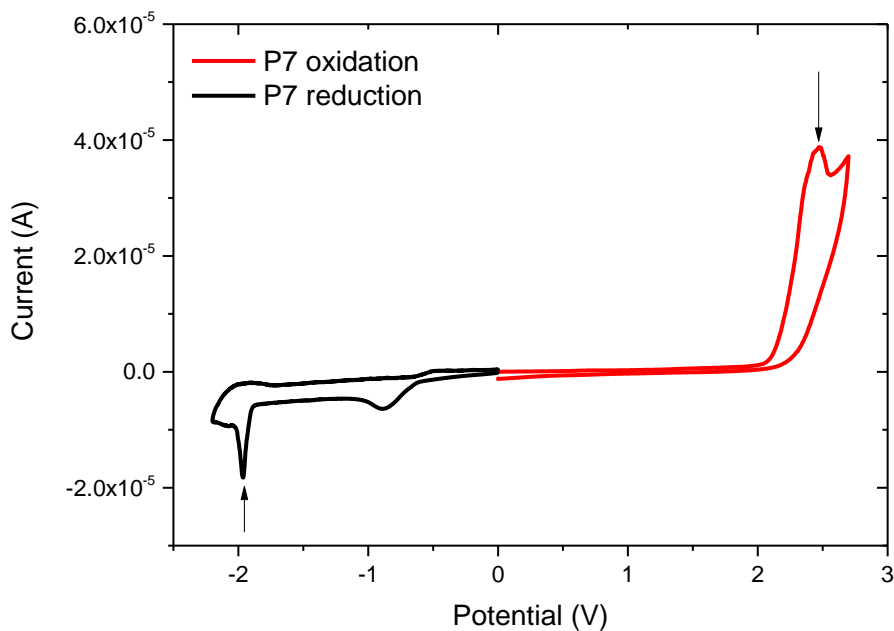


**Figure 30.** Exemplary cyclic voltammogram of polymer **P7**. The oxidation and reduction potential were taken from the onset of the corresponding peak.

### 3.2.5 Solution processed multilayer OLEDs

The polymers potential as electron-transport materials was investigated in optoelectronic devices. Polymers were used integrated in the emissive layer of green OLEDs (Figure 31a).

These devices consist of a bilayer structure of organic materials (HTL and EML) between the electrodes. While hole transport to the EML is provided by the HTL, electron transport and charge recombination occur simultaneously in the EML. Therefore, this layer is a multicomponent blend composed of an emitter, a host and an electron transport material.<sup>86</sup> In this devices it is required to shift the recombination zone from the cathode vicinity because otherwise it could result in exciton quenching. Thus, an electron transport material with high electron mobility it is crucial to achieve high current efficiencies, as well as the optimization of the components mixing ratio and layer thickness.

The devices were fabricated by subsequent solution deposition of the organic layers by spin-coating. After deposition of PEDOT:PSS and HIL-12, the stack was thermally cured at 180 °C for 30 minutes rendering a very thin surface of insoluble HIL-12 on top of PEDOT:PSS. This strategy allows next layer deposition avoiding redissolution problems of the underlying layer. The components of the emissive layer blend are a green emitter (TEG01) a host material (co-host) and the electron transport polymers **P7-P10** (TEG01/co-host/**P7-P10** in a weight ratio of 0.5:2:1) dissolved in toluene (Figure 31c). This layer is about 95 nm thick and has been annealed at 180 °C for 30 minutes in order to remove residual solvent. Except the ITO anode and the evaporated Ba/Ag cathode, these multilayer devices are fully solution processed. Figure 31d depicts the current density-voltage and luminance-voltage characteristic of representative OLED samples. Due to the good film forming properties of the materials used, the OLEDs exhibit diode behaviour with very low leakage currents at negative voltages. Very similar device characteristics are observed for polymers **P7- P10**. This is in agreement with the similar electrochemical properties (Table 7) and LUMO distributions (Figure 28). Rather high current efficacies are achieved. We attribute these values to the high triplet energies and deep HOMO levels. **P10** has a slightly higher on-set voltage of the current density and luminance than the rest of the series. Since it does not obviously correlate with the electrochemical properties in Table 7, we might hypothesize that the higher voltages are related to a slightly

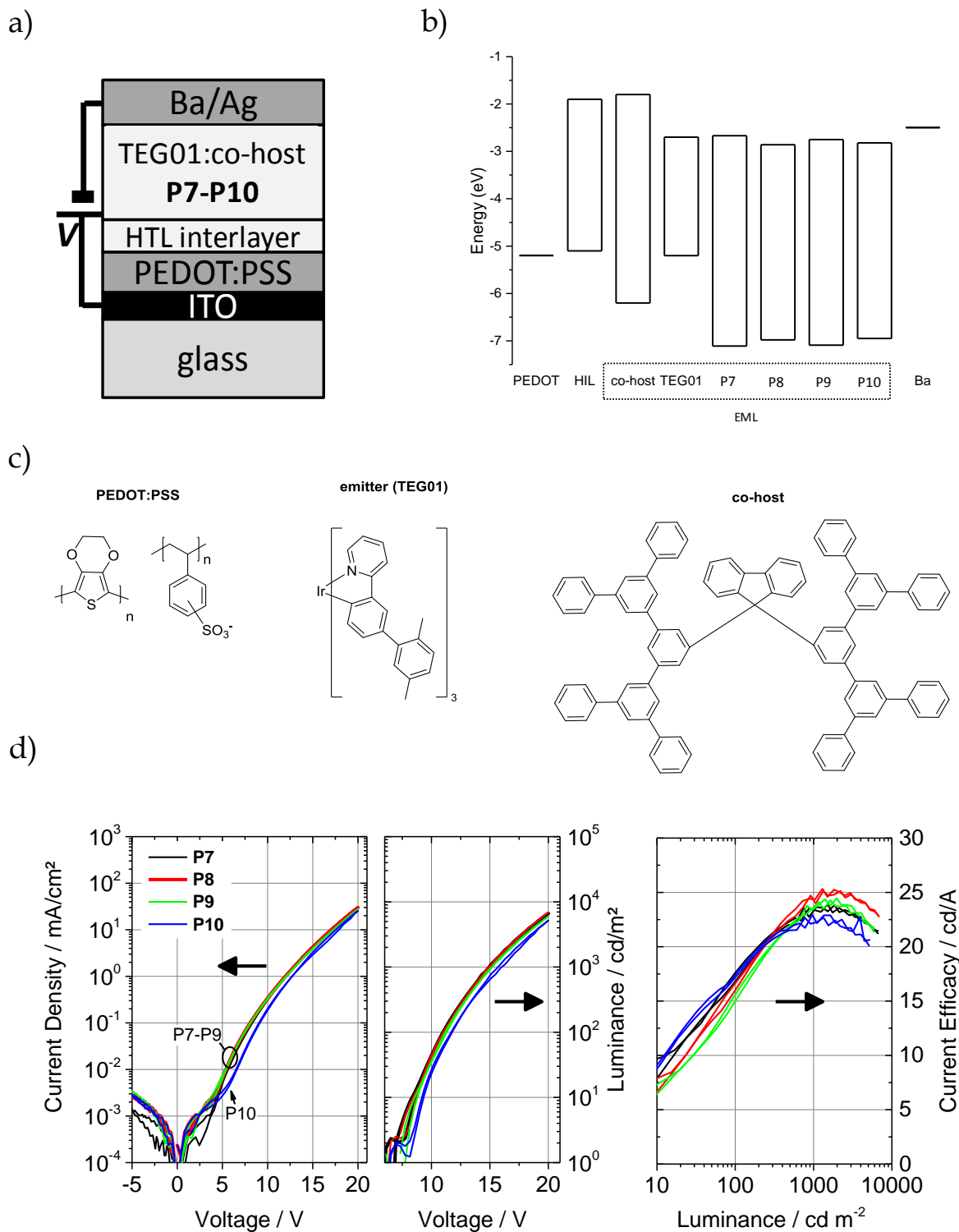


**Figure 31.** a) Device structure, b) energy level diagrams and c) chemical structures of additional OLED materials. d) Current-density and luminance characteristics of multilayer OLEDs with P7-P10 as ETMs.

lower electron mobility. This, in turn, might be related to the different location of the LUMO of **P10**, as seen in Figure 28. The high current efficiencies observed ranging from 22.8 to 25.3 cd/A (Table 8) are most likely to the good hole blocking properties due to the deep HOMOs and high triplet energies ( $> 2.7$  eV) of the series.

**Table 8.** Physical parameters of the OLEDs with polymers **P6-P10** as electron transport material in combination with co-host and TEG001 (1:2:0.5)

Polymer	Current on-set voltage (V) <sup>a</sup>	Luminance on-set voltage (V) <sup>b</sup>	Max. current efficacy (cd/A) <sup>c</sup>
P6*	-	-	-
P7	5.7	8.2	23.8 (1535 cd/m <sup>2</sup> )
P8	5.3	8.3	25.3 (1356 cd/m <sup>2</sup> )
P9	5.3	8.6	24.4 (1951 cd/m <sup>2</sup> )
P10	6.6	9.2	22.8 (1395 cd/m <sup>2</sup> )

<sup>a</sup> At 10<sup>-2</sup> mA/cm<sup>2</sup>, forward sweep. <sup>b</sup> At 10 cd/m<sup>2</sup>, forward sweep. <sup>c</sup> According luminance is denoted in brackets. \* no ET properties expected.

### 3.3 Conclusions

A series of polystyrenes containing either triarylborane-derivatives, tetraphenylsilane or both motives combined was synthesized. The motifs were incorporated as side-chain onto polystyrene backbones by free-radical polymerization of the corresponding functionalized polystyrenes. High  $T_g$ s up to 214 °C and no additional thermal processes were detected by following the polymer approach, ensuring materials high thermal stability. Additionally, polymers show good solubility in common organic solvents, such as halogenated and aromatics, rendering typical glassy films upon spin-coating.

The molecular design of the side-chains led to high triplet energy for electron transport materials in the range of 2.75 to 2.95 eV, which allows for potential application in a wide-range of emitter classes. Lower  $E_T$  is obtained when biphenyl unit is included in the side-chains (**P9**), while higher  $E_T$  is achieved when this motif is not present (**P7**, **P8**, **P10**). Furthermore, the introduction of several  $\text{BMes}_2$  units has a negligible influence in  $E_T$  (**P10**). The utilization of tetraphenylsilane and dimesitylborane lead to materials with wide band gaps, with very deep HOMO levels around -7.0 eV.

The polymers with expected electron transport properties (**P7-P10**) were tested in green Ir-based devices. All the materials show similar current efficacies around 24 cd/A at 1000 cd/m<sup>2</sup> luminance, independently of the modifications in the side-chain structure. This observation suggests that the electron mobility of the polymers it is determined by the  $\text{BMes}_2$  motif (**P7-P10**) and that the tetraphenylsilane core plays a negligible effect in the polymers transport properties. Furthermore, the similar performance of **P8** and **P10** suggests that no significant delocalization occurred through the Si atom and no effect on the transport properties was achieved, as conversely suggested by the DFT calculations.

In conclusion, the materials are good candidates for application into solution processed devices and for application as ETM the more synthetic feasible polymer (**P7**) could be used. Additionally, the effective disruption of the conjugation among the  $\text{BMes}_2$  units through the Si atom indicates that this core could be further used, for instance with electron-rich groups, to develop ambipolar host materials.





## 4. Orthogonal solution processable electron transport layers

Application of the HTL and EML of OLEDs from solutions in multilayer OLEDs has been successfully established by the use of cross-linkable HTLs and applied in Chapter 2.<sup>88</sup> A natural step to continue device fabrication (i.e., by deposition of the ETL) via solution-processing would be to crosslink the emission layer materials; however, this approach requires laborious efforts, because the emission layer does normally consist of at least two materials (host and emitter) and the modification of established emitter materials is often not feasible. Consistently, there are only few reported examples of efficient OLEDs with crosslinked emission layer.<sup>111,112</sup>

A different approach involves the use of orthogonal solvents (e.g. toluene and ethanol) to deposit organic layers consecutively without “harming” the underlying layers.<sup>113</sup> In this context, two classes of materials can be used. On the one side, small molecules such as 1,3,5-tris(4-phenylquinolin-2-yl)benzene (TQB) which can be dissolved into formic acid/water mixtures<sup>77</sup> or 1,3,5-tris(1-phenyl-1H-benzo[d]imidazol-2-yl)benzene (TPBi) and [1,1':3',1''-terphenyl]-4,4''-diylbis(diphenylphosphine oxide) (BPOPB), which have been reported to show solubilities up to 7 g/L in methanol.<sup>83</sup> However, the achievement of homogeneous films is difficult and recrystallization easily occurs after curing the thin layers. On the other side, polymers which provide homogenous and morphologically stable films are of big interest and can also show solubility into alcohols. That is the case of conjugated polyfluorenes with amine functionalized aliphatic side-chains. Quaternization of the amine with counter ions (e.g. Cl<sup>-</sup> or I<sup>-</sup>)<sup>75</sup> or sultones (e.g., 1,3-propane sultone)<sup>76</sup> renders alcohol soluble polymers. However, the ionic groups in such polyelectrolytes can result in undesired electrochemical effects and reduce the air-stability of high work function electrodes such as Al.<sup>77,114</sup> Conversely, Sax et al. attached neutral aliphatic chains such as ethylene glycol providing alcohol soluble materials whose optoelectronic properties are slightly affected.<sup>114</sup> However, the presence of long alkyl chains results in a large decrease of the glass transition temperature of the materials,<sup>88</sup> which results in detrimental effects for morphological stability and life time of the devices. A much more attractive approach involves the combination of small molecules and polymers. Lithium quinolate (Liq) has been shown to provide excellent injection properties and is soluble into alcohols.<sup>115</sup> However, since Liq shows poor film forming properties. Chiba et al. combined poly-

vinylpyridines and poly-vinylphenylpyridines with Liq to create homogeneous films, since these polymers are also soluble into alcohols.<sup>116</sup> These structures are summarized in Figure 32.

As discussed in Chapter 3, besides the required solubility in orthogonal processable organic solvents the materials used in electron transport layers should meet the following requirements: i) deep HOMO to prevent the flow of holes from reaching the cathode without recombination in the EML, ii) high triplet energy to confine the triplet excitons within the EML, iii) high electron mobility and iv) high  $T_g$ s to ensure thermal and morphological stability. Kido et al. demonstrated that dendritic phenylpyridines can meet this requirements effectively by the rational combination of pyridine and phenyl rings.<sup>46,51,117</sup>

In this chapter we aim the development of electron transport materials based on phenylpyridines which fulfil the general requirements of ETMs and can be applied orthogonally from solution.

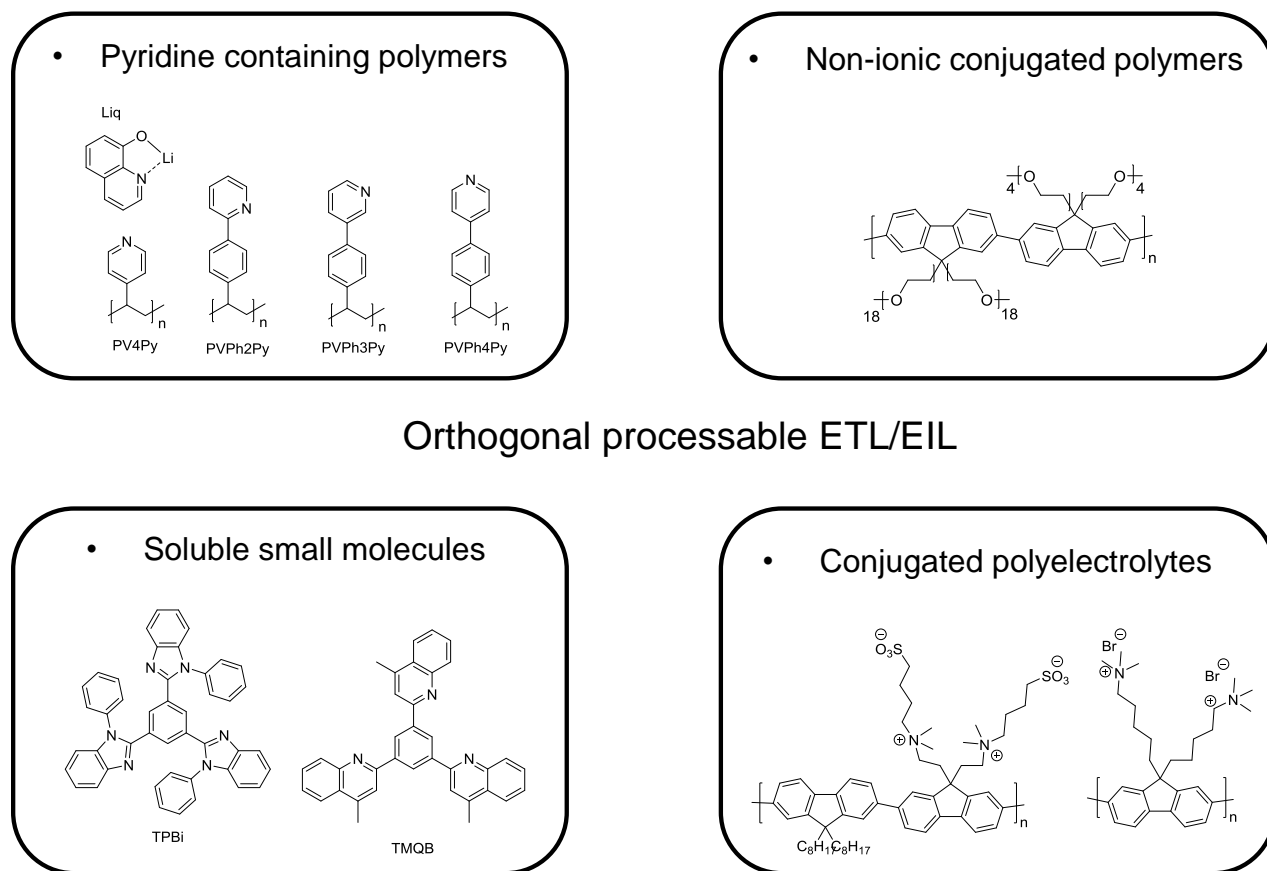


**Figure 32.** Overview of different examples of orthogonal processable electron transport layers.

## 4.1 Choice of materials

A strategy previously used by Kido et al. in the development of electron transport materials was adapted to develop a series of materials with suitable optoelectronic properties. In this strategy, *meta*-terphenyl (mTP, Figure 33) is used as a central core due to its high triplet energy ( $\approx 2.8$  eV).<sup>30</sup> Functionalization in the periphery with pyridines as electron-deficient heterocycle improves the ability to stabilize negative charges and therefore promote charge transport. Two widely used small molecules in vacuum-processed devices designed with this strategy are 1,3,5-tri(*p*-pyrid-3-yl-phenyl)benzene (TpPyPB) and 1,3,5-tri(*m*-pyrid-3-yl-phenyl)benzene (TmPyPB, Figure 33).<sup>117</sup> Both structures feature electron mobility around  $1 \times 10^{-3} \text{ cm}^2 \text{ V}^{-1} \text{ s}^{-1}$ , which is several orders of magnitude higher than other conventional ETMs such as bathophenanthroline (BPhen) or aluminium-tris(8-hydroxyquinolin) ( $\text{Alq}_3$ ). Concretely, TpPyPB shows higher electron mobility than TmPyPB due to its planer structure and more delocalized  $\pi$ -conjugation, which induce an easier electron hopping among adjacent molecules.<sup>94</sup> Additionally, hydrogen-bonding interactions also provide an additional channel for charge transport since it increases the interactions between the molecules.<sup>46,94,118</sup> The molecules are incorporated as side-chains into polymer backbones by substituting one of the arms by a terminal alkene function.

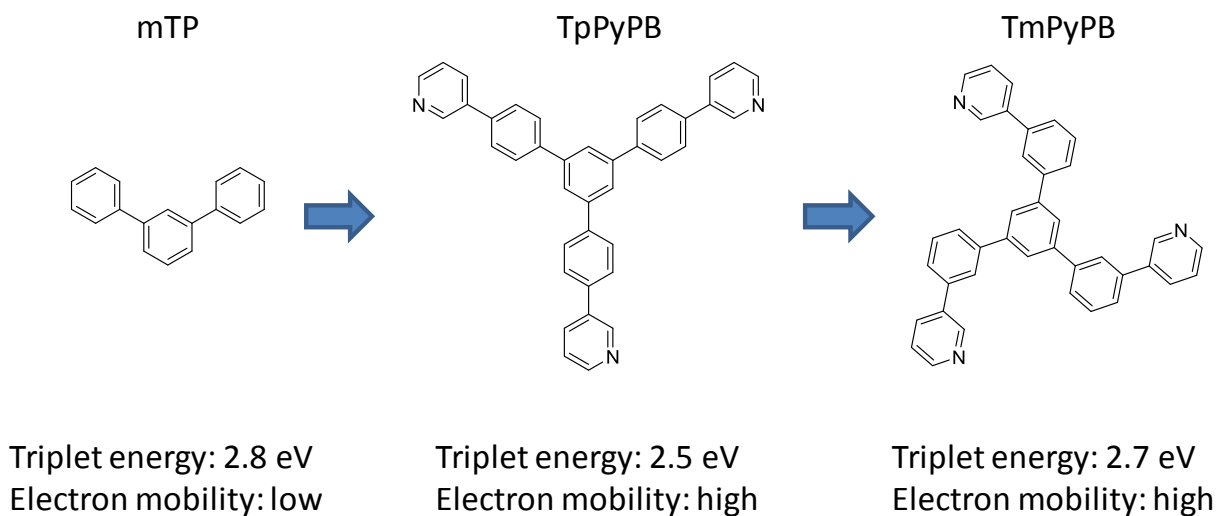
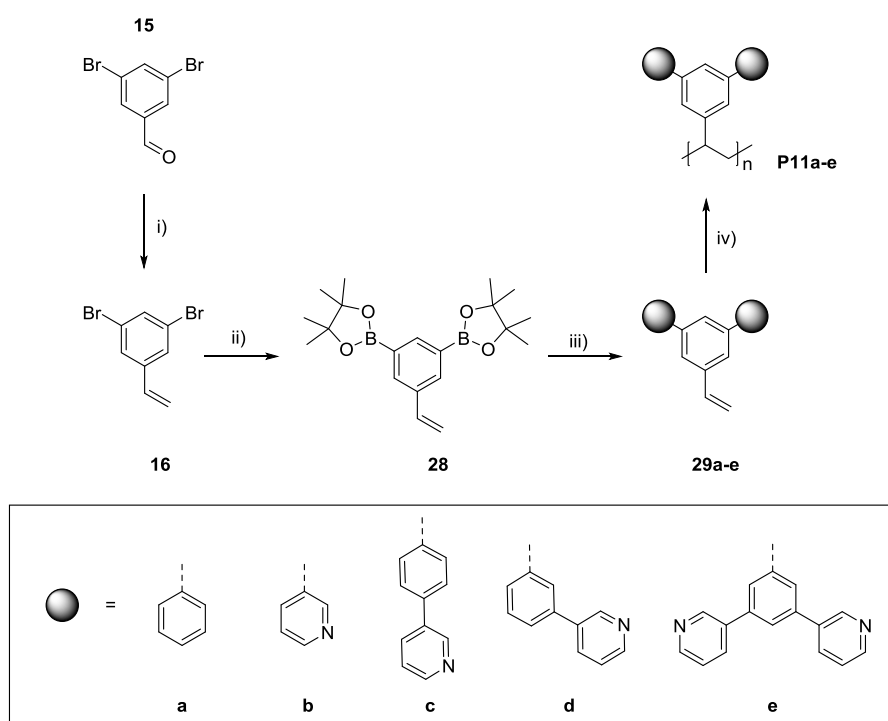


**Figure 33.** 1,3,5-Tri(*p*-pyrid-3-yl-phenyl)benzene (TpPyPB) and 1,3,5-tri(*m*-pyridin-3-ylphenyl)benzene (TmPyPB) by Kido et al. for high triplet ETMs.<sup>117</sup>

## 4.2 Synthesis

Monomers were synthesized by a three-step route depicted in Scheme 5. The alkene function was firstly introduced by Wittig reaction using 3,5-dibromobenzaldehyde **15** and MePPh<sub>3</sub>Br, giving **16** in good yields. Subsequent cross-coupling reaction of **16** with bis(pinacolato)diboron, catalyzed by bis(diphenyl-phosphino)ferrocene dichloropalladium (Pd(dppf)Cl<sub>2</sub>), yield the styryl diboronic ester **28**. The last step in monomer synthesis was realized by the Suzuki cross-coupling of the precursor **28** with the corresponding aryl- or pyridyl-bromide giving **29a-e** from good to moderate yields.



**Scheme 5.** Synthesis of polymers **P11a-e**. *Reagents and conditions:* i) MePPh<sub>3</sub>Br, *t*-BuOK, THF, 2h, 0 °C, 65% **16**. ii) Bis(pinacolato)diboron, Pd(dppf)Cl<sub>2</sub> · CH<sub>2</sub>Cl<sub>2</sub>, KOAc, 1,4-dioxane, 80 °C, 53% **28**. iii) Pd(PPh<sub>3</sub>)<sub>4</sub>, K<sub>2</sub>CO<sub>3</sub>, arylbromide **a-e** (bromobenzene **a**, 3-bromopyridine **b**, 3-(4-bromophenyl)pyridine **c**, 3-(3-bromophenyl)pyridine **d**, 3,3'-(5-bromo-1,3-phenylene)dipyridine **e**, Toluene:EtOH:H<sub>2</sub>O, reflux, 40-85%, **29a-e**. iv) AIBN, THF, 50 °C, 72 h, 55-83%, **P11a-e**.

Polymers **P11a-e** were synthesized by free radical polymerization (Scheme 5). The reaction was conducted in a N<sub>2</sub> atmosphere glove box system using AIBN as radical initiator. Polymerization of monomers **P11a-d** was realized in THF. . Reaction conditions were settled at 50 °C for 3 days.

Due to the low solubility of monomer **29b** and **29e** in THF, these polymerizations were realized in DMF. Polymers were quenched with methanol and demonomerized by repeated precipitation into methanol, ethyl acetate/ heptane mixtures, or ethyl acetate.

### 4.3 Characterization

#### 4.3.1 Solubility

All polymers show good solubility in halogenated solvents, e.g., chloroform or dichloromethane. Furthermore, polymers **P11b** and **P11e** (Figure 34), with a relative pyridine content ( $RPC = n_{\text{pyridines}} / [n_{\text{pyridines}} + n_{\text{phenyl}}]$ ) of 0.66 and 0.57 respectively, show good solubility in methanol. One of the main variations through the series is the relative amount of phenyl and pyridyl rings incorporated into the side-chains. This observation suggests that, due to the increase of CH-N hydrogen-bond interactions in solution, polymers **P11b** and **P11e** turn soluble into methanol (up to 7 g/L). During the series synthesis, monomers purification required chloroform/methanol mixtures, which also suggest strong hydrogen-bonding interactions between the monomers and the SiO structure of the stationary phase.<sup>119</sup> On the other side, recent studies on polymers with high relative pyridine content such as **PV4Py** and **PVph3Py** in the side-chains (1 and 0.5, respectively) show also solubility into alcohols.<sup>116</sup> Adversely, polymers **P11c** and **P11d** (with 0.4 as RPC, Figure 34) precipitate into methanol. These observations allow us establishing an empirical relation where if the relative pyridine content is  $\geq 0.5$  solubility into methanol is expected (Figure 35).

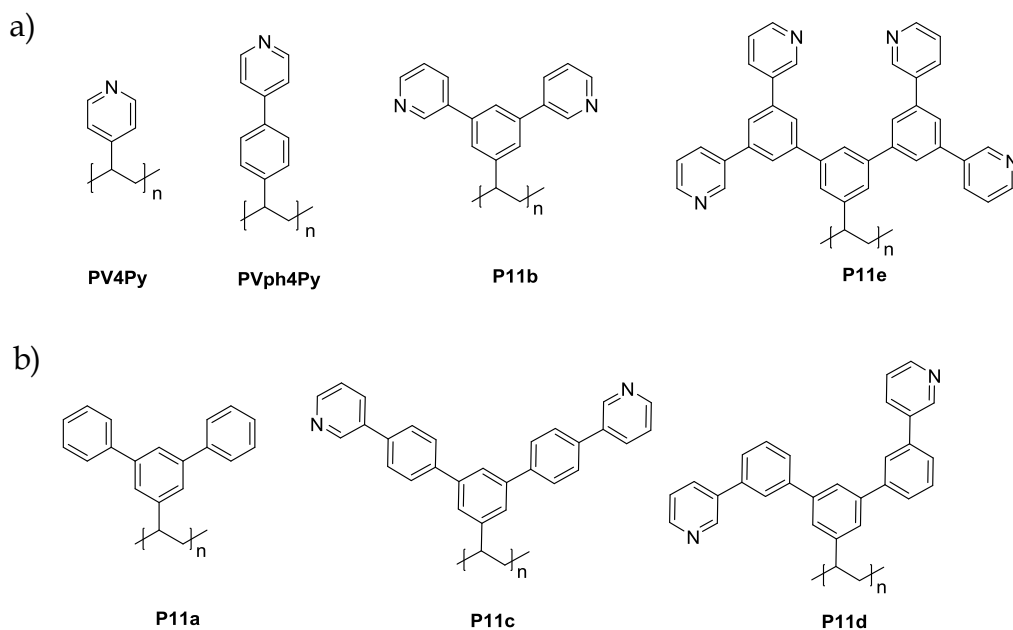


**Figure 34.** a) Methanol soluble pyridine-containing polymers with relative pyridine content  $\geq 0.5$ . b) Non-methanol soluble polymers.

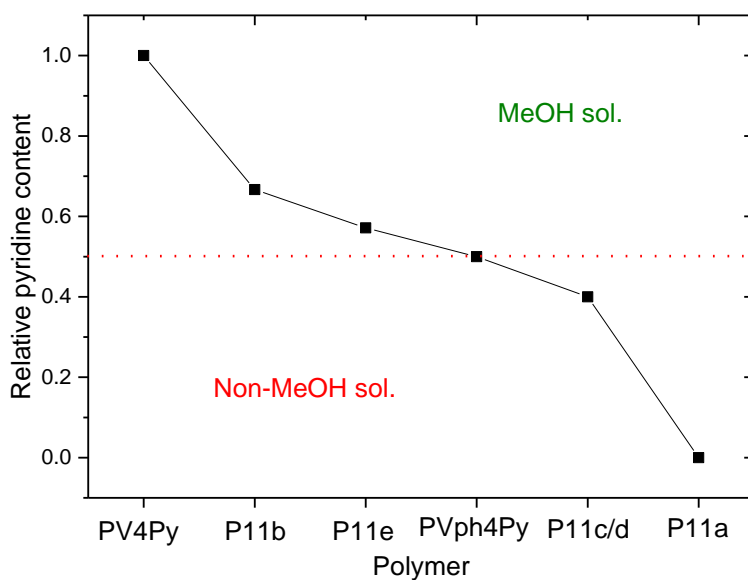


**Figure 35.** Methanol solubility of different pyridine- and phenylpyridine-based side-chain polymers. Those with a RPC  $\geq 0.5$  can be dissolved in methanol.

### 4.3.2 GPC and DSC

Gel permeation chromatography (GPC) was used to characterize polymers' molecular weights. Nevertheless, when THF was used as elution solvent for pyridine containing polymers (**P11b-P11e**) no elution of the polymers was observed. As an alternative, polymers were dissolved in chloroform and chloroform with 4% trimethylamine (TMA) was used as eluent using polystyrene as standard (Table 9). The distributions detected may not correspond to the coil conformation as a result of the strong N-H interactions. Number average molar masses ( $M_n$ ) of **P11a-e** were determined to be in the range from 17.6 to 48.8 kg mol<sup>-1</sup> with a polydispersity index (PD) ranging from 2.50 to 7.39. The higher PD observed for **P11e** and **P11d** are related to a bimodal distribution, which may be associated to chain-transfer reaction during polymerization. However, this process was not further studied. DPs corresponding to the polymers range from 42 for **P11d** to 140 for **P11a**.

**Table 9.** GPC and thermal properties of polymers **P11a-e**

Polymer	$M_n$ (kg mol <sup>-1</sup> ) <sup>a</sup>	$M_w$ (kg mol <sup>-1</sup> ) <sup>a</sup>	PD <sup>a</sup>	$T_g$ (°C) <sup>b</sup>	DP <sup>c</sup>
P11a	36.1	90.1	2.50	161	140
P11b	21.5	50.8	2.36	192	83
P11c	48.8	280.8	5.75	241	118
P11d	17.6	133.7	7.59	136	42
P11e	48.1	355.6	7.39	247	85

<sup>a</sup>Determined from GPC measured in CHCl<sub>3</sub> with 4% TMA. <sup>b</sup>Determined from DSC measurements. <sup>c</sup>DP =  $M_n/M_{\text{monomer}}$

Differential scanning calorimetry (DSC) measurements were performed to determine the thermal behaviour and  $T_g$ s of the series (Table 9, Figure 36). Polymer **P11a**, synthesized as a reference polymer, shows a glass transition at 161 °C. **P11b** with pyridines incorporated into the



framework of mTP has a  $T_g$  of 192 °C. This could be related to an increase in the polarity of the side-chain moiety and thus stronger molecular interactions. These stronger N-H interactions are similarly observed when comparing boiling points of benzene (80 °C) and pyridine (115 °C). **P11c** and **P11e** show a  $T_g$  of 241 and 247 °C, respectively. This can be attributed to the bulkiness and planarity of the side-chains, which require more space, leading to a more rigid polymer backbone. Comparatively, **P11d** has higher rotational freedom which results in lower rigidity in the side-chains and therefore a lower  $T_g$  of 136 °C is observed. Observed  $T_g$ s for the series are in a suitable range to ensure thermal and morphological stability during OLEDs operation.

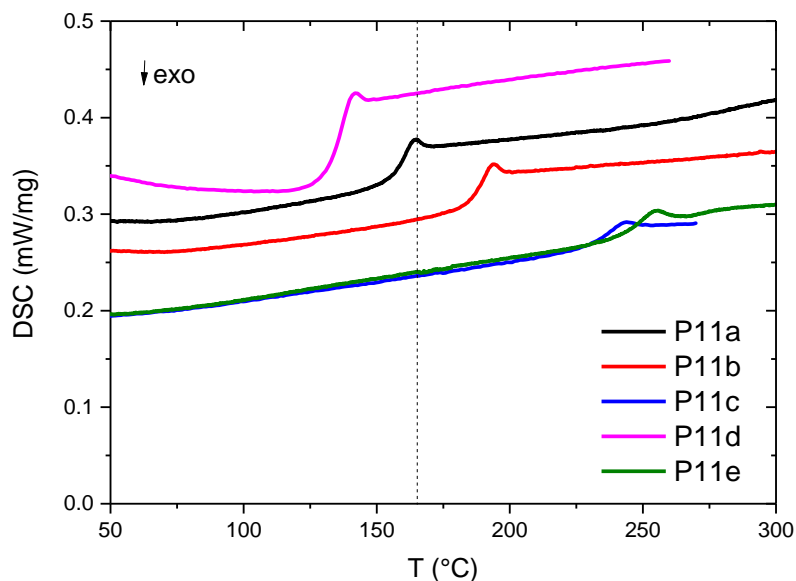


**Figure 36.** Differential-scanning calorimetry scans for polymers **P11a-e**. The 2<sup>nd</sup> heating cycles are displayed.

### 4.3.3 Theoretical calculations

Quantum chemical calculations were performed on the side-chain units of **P11a-e** at the B3LYP/6-31G\* level in order to examine the relationship between the chemical structure and the location of the HOMO and LUMO within the series. According to DFT calculation results shown in Figure 37, HOMO levels are mainly located on the central mTP core. In the case of **P11c** some delocalization is also observed on the pyridines due to the para linkage. Reference

polymer **P11a** and **P11b** exhibit their LUMO located as well in the mTP core. Differently, polymers **P11c-e**, with a larger molecular structure, show their LUMOs predominantly located in the phenylpyridyl arms. This is most likely to the higher electron affinity of the pyridyl substituents. Overall, among the polymer series higher electron mobility can be expected for those side-chains with a largely delocalized LUMO.<sup>94</sup>

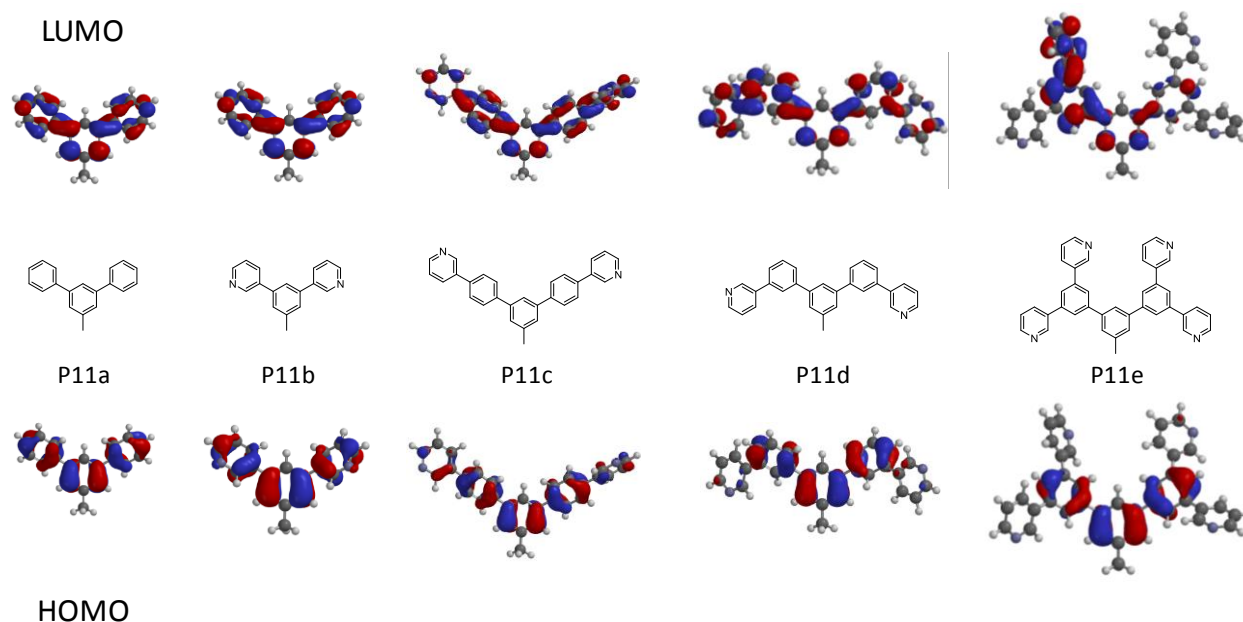


**Figure 37.** Calculated spatial distributions of the LUMO (top) and HOMO (bottom) of the corresponding **P11a-e** side-chains employing B3LYP/6-31G\* theoretical level.

#### 4.3.4 Optical properties

The normalized optical absorption and photoluminescence (PL) spectra of polymers **P11a-e** are shown in **Figure 38**. Table 10 summarizes the optical transitions extracted from the spectra. Reference polymer **P11a** exhibits a major intense band ( $\lambda_{\max}$ ) at 253 nm originating from  $\pi$ - $\pi^*$  transition. **P11b**, **P11d** and **P11e** exhibit similar absorption bands at 248, 253 and 257 nm, respectively. This can be attributed to the confinement of the conjugation within the mTP unit, despite the introduction of pyridines in *meta*-position.<sup>94</sup> Comparatively, **P11c** with pyridines connected in the *para*-position of mTP, show a highly red shifted absorption band at 293 nm due to the extended conjugation in the polymer side-chain. From the low energy onset of the absorption bands, the optical energy gaps were found to be in the range from 3.61 to 4.18 eV.

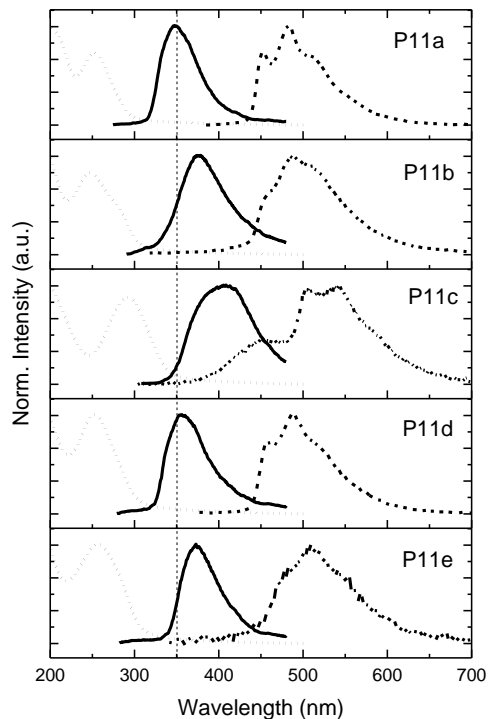


**Figure 38.** UV-vis (point) and PL emission (solid) low-temperature phosphorescence (dash) spectra of polymers **P11a-e**. The read out of the triplet energy was taken from the onset of the low-temperature phosphorescence.

The PL emission spectra were measured upon excitation at the respective  $\lambda_{\text{max}}$ . PL emission maximum ( $\lambda_{\text{em}}$ ) of reference compound **P11a** is observed at 347 nm. **P11d** shows a small difference in  $\lambda_{\text{em}}$  (353 nm), which indicates that the extension of the conjugation is minimized by insertion of pyridines in the *meta*-position. The slight red shift observed could be due to electron withdrawing inductive effect of pyridine. **P11b** and **P11e** show similar emission maximum at 371 and 373 nm, respectively. This suggest that the emission could be generated form the 1,3-di(pyridin-3-yl)benzene moiety instead of the mTP core. In the case of **P11c**, a strong bathochromic shift up to 406 nm is observed due to a higher conjugation in the side-chain moiety.

Low-temperature phosphorescence spectra recorded for delay time of 30 ms were used to determine polymers  $E_{\text{T}}$ . Reference polymer **P11a** shows an  $E_{\text{T}}$  of 2.83 eV. This value is in a good

agreement with the  $E_T$  of mTP.<sup>120</sup> Incorporation of pyridine in its frame work (**P11b**) or in *meta*-position (**P11d** and **P11e**) results in triplet energies of 2.84, 2.82 and 2.78 eV, respectively. These results suggest that conjugation is not further delocalized within the side-chains and therefore such high  $E_T$  can be obtained. On the other side, polymer **P11c** showed lower  $E_T$  value (2.62 eV), which is consistent with red-shift of absorption and PL spectra and confirms elongated conjugation of side-chains.

**Table 10.** Photophysical properties of polymers **P11a-e**

Polymer	$\lambda_{\max, \text{abs}}$ (nm) <sup>a</sup>	$\lambda_{\text{em}}$ (nm) <sup>a</sup>	$E_g$ (eV) <sup>b</sup>	$E_T$ (eV) <sup>c</sup>
P11a	253	347	4.18	2.83
P11b	248	371	4.00	2.84
P11c	293	406	3.61	2.62
P11d	253	353	3.76	2.82
P11e	257	373	3.96	2.78

<sup>a</sup> Measured as thin films over quartz substrates. <sup>b</sup> Calculated from the onset of the absorption. <sup>c</sup> Calculated from the onset of the phosphorescence spectra.

#### 4.3.5 Electrochemical properties

HOMO and LUMO level values were investigated by cyclic voltammetry (CV) studies with thin films on a glassy carbon electrode. Photoelectron spectroscopy in air (PESA) was not a suitable method for HOMOs determination due to the deep values expected for the polymers ( $\leq -6.2$  eV).<sup>46,94</sup>

All polymers exhibited irreversible reduction and oxidation waves. Read-out of oxidation and reduction potentials ( $E_{\text{red/ox}}$ ) was taken from the peak of the respective wave (marked with an arrow in Figure 39). HOMO level of reference compound **P11a** was estimated to be -6.8 eV. The introduction of pyridines results in lower-lying HOMOs in the range of -7.3 eV to -7.1 eV for **P11b-e**, indicating improved hole blocking properties.

LUMO level of polymer **P11b** was estimated to be -2.6 eV. For polymers **P11c**, **P11d** and **P11e** LUMO levels of -2.7 eV were estimated. This could be related to a larger LUMO distribution in the side-chains.<sup>121,122</sup>

**Table 11.** Oxidation/reduction peaks and HOMO/LUMO estimation for polymers **P11a-e**

Poylmer	$E_{\text{ox, peak}}$ (V) <sup>a</sup>	HOMO (eV) <sup>b</sup>	$E_{\text{red, peak}}$ (V) <sup>a</sup>	LUMO (eV) <sup>b</sup>
P11a	2.0	-6.8	-2.0	-2.8
P11b	2.5	-7.3	-2.2	-2.6
P11c	2.4	-7.2	-2.1	-2.7
P11d	2.4	-7.2	-2.1	-2.7
P11e	2.3	-7.1	-2.1	-2.7

<sup>a</sup> Determined by cyclic voltammetry. <sup>b</sup> Cyclic voltammetry peak potential against ferrocene standard.

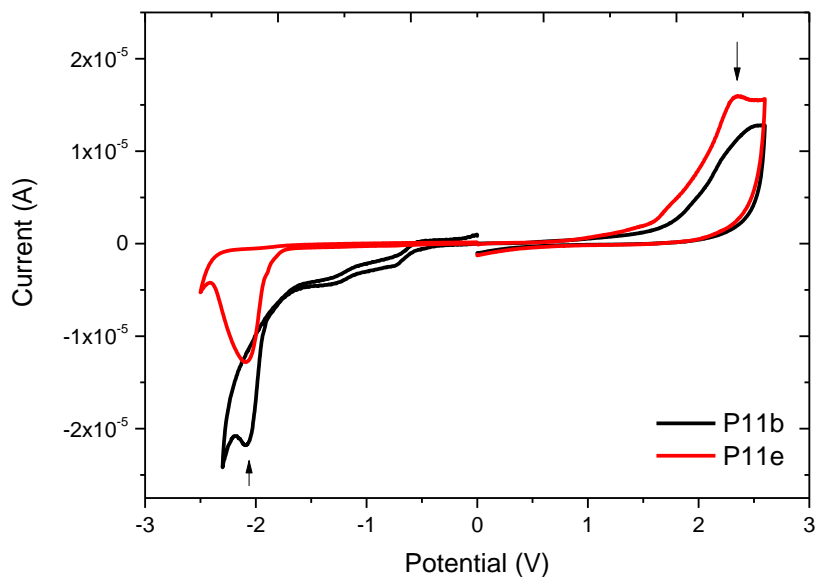


**Figure 39.** Oxidation and reduction cycles of methanol soluble polymers **P11b** and **P11e**. The arrow points the read-out of the peak potential.

### 4.3.6 Solution processed devices

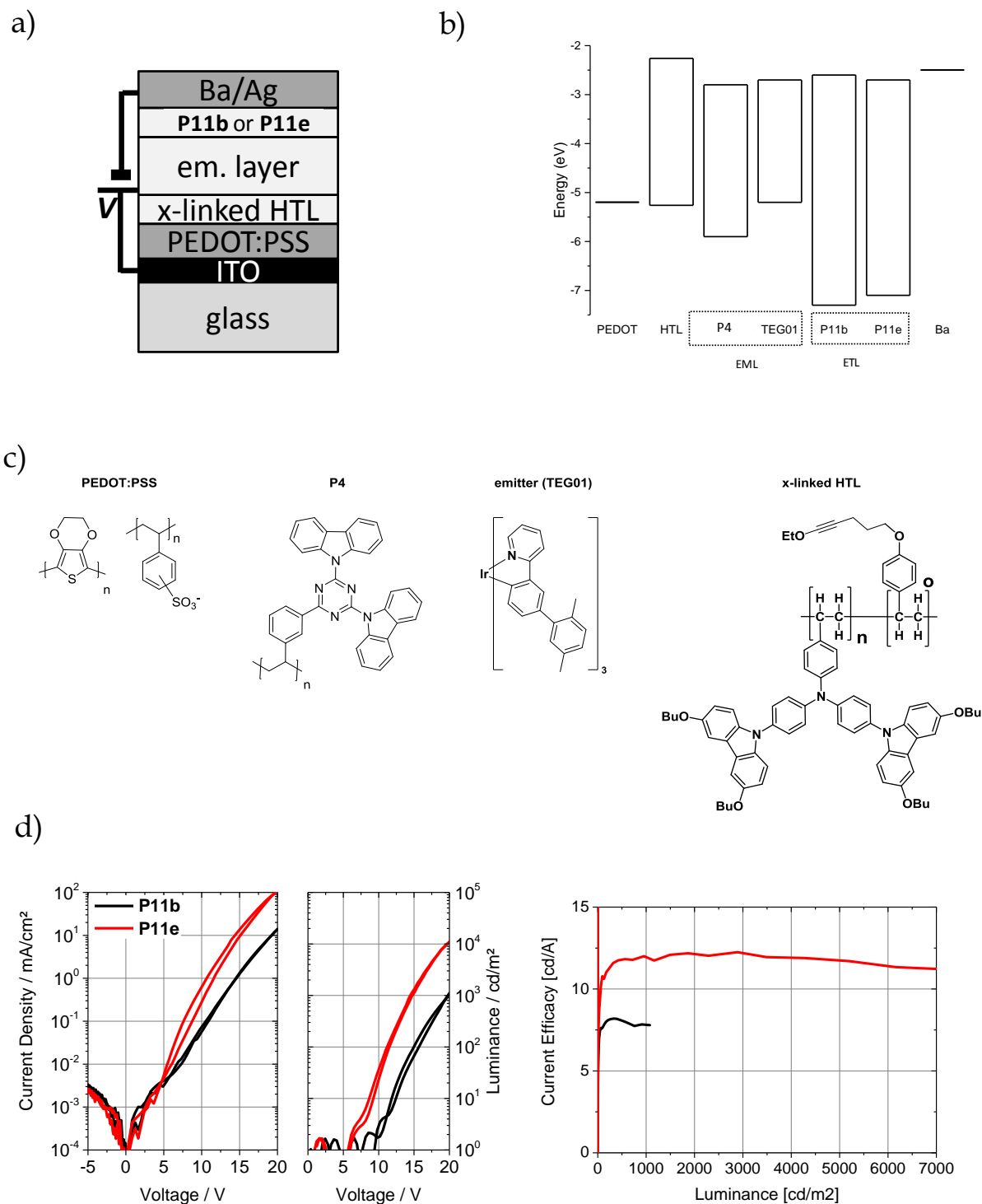
Polymers **P11b** and **P11e** are identified to be suitable for orthogonal processing from methanol on top of an emission layer. In order to demonstrate this application, we fabricated multilayer OLEDs similar to those presented in Chapter 2, and are showed in Figure 40a.<sup>123</sup> In short, HTL, emission layer, and ETL were prepared on a glass/ITO/PEDOT:PSS substrate by subsequent spin-coating. The HTL consists of a hole transporting side-chain polymer, poly-(3,6-(BuO)<sub>4</sub>TCTA),<sup>88</sup> which has been equipped with cross-linker groups for thermal curing. The emission layer is composed of a polymer host with [9,9'-(6-(3-vinylphenyl)-1,3,5-triazine-2,4-diyl)bis(9H-carbazole)] as side-chains (**P4**, described in Chapter 2) and the green emitting Ir-complex TEG001,<sup>103</sup> which have been deposited from a blend solution in chlorobenzene. In the present devices, the ETL is prepared by spin-coating from 5 g/l solutions of polymer **P11b** or **P11e** in methanol. The layer thicknesses were 30 and 40 nm, respectively. Ba and Ag were thermally evaporated to complete the device and to form 9 mm<sup>2</sup>-sized pixels.

Figure 40d displays representative current density- and luminance-voltage characteristics of these OLEDs and Table 12 denotes the on-set voltages and maximum current efficacies. We achieve moderate current efficacies around 10 cd/A and luminance on-set voltages around 10 V with both ETL polymers, which could be related to the high triplet energies and deep HOMO levels. In detail, we observe higher current density and luminance for the devices with polymer **P11e** as ETL. We relate this to improved electron transport in the ETL as compared to devices with polymer **P11b**, due to the higher delocalization of **P11e** LUMO.

**Table 12.** Physical parameters of the OLEDs with polymers **P11b** and **P11e** as ETL material

Polymer	Current on-set voltage (V) <sup>a</sup>	Luminance on-set voltage (V) <sup>b</sup>	Max. current efficacy (cd/A) <sup>c</sup>
P11b	7.3	11.8	8.2 (330 cd/m <sup>2</sup> )
P11e	6.1	9.3	12.2 (2900 cd/m <sup>2</sup> )

<sup>a</sup>at 10<sup>-2</sup> mA/cm<sup>2</sup>, forward sweep. <sup>b</sup>at 10 cd/m<sup>2</sup>, forward sweep. <sup>c</sup>According luminance is denoted in brackets .



**Figure 40.** a) Device structure consisting of a glass substrate, ITO anode, PEDOT:PSS, crosslinked HTL, EML, **P11b** or **P11e** and Ag/Ba cathode. b) Energy diagram of the different compounds molecular orbitals. c) Additional structures of the materials used for the device fabrication. d) Current density-voltage and luminance-voltage characteristics of representative OLEDs.

## 4.4 Conclusions

A series of electron transport polymers based on phenylpyridines was synthesized. Free radical polymerization was used to incorporate the moieties as side-chain in polystyrene backbones. High  $T_g$ s were obtained by following the polymer approach, while high triplet energies were achieved for those polymers which connect their side-chain aromatic rings through meta-linkages. It was observed that the solubility changes drastically upon changing relative pyridine content within the side-chains. While polymers containing an equal or higher RPC-ratio of 0.5 are soluble into methanol (**P11b** and **P11e**), those with a lower content remain insoluble (**P11a**, **P11c**, **P11d**).

Polymers soluble in methanol were tested in green three-layered full solution processed OLEDs. High current efficiencies are obtained due to the materials deep HOMO and high  $E_T$ . A higher delocalization of the LUMO features a higher current efficacy for polymer **P11e**.<sup>124</sup> High driven voltages in the polymers were observed. The reason could be that due to a hindrance of the molecular interactions within electron transport moieties, such as  $\pi$ - $\pi$  stacking and hydrogen bonds,<sup>27</sup> due to the attachment of the side-chains to the inert polymer backbone. These interactions have been proved to effectively enhance electron transport in related molecular compounds.<sup>122</sup> Nevertheless, conversely to other methanol soluble polymers, **P11b** and **P11e** can work as ETL without the combination of additional small molecules as dopants to enhance electron injection.<sup>113</sup>

In conclusion, the introduction of sufficient pyridines units combined with our side-chain approach is a promising strategy for further development of solution processable electron transport materials which do not require an underlying crosslinked EML. These early all-solution processed three-layered devices show as well, a high potential for further improvement of their performances.



## 5. Summary

Charge transport materials crucially determine the efficacy achievable in OLED devices. They decrease energy barriers between the electrodes and the emissive layer, lowering driving voltages. They also prevent from exciton quenching during OLED operation, either at the electrodes or by energy transfer reactions, enhancing the amount of light generated respect to the excitons formed. Therefore, in the pursuit of fabricating OLEDs approaching the efficacy theoretical limits, charge transport materials well adapted to the emitter's requirements are highly demanded.

Addressed to this purpose many efforts have been done by the scientific community to explore organic materials with semiconducting properties. Extensive libraries and catalogues with many different molecular motives have been studied and applied into OLEDs, providing high performance devices. Among all applicable organic materials into OLEDs, electron-rich and electron-poor *N*-heterocycles, such as triarylmines and pyridines, provide an excellent compromise in terms of device lifetime and performance.

Most of these small molecules are thought to be applied by vacuum deposition techniques. Such techniques allow for fabrication of complex multilayer structures with precisely controlled thicknesses. Optimization of devices by these methods leads to the highest efficient OLEDs at this time. However, these techniques require large amounts of product because during evaporation most of the materials are lost at the deposition chambers. Furthermore, it can result in a slow and tedious process when many layers are involved, due to the time required to achieve high vacuum. These drawbacks increase production costs and limit large scale production of OLEDs. As alternative, printing techniques provide better materials use, since deposition can be done precisely (e.g. ink-jet printing), and simplify the manufacture process.

However, these relatively low molecular weight small molecules cannot always be applied from solutions. They tend to crystallize during the evaporation and curing processes, resulting in inhomogeneous films. Therefore, they require structural modifications. In this doctoral thesis, this problem was addressed and circumvented by increase of small molecules molecular weight. A straightforward strategy to rapidly increase molecular weights of small molecules is

to incorporate them as side-chains in inert polystyrene backbones. In this approach, charge transport small molecules are modified to be converted into styrene derivatives and subsequently polymerized by free-radical polymerization. This leads to high molecular weight materials with increased thermal stability, when compared with the respective small molecules. Furthermore, due to the non-conjugated nature of polystyrene, the optoelectronic properties of the adapted small molecules stay mainly constant.

In this context, new solution processable host polymers were developed. Side-chain polystyrenes were used as ambipolar host materials in the EML of phosphorescent OLEDs. To feature hosts requirements, the molecules must incorporate electron-rich and electron-poor heterocycles in the same molecular structure to be able to transport electron and holes. Therefore, the side-chain chemical structures consist of carbazole, pyridine and triazine as heterocycles. The design of the side-chains was based in more extensive literature reports and just the best candidates were adapted into solution processable materials. The application of the polymer approach lead to increased thermal stability, illustrated in the high  $T_g$ s of the series ( $> 211$  °C). The optoelectronic properties, e.g. triplet energy, remained almost identical to that of the corresponding small molecules, confirming the suitability of the polymer approach. Upon application into green Ir-based devices, observations indicate that the materials' performance is highly dependent on the balance between electron and hole transport properties in the EML. The electron transport character was gradually increased by incorporating electron-poor heterocycles and extending the conjugation with phenyl bridges. A current efficacy increase over 10-fold was achieved when comparing **P1** and **P4** (28.9 cd/A for **P4**). Polymer **P4** resulted in the series optimal ambipolar host. No further increase in current efficacy was possible for the last polymer of the series (**P5**) due to its low triplet energy (2.52 eV).

In the second part the focus was on the development of electron-only transport materials applied in a blended EML of green Ir-based phosphorescent OLEDs. The molecular motives studied are dimesitylborane and tetraphenylsilane. Triarylboranes have attracted much attention in the last years due to boron  $sp^2$  hybridization and its vacant p-orbital. They possess high triplet energy, similar to that of triaryl amines, but conversely are able to transport electrons due to its electropositive nature. Polymers show high thermal stability, reflected in their high  $T_g$ s ( $> 187$  °C). Dimesitylborane performance was evaluated as independent side-

chain (**P7**) and in combination with a tetraphenylsilane core (**P8-P10**). The combination of these two motives was in pursuit of enhancing the electron transport mobility when several dimesitylborane units were incorporated in the side-chain (**P10**). However, all polymers show almost identical performances (around 24 cd/A). This indicates that no delocalization occurs through the silicon atom and that the electron transport properties are therefore determined by a single dimesitylborane unit. Nevertheless, high triplet energy materials were obtained, ranging from 2.71 to 2.95 eV.

Another trend addressed in this work was the solution deposition of ETLs separately from the EML. Many current solution-processed devices combine solution process of HTL and EML with vacuum deposition of ETLs. This is mainly due to re-dissolution problems occurring when ETLs with similar solubility to the underlying layer are applied from solutions. Although this combination is a significant step forward in order to decrease fabrication costs of OLEDs it is still not ideal. Significant efforts have been attempted to insolubilize organic transport layers, for instance HTL and EML, by the use of crosslinking techniques which render solution stable layers. However, modification of the charge transport layers and emitters is not always feasible, and the application of high curing temperatures to achieve full cross-link can result in layer morphology defects. Therefore, we focused on the development of orthogonally processable materials which allow deposition of ETLs without applying high curing temperatures. Orthogonal strategies base on the insolubility of the underlying layer in the solvent used to process the upcoming layer.

Chapter 4 presents the products developed in this direction. The small molecules are adapted from dendritic phenylpyridines, which are among the best electron transport materials for vacuum-processed devices to date. The polymer approach provides highly thermal stable materials ( $137\text{ }^{\circ}\text{C} < T_g < 247\text{ }^{\circ}\text{C}$ ) and triplet energies analogue to the corresponding small molecules. Methanol solubility, which would allow materials orthogonal processing, was not observed for all the polymer series. Nevertheless, we found that solubility into methanol is possible for those polymers with a relative pyridine content (RPC)  $\geq 0.5$  (**P11b** and **P11e**). This behaviour was already known for lower molecular side-chains, such as in poly-vinylpyridines and poly-vinylphenylpyridines. However, these polymers show no adequate electron transport ability in OLEDs. Therefore, these polymers were doped with electron transporting small

molecules such as Liq. Such blends were used as electron transport layers in full solution processed OLEDs. Contrarily, it was possible to apply polymers **P11b** and **P11e** without additional doping showing moderate efficacies in early devices. This seems to be a first example of standalone application of side-chain polystyrenes as electron transport materials by orthogonal deposition.

## 6. Outlook

The research presented within this work provides knowledge in order to further develop charge transport materials for solution processed OLEDs.

Concerning the series of ambipolar host developed in Chapter 2, the primary strategy was conducted up to the end. Nevertheless, the last product of the series shows low triplet energy. This is insufficient to avoid exciton quenching and therefore features a lower current efficacy. New products should focus in achieving higher triplet energies while providing a balanced ambipolar charge transport. A new series of materials could use similar *N*-heterocycles but explore a different connectivity within the electron-rich and electron-poor motifs, for instance situating carbazole as the central unit and modifying the periphery with electron-deficient groups.

Chapter 3 materials performance revealed a significant result concerning the devices performance. Current efficacy was independent from the number of triarylborane units due to the disruption of the conjugation through the silicon bond. An interesting group of products which could result in better electron transport properties should most likely incorporate a central  $sp^2$ -hybridized atom. For instance, the use of boron instead of silicon could provide an extended delocalization of the LUMO, better electron transport properties while retaining a high triplet energy.

The materials developed in Chapter 4 possess an interesting property, which has not been widely reported in the literature. That is the solubility into methanol of high molecular weight side-chains when incorporated into polystyrene. The materials show limited electron transport properties, however substitution of the central phenyl ring by a more electron-poor heterocycle could significantly increase the electron transport of such polymers. Functionalization retaining a  $RPC \geq 0.5$  could result in new series of orthogonal processable electron transport layers.

In conclusion, a further step in the development of all solution processed OLEDs has been presented within this work, which contributes to further development of semiconductor materials for optoelectronic applications.

## 7. Experimental

### 7.1 Methods

#### 7.1.1 Characterization

Thin layer chromatography (TLC) was done with POLYGRAM SIL G/UV254 TLC-plates.

High-resolution  $^1\text{H}$  NMR (500 MHz) and  $^{13}\text{C}$  NMR (125 MHz) spectra were recorded on a UNITY INOVA 500 spectrometer from Varian at room temperature.

Thermal analysis of 3-10 mg per polymer sample was performed with differential scanning calorimetry (DSC) using a Netzsch DSC 204 Phoenix with a scanning rate of  $10\text{ K min}^{-1}$ . The glass transition was obtained from the inflexion point (maximum of the first derivative of the heating curve) of the second heating cycles.

Photoelectron spectroscopy on air (PESA) was performed using a Riken Keiki AC-2 at a power of 50 nW. Investigated polymer layers were prepared by drop-casting onto glass substrates. All measurements were carried out at least three times and the read-out was done from curves onset.

UV/Vis and photoluminescence (PL) spectra: About 30 nm thick films were spun from toluene solutions (concentrations  $5\text{ g L}^{-1}$ , 1000 rpm) onto silica glass substrates. Absorption was measured using a Cary 5000 UV/Vis spectrometer. Photoluminescence spectra were recorded on a Perkin Elmer LS50B spectrometer. Low temperature phosphorescence spectra of **P1-P10** were made with a HORIBA Fluoromax system. The excitation wavelength was set to the absorption maximum. The measurements were performed in nitrogen cooled 2-Me-THF solutions with a concentration of  $0.01\text{ g L}^{-1}$ . Low temperature phosphorescence spectra of **P11a-e** in chloroform were measured in closed-cycle helium cryostat at 170 K temperature by utilizing the time-gated intensified CCD camera iStar (Andor). As an excitation source was used a picosecond laser EKSPLA PL2140 YAG:Nd $^{3+}$  (25ps, 266 nm).

Density Functional Theory (DFT): All quantum chemical calculations were performed using the Spartan program package. Geometry optimization was performed using the B3LYP functional with the 6-31G\* basis set.

Size exclusion chromatography (SEC) has been performed at 25 °C in THF for polymers **P1-P10** and at 30 °C in chloroform with 4% trimethylamine for polymers **P11a-e** to determine the molecular weights using a combination of Separation module 2695e (Waters), Dual  $\lambda$  Absorbance Detector 2487, and Refractive Index Detector 2414. A SEC-column set with 5  $\mu\text{m}$  high crosslinked porous polystyrene-divinylbenzene matrix from Waters (7.8 mm  $\times$  300 mm; Styragel Guard column, HR3, HR4, HR5) for separation and narrowly distributed, linear polystyrene standards from Agilent Polymer Laboratories (Varian) for weight determination were used. Polymer solutions (2 mg mL<sup>-1</sup> in THF for **P1-P10** and in chloroform for **P11a-e**) were stirred for 24 h at 22 °C and filtered (1  $\mu\text{m}$  PTFE) before 2  $\times$  100  $\mu\text{L}$  of the solution were injected. Molecular weights were calculated with the Empower software from Waters.

Cyclic voltammetry (CV) measurements: cyclovoltammograms were obtained with an EG&G Parc model 273 potentiostat. A three electrode configuration was used in an undivided cell from RHD Instruments GmbH, which consisted of a glassy carbon electrode (3 mm diameter) onto which the polymer film was deposited, a platinum crucible as the counter electrode with a maximum capacity of 1.6 mL, and a pseudoreference type "Ag" electrode. 0.1 M Bu<sub>4</sub>NBF<sub>4</sub> in acetonitrile was used as electrolyte and prior to each measurement the electrochemical cell has been deoxygenated with argon. The electrochemical cell was calibrated by the use of a ferrocene standard (-4.4 eV against standard hydrogen electrode when the read-out was taken from the onset and -4.8 eV when the read-out was taken from the peak)<sup>125-127</sup> and the ferrocene half-wave potential has been determined to be 611 mV for polymers **P1-P5** assembly, 574 mV for polymers **P6-P10** assembly, and 606 mV for polymers **P11a-P11e** assembly. 1 wt% polymer solutions in CHCl<sub>3</sub> were prepared and 5  $\mu\text{L}$  were deposited on the glassy carbon electrodes. The prepared electrodes were kept under vacuum and dried at 60 °C for 2 hours. The oxidation potential was determined from the on-set potential for **P1-P5**, and by the peak potential for **P6-P10** and **P11a-e** of measured polymer films. The corresponding HOMO energies are obtained from Equation 1 and Equation 2.

$$E_{\text{Fc/Fc}^+}^{\text{red/oxX}}(\text{Polymer}) = -\left(E_{\text{Ag/AgCl}}^{\text{red/ox}}(\text{Polymer}) - E_{1/2}(\text{Ferrocene})\right) \text{V} \quad \text{Equation 1}$$

$$E^{\text{HOMO}}(\text{Polymer}) = -\left(4.8 + E_{\text{Fc/Fc}^+}^{\text{red/ox}}(\text{Polymer})\right) \text{eV} \quad \text{Equation 2}$$

## 7.1.2 Device fabrication and characterization

### General

Glass substrates with an ITO pattern (Xin Yan Technology Ltd., 15 Ohm/sq ITO sheet resistance) were thoroughly cleaned by ultrasonification in diluted Mucosol™ detergent, deionized water, acetone, and isopropanol. The substrates were treated with oxygen plasma at low pressure in a microwave plasma chamber (Diener Femto) for 10 min at 80 W. A 50-nm-thick layer of PEDOT:PSS (Clevios™ P VP AI4083) was spin-coated under ambient conditions. All further preparation steps and the measurements were done in the N<sub>2</sub>-filled glovebox. The PEDOT:PSS layer was dried at 180 °C for 10 min.

### Devices fabrication Chapter 2

A 20-nm-thick hole transport layer of poly-(3,6-(BuO)<sub>4</sub>TCTA) equipped with cross-linkable comonomers was spin-coated from toluene solution over the PEDOT:PSS layer. Solvent stability of this layer was achieved by thermal curing at 185 °C for 5 min. The emission layer has been spin-coated from 14 g L<sup>-1</sup> blend solutions of the polymer **P1-P5** and the green phosphorescent emitter TEG001 (86:14 polymer:emitter weight ratio) in chlorobenzene. After this, the sample underwent heating at 180 °C for 30 min. The thickness of the emission layer was ca. 45 nm, as has been determined by profilometry (DEKTAK 150). The electron transport layer was spin-coated from a solution of an alcohol-soluble fluorene co-polymer in isopropanol. This layer was ca. 20 nm thick. The cathode was formed by high-vacuum thermal evaporation of 7 nm Ba and 100 nm Ag at 0.4 Å s<sup>-1</sup> and 5 Å s<sup>-1</sup>, respectively.

### Device fabrication Chapter 3



Spin-coating of a HIL-12 layer from 5 g/l in toluene. Heating for 30 min at 180°C renders a very thin surface layer of HIL-12 on PEDOT:PSS insoluble (interlayer approach). Spin-coating of the TEG01:co-host:**P7-P10** emission layer from a blend 20 g/l solution in toluene with materials' weight ratio of 0.5:2:1. Heating at 180°C for 30 min. This layer was about 95 nm thick. The cathode was formed by high-vacuum thermal evaporation of 5 nm Ba and 100 nm Ag.

#### **Devices fabrication Chapter 4**

A 20-nm-thick hole transport layer of poly-(3,6-(BuO)<sub>4</sub>TCTA) equipped with cross-linkable comonomers was spin-coated from toluene solution. Solvent stability of this layer was achieved by thermal curing at 185 °C for 5 min. The emission layer has been spin-coated from 14 g L<sup>-1</sup> blend solutions of polymer **P4** and the green phosphorescent emitter TEG001 (86:14 polymer:emitter weight ratio) in chlorobenzene. After this, the sample underwent heating at 180 °C for 30 min. The thickness of the emission layer was ca. 45 nm, as has been determined by profilometry (DEKTAK 150). The electron transport layers were spin-coated from 5 g/L solutions of **P11b** and **P11e** in methanol with layer thickness of 30 and 40 nm, respectively. The cathode was formed by high-vacuum thermal evaporation of 7 nm Ba and 100 nm Ag at 0.4 Å s<sup>-1</sup> and 3 Å s<sup>-1</sup>, respectively.

#### **Devices characterization**

ITO and cathode patterns define an active pixel area of 9 mm<sup>2</sup> and 6 pixels per substrate. Current-voltage and luminance characteristics were recorded using a Keithley 2636A dual source meter and a Gigahertz integrating sphere assembly with a photosensor with photooptic correction.

## 7.2 Synthesis

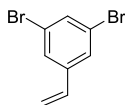
### 7.2.1 Materials

All materials were obtained from Sigma-Aldrich (Munich, Germany), Acros Organics (Geel, Belgium), Lumtec (Taiwan), TCI Deutschland GmbH, Alfa Aesar®, Th. Geyer GmbH & Co. KG, Fischer Scientific Deutschland or Synthon Chemical GmbH (Wolfen, Germany) and used without any further purification unless otherwise stated. The green emitter TEG01 was provided by Merck KGaA (Darmstadt, Germany). Silica gel 60 (Merck, Darmstadt, Germany) was used in the separation and purification of compounds by column chromatography. Separations with column chromatography were obtained using a TELEDYNE ISCO CombiFlash Rf system. Solvents for column chromatography, recrystallization, and purification were received from Th. Geyer GmbH (Berlin, Germany) and J. T. Baker (Deventer, Netherlands). Dry solvents were received from Sigma-Aldrich, stored over molecular sieve and sealed under an inert atmosphere. All reactions were done in inert atmosphere (argon or nitrogen) by using common Schlenk techniques.

## Chapter 2

**General:** Intermediates 9-(3-(4,4,5,5-tetramethyl-1,3,2-dioxaborolan-2-yl)phenyl)-9H-carbazole **8**<sup>117</sup> and 9,9'-(6-chloro-1,3,5-triazine-2,4-diyl)bis(9H-carbazole) **12a**<sup>97</sup> were synthesized by previously reported procedures.

### 7.2.2 1,3-Dibromo-5-vinylbenzene (2)

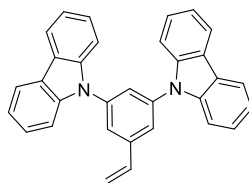


A mixture of potassium *tert*-butoxide (2.77 g, 24.7 mmol) and methyltriphenylphosphonium bromide (8.17 g, 22.9 mmol) was suspended in *anhydrous* tetrahydrofuran (50 mL). The reaction mixture was cooled to 0 °C and stirred for 0.5 hours. 3,5-Dibromobenzaldehyde **1** (4.00 g, 15.2 mmol) was dissolved in tetrahydrofuran (25 mL), added dropwise to the mixture and stirred for 1.5 hours at room temperature. After completion of the reaction, the mixture was poured into water. After evaporation of tetrahydrofuran, the aqueous phase was extracted with dichloromethane. The combined organic phases were dried over MgSO<sub>4</sub>. The crude was

purified with silica gel column chromatography using heptane as eluent giving **2** as clear oil. Yield: 2.65 g (65%).<sup>85</sup>

<sup>1</sup>H NMR (500 MHz, CDCl<sub>3</sub>, δ): 7.54 (t, J = 1.6 Hz, 1H), 7.46 (d, J = 1.6 Hz, 2H), 6.57 (dd, J = 17.5, 10.9 Hz, 1H), 5.76 (d, J = 17.5 Hz, 1H), 5.35 (d, J = 10.9 Hz, 1H). <sup>13</sup>C NMR (126 MHz, CDCl<sub>3</sub>, δ): 141.12, 134.40, 133.13, 128.11, 123.23, 117.02.

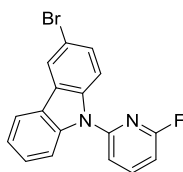
### 7.2.3 9,9'-(5-Vinyl-1,3-phenylene)bis(9H-carbazole) (**3**)



A mixture of 1,3-dibromo-5-vinylbenzene **2** (1.93 g, 7.4 mmol), carbazole (2.71 g, 16.2 mmol), sodium *tert*-butoxide (1.70 g, 17.7 mmol) tris(dibenzylideneacetone)-dipalladium(0) (0.14 g, 0.15 mmol) and tri-*tert*-butylphosphine (0.02 g, 0.11 mmol) was dissolved in *anhydrous* toluene (50 mL). The reaction mixture was heated to 110 °C for 4 hours. After completion of the reaction, the mixture was cooled to room temperature and acidified with HCl 2 M (50 mL). Phase separation was followed by extraction with dichloromethane. The combined organic phases were dried over MgSO<sub>4</sub>. The crude was purified with silica gel column chromatography using heptane/toluene (gradient) as eluent. Recrystallization with tetrahydrofuran/ethanol mixture gave **3** as a white solid. Yield: 0.85 g (26%).<sup>128</sup>

<sup>1</sup>H NMR (500 MHz, CDCl<sub>3</sub>, δ): 8.17 (m, 4H), 7.74 (d, J = 2.0, 2H), 7.72 (t, J = 2.0, 1H), 7.56 (dt, J = 8.3, 0.9, 4H), 7.46 (m, 4H), 7.33 (m, 4H), 6.89 (dd, J = 17.6, 10.9 Hz, 1H), 5.92 (d, J = 17.5, 1H), 5.48 (d, J = 11.1, 1H). <sup>13</sup>C NMR (126 MHz, CDCl<sub>3</sub>, δ): 141.30, 140.72, 139.70, 135.49, 126.32, 124.58, 123.72, 120.61, 120.49, 116.78, 109.84.

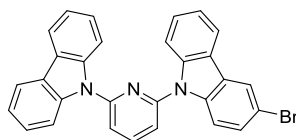
### 7.2.4 3-Bromo-9-(6-fluoropyridin-2-yl)-9H-carbazole (**5**)



A suspension of 3-bromo-9H-carbazole (16.53 g, 67.2 mmol) and sodium hydride (3.22 g, 134 mmol) in *anhydrous* tetrahydrofuran (120 mL) was heated at 60 °C for 30 minutes. Afterwards, 2,6-difluoropyridine **4** (7.73 g, 67.2 mmol) was added dropwise and the reaction was heated at 80 °C for 6 hours. After completion the reaction was cooled to room temperature, quenched with ethanol and then poured into water. After evaporation of tetrahydrofuran, the aqueous phase was extracted with dichloromethane and dried over MgSO<sub>4</sub>. The crude was purified on silica gel column chromatography using toluene/ heptane (1:9) as eluent. Yield: 16.6 g (72%).

<sup>1</sup>H NMR (500 MHz, THF-*d*<sub>8</sub>, δ): 8.33 (d, *J* = 2.0 Hz, 1H), 8.19 – 8.13 (m, 2H), 7.94 (dt, *J* = 8.4, 0.8 Hz, 1H), 7.90 (dd, *J* = 8.8, 0.4 Hz, 1H), 7.67 (dd, *J* = 7.7, 1.6 Hz, 1H), 7.55 (dd, *J* = 8.8, 2.0 Hz, 1H), 7.47 (ddd, *J* = 8.4, 7.2, 1.3 Hz, 1H), 7.33 (ddd, *J* = 8.0, 7.2, 0.9 Hz, 1H), 7.06 (dd, *J* = 8.1, 2.4 Hz, 1H). <sup>13</sup>C-NMR (126 MHz, THF-*d*<sub>8</sub>, δ): 164.71, 160.24, 144.44, 142.79, 133.10, 133.02, 126.61, 126.03, 124.76, 122.55, 119.78, 133.27, 110.71, 109.49, 106.35, 103.01.

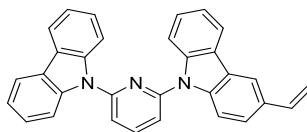
## 7.2.5 9-(6-(9H-carbazol-9-yl)pyridin-2-yl)-3-bromo-9H-carbazole (**6**)



Following the same procedure as in 3-Bromo-9-(6-fluoropyridin-2-yl)-9H-carbazole **5**, carbazole (2.11 g, 12.6 mmol), **5** (4.3 g, 12.6 mmol) and sodium hydride (0.60 g, 25.2 mmol) were used. Yield: 4.96 g (80%).

<sup>1</sup>H NMR (500 MHz, CDCl<sub>3</sub>, δ): 8.10 (d, *J* = 1.6 Hz, 1H), 8.01 (d, *J* = 7.7 Hz, 2H), 7.96 – 7.91 (m, 2H), 7.88 (d, *J* = 8.3 Hz, 2H), 7.85 (d, *J* = 8.3 Hz, 1H), 7.79 (d, *J* = 8.8 Hz, 1H), 7.48 (d, *J* = 7.9 Hz, 1H), 7.41 (d, *J* = 7.9 Hz, 1H), 7.36 – 7.26 (m, 4H), 7.21 (t, *J* = 7.4 Hz, 3H). <sup>13</sup>C (126 MHz, CDCl<sub>3</sub>, δ): 151.66, 151.14, 140.61, 139.75, 139.48, 138.27, 129.10, 127.15, 126.49, 126.41, 124.70, 123.56, 122.96, 121.70, 121.47, 120.48, 120.30, 115.21, 114.79, 114.20, 113.78, 112.03, 111.99.

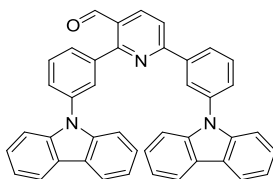
## 7.2.6 9-(6-(9H-carbazol-9-yl)pyridin-2-yl)-3-vinyl-9H-carbazole (**7**)



Potassium vinyltrifluoroborate (2.19 g, 16.4 mmol), 9-(6-(9H-carbazol-9-yl)pyridin-2-yl)-3-bromo-9H-carbazole **6** (4.00 g, 8.19 mmol), sodium carbonate (3.47 g, 32.8 mmol) and tetrakis(triphenylphosphine)-palladium(0) (0.47 g, 0.41 mmol) were dissolved in a tetrahydrofuran/water (9:1, 100 mL) mixture. The reaction was heated at 110 °C for 20 hours. After completion, the reaction was cooled to room temperature and poured into water. Phase separation was followed by extraction of the aqueous phase with dichloromethane. The combined organic fractions were dried over MgSO<sub>4</sub>. The crude was purified on silica gel column chromatography using toluene/heptane (1:9) as eluent. The product was recrystallized from dichloromethane/ethanol mixtures. Yield: 2.67 g (75%).

<sup>1</sup>H NMR (500 MHz, THF-*d*<sub>8</sub>, δ): 8.31 (td, *J* = 7.9, 0.7 Hz, 1H), 8.25 (d, *J* = 1.6 Hz, 1H), 8.20 (d, *J* = 7.7 Hz, 1H), 8.17 (d, *J* = 7.7 Hz, 2H), 8.05 (d, *J* = 8.3 Hz, 3H), 8.02 (d, *J* = 8.6 Hz, 1H), 7.79 (dd, *J* = 7.9, 2.7 Hz, 2H), 7.54 (dd, *J* = 8.6, 1.7 Hz, 1H), 7.40 (ddt, *J* = 8.4, 7.3, 1.4 Hz, 3H), 7.34 – 7.28 (m, 3H), 6.92 (dd, *J* = 17.6, 10.9 Hz, 1H), 5.83 (dd, *J* = 17.6, 1.0 Hz, 1H), 5.20 (dd, *J* = 10.9, 0.9 Hz, 1H).  
<sup>13</sup>C NMR (126 MHz, THF-*d*<sub>8</sub>, δ): 152.56, 152.44, 142.14, 140.99, 140.58, 140.30, 138.41, 132.43, 129.83, 129.07, 127.37, 126.20, 125.94, 125.71, 125.56, 122.31, 122.17, 121.06, 120.95, 118.94, 116.26, 116.10, 113.04, 112.92, 112.08.

### 7.2.7 2,6-Bis(3-(9H-carbazol-9-yl)phenyl)-nicotinaldehyde (**9**)

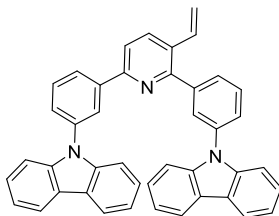


A mixture of 9-(3-(4,4,5,5-tetramethyl-1,3,2-dioxaborolan-2-yl)phenyl)-9H-carbazole **8** (7.54 g, 20.4 mmol), 2,6-dibromonicotinaldehyde (2.42 g, 9.28 mmol), potassium carbonate (5.13 g, 37.1 mmol) and tetrakis(triphenylphosphine)palladium(0) (0.53 g, 0.46 mmol) was dissolved in a toluene/water/ethanol (2:1:1, 200 mL) mixture and refluxed at 110 °C for 20 hours. After cooling to room temperature, the mixture was poured into water. Phase separation was

followed by extraction with dichloromethane. The combined organic fractions were dried over  $\text{MgSO}_4$ . The crude was purified on silica gel chromatography using ethyl acetate/heptane (9:1) as eluent. Yield: 5.00 g (91%).<sup>117</sup>

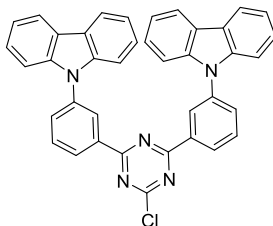
$^1\text{H}$  NMR (500 MHz,  $\text{CDCl}_3$ ,  $\delta$ ): 10.30 (s, 1H), 8.44 (d,  $J = 8.2$  Hz, 1H), 8.40 (t,  $J = 1.9$  Hz, 1H), 8.27 (d,  $J = 7.8$  Hz, 1H), 8.17 (d,  $J = 7.7$  Hz, 2H), 8.14 (d,  $J = 7.3$  Hz, 2H), 8.00 (s, 1H), 7.95 (d,  $J = 8.2$  Hz, 1H), 7.78 – 7.74 (m, 3H), 7.74 – 7.68 (m, 2H), 7.49 (d,  $J = 7.3$  Hz, 2H), 7.44 (d,  $J = 8.2$  Hz, 2H), 7.37 (t,  $J = 7.6$  Hz, 2H), 7.32 – 7.26 (m, 6H).  $^{13}\text{C}$  NMR (126 MHz,  $\text{CDCl}_3$ ,  $\delta$ ): 190.81, 161.09, 159.62, 140.91, 140.69, 139.99, 139.33, 138.61, 138.37, 137.50, 130.63, 130.14, 129.57, 129.10, 128.93, 128.41, 128.12, 126.70, 126.48, 126.19, 126.18, 123.63, 123.56, 120.50, 120.48, 120.35, 120.25, 119.50, 109.77.

### 7.2.8 9,9'-((3-Vinylpyridine-2,6-diyl)bis(3,1-phenylene))bis(9H-carbazole) (10)



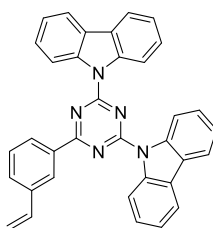
Following the same procedure as in **2**, potassium *tert*-butoxide (0.99 g, 8.85 mmol), methyltriphenylphosphonium bromide (2.96 g, 8.29 mmol) and 2,6-Bis(3-(9H-carbazol-9-yl)phenyl)-nicotinaldehyde **9** (3.26 g, 5.53 mmol) were used. Purification on silica gel column chromatography using ethyl acetate/hexane (1:9) as eluent gave **10** as a white solid. Yield: 2.57 g (79%).

$^1\text{H}$  NMR (500 MHz,  $\text{CDCl}_3$ ,  $\delta$ ): 8.21 (s, 1H), 8.12 (d,  $J = 7.8$  Hz, 1H), 8.07 (dd,  $J = 13.4, 7.7$  Hz, 4H), 7.93 (d,  $J = 8.2$  Hz, 1H), 7.83 (s, 1H), 7.70 (dd,  $J = 12.3, 7.9$  Hz, 2H), 7.61 (q,  $J = 7.6$  Hz, 2H), 7.55 (d,  $J = 7.9$  Hz, 1H), 7.52 (d,  $J = 7.8$  Hz, 1H), 7.43 (d,  $J = 8.2$  Hz, 2H), 7.36 (d,  $J = 8.2$  Hz, 2H), 7.29 (t,  $J = 7.6$  Hz, 2H), 7.26 – 7.21 (m, 3H), 7.19 – 7.15 (m, 3H), 6.90 (dd,  $J = 17.5, 11.0$  Hz, 1H), 5.73 (d,  $J = 17.5$  Hz, 1H), 5.33 (d,  $J = 11.0$  Hz, 1H).  $^{13}\text{C}$  NMR (126 MHz,  $\text{CDCl}_3$ ,  $\delta$ ): 156.13, 155.19, 141.77, 141.08, 140.88, 138.39, 137.66, 135.56, 134.38, 130.71, 130.47, 129.78, 129.05, 128.78, 127.90, 126.92, 126.22, 126.16, 126.10, 125.86, 123.59, 123.55, 120.49, 120.45, 120.16, 120.14, 119.56, 117.21, 110.04, 109.99.

7.2.9 9,9'-((6-Chloro-1,3,5-triazine-2,4-diyl)bis(3,1-phenylene))bis(9H-carbazole) (**12b**)

Cyanuric chloride **11** (1.10 g, 5.97 mmol) was dissolved in tetrahydrofuran (100 mL). In a separated flask, a solution of 9-(3-bromophenyl)-9H-carbazole (3.85 g, 12.0 mmol) in tetrahydrofuran (100 mL) was cooled to  $-78\text{ }^{\circ}\text{C}$  before addition of *n*-butyllithium 1.6 M in hexanes (7.47 mL, 12.0 mmol). The mixture was stirred at this temperature for 2 hours. Afterwards the mixture was transferred to the first solution and refluxed overnight at  $70\text{ }^{\circ}\text{C}$ . After cooling to room temperature, the crude was filtered through celites. Purification on silica gel column chromatography using ethyl acetate/hexane (1:9) as eluent gave **26b**. Yield: 0.69 g (19%).

$^1\text{H}$  NMR (500 MHz, THF- $d_6$ ,  $\delta$ ): 8.85 (s, 1H), 8.69 (d,  $J=7.4$ , 1H), 8.14 (d,  $J=7.7$ , 2H), 7.89 (d,  $J=7.7$ , 1H), 7.82 (t,  $J=7.8$ , 7.8, 1H), 7.38 (d,  $J=8.1$ , 2H), 7.32 (t,  $J=7.5$ , 7.5, 2H), 7.23 (t,  $J=7.4$ , 7.4, 2H).  $^{13}\text{C}$  NMR (126 MHz, THF- $d_6$ ,  $\delta$ ): 173.89, 173.39, 141.84, 139.71, 137.61, 133.25, 131.71, 129.27, 128.77, 127.02, 124.67, 121.17, 110.38.

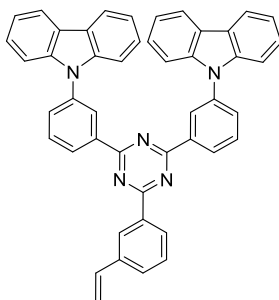
7.2.10 9,9'-(6-(3-Vinylphenyl)-1,3,5-triazine-2,4-diyl)bis(9H-carbazole) (**13a**)

3-Vinylphenylboronic acid (1.48 g, 10.0 mmol), 9,9'-(6-chloro-1,3,5-triazine-2,4-diyl)bis(9H-carbazole) **12a** (3.80 g, 8.33 mmol), caesium carbonate (8.96 g, 27.5 mmol) and tetrakis(triphenylphosphine)palladium(0) (0.48 g, 0.41 mmol) were dissolved in a toluene/water (2:1) mixture (150 mL) and heated for 20 hours at  $100\text{ }^{\circ}\text{C}$ . After completion of the reaction the reaction was cooled to room temperature. Phase separation was followed by extraction with

dichloromethane. The combined organic phases were dried over  $\text{MgSO}_4$ . The crude was purified on silica gel column chromatography using toluene/ heptane (1:9) as eluent. The product crystallized upon concentration. Filtration and washing with ethanol gave **13a**. Yield: 2.23 g (52%).

$^1\text{H}$  NMR ((500 MHz,  $\text{CDCl}_3$ ,  $\delta$ ): 9.02 (d,  $J = 8.3$  Hz, 4H), 8.76 (s, 1H), 8.56 (d,  $J = 7.6$  Hz, 1H), 8.06 (d,  $J = 7.4$  Hz, 4H), 7.66 (d,  $J = 7.5$  Hz, 1H), 7.56 (t,  $J = 7.6$  Hz, 1H), 7.50 (t,  $J = 7.5$  Hz, 4H), 7.41 (t,  $J = 7.3$  Hz, 4H), 6.87 (dd,  $J = 17.5, 10.8$  Hz, 1H), 5.96 (d,  $J = 17.5$  Hz, 1H), 5.41 (d,  $J = 10.8$  Hz, 1H).  $^{13}\text{C}$  NMR (126 MHz,  $\text{CDCl}_3$ ,  $\delta$ ): 172.81, 164.72, 138.99, 138.24, 136.47, 130.73, 129.26, 128.55, 127.05, 126.97, 126.66, 123.46, 119.81, 117.70, 114.99.

### 7.2.11 9,9'-((6-(3-Vinylphenyl)-1,3,5-triazine-2,4-diyl)bis(3,1-phenylene))bis(9H-carbazole) (**13b**)

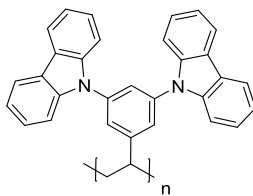


Following the same procedure as in **13a**, 3-vinylphenylboronic acid (0.88 g, 5.98 mmol), caesium carbonate (5.23 g, 9.90 mmol), 9,9'-((6-Chloro-1,3,5-triazine-2,4-diyl)bis(3,1-phenylene))bis(9H-carbazole) **12a** (1.79 g, 2.99 mmol) and tetrakis(triphenylphosphine)palladium(0) (0.17 g, 0.15 mmol) were used. The crude was purified on silica gel column chromatography using ethyl acetate/ heptane (1:9) as eluent. Yield: 1.07 g (53%).

$^1\text{H}$  NMR (500 MHz,  $\text{CDCl}_3$ ,  $\delta$ ): 8.98 (s, 2H), 8.83 (d,  $J=5.9$ , 2H), 8.74 (s, 1H), 8.61 (d,  $J=7.4$ , 1H), 8.18 (d,  $J=7.5$ , 4H), 7.80 (d,  $J=6.9$ , 4H), 7.65 (d,  $J=7.3$ , 1H), 7.49-7.41 (m, 5H), 7.41 (t,  $J=7.2, 7.2$ , 4H), 7.32 (t,  $J=7.1, 7.1$ , 4H), 6.84 (dd,  $J=17.4, 10.9$ , 1H), 5.86 (d,  $J=17.5$ , 1H), 5.33 (d,  $J=10.7$ , 1H).  $^{13}\text{C}$  NMR (126 MHz,  $\text{CDCl}_3$ ,  $\delta$ ): 171.91, 171.17, 140.83, 138.31, 138.23, 138.12, 136.30, 135.95, 131.18, 130.29, 128.95, 128.47, 128.01, 127.59, 126.92, 126.11, 123.47, 120.37, 120.14, 114.93, 109.71.

### 7.2.12 Poly[9,9'-(5-vinyl-1,3-phenylene)bis(9H-carbazole)] (**P1**)

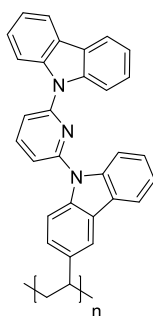




**Polymer P1**, from **3**: The monomer concentration was set to be 100 g/L in freshly distilled tetrahydrofuran. *N,N*-azobisisobutyronitrile (2 mol%) was used as initiator. The reaction was carried out in a glove box system under nitrogen atmosphere at 50 °C for 72 hours. After cooling to room temperature the reaction was quenched with methanol. Demonomerization was achieved by repeated precipitation into methanol. The residue was dissolved again in tetrahydrofuran and filtered through syringe PTFE filter 0.2 μm. The solution was concentrated and precipitated again into methanol. The precipitate was filtered by the use of PTFE filters pore size 0.45 μm. The polymer was dried overnight at 50 °C in vacuum. Yield: 0.15 g (62%).

<sup>1</sup>H NMR (500 MHz, CDCl<sub>3</sub>, δ): 8.40-6.55 (aromatic), 2.91-0.89 (backbone). Elemental analysis, calculated: C, 88.45; H, 5.10; N, 6.45; found: C, 84.82; H, 4.96; N, 6.09. T<sub>g</sub> = n.d.; M<sub>n</sub> = 9.0 kg mol<sup>-1</sup>; M<sub>w</sub> = 88.5 kg mol<sup>-1</sup>; PD = 9.88; DP = 20.

### 7.2.13 Poly(9-(6-(9H-carbazol-9-yl)pyridin-2-yl)-3-vinyl-9H-carbazole) (P2)

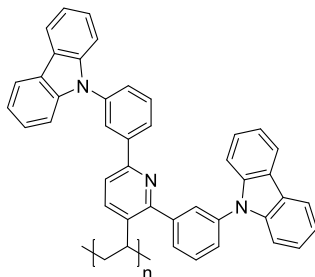


**Polymer P2**, from **7**: The same procedure as for **P1** was employed. After cooling to room temperature and quenching with methanol, the mixture was diluted with tetrahydrofuran. Precipitations were carried out in methanol/ ethyl acetate (2:1) mixtures. Yield: 0.37 g (68%).

<sup>1</sup>H NMR (500 MHz, CDCl<sub>3</sub>, δ): 8.05-7.75 (aromatic), 7.75-7.54 (aromatic), 7.20-6.85 (aromatic), 6.80-6.65 (aromatic), 2.50-1.13 (backbone). Elemental analysis, calculated: C, 85.49; H, 4.86; N,

9.65; found: C, 84.83; H, 4.83; N, 9.21.  $T_g = 211\text{ }^\circ\text{C}$ ;  $M_n = 38.4\text{ kg mol}^{-1}$ ;  $M_w = 123.5\text{ kg mol}^{-1}$ ; PD = 3.21; DP = 88.

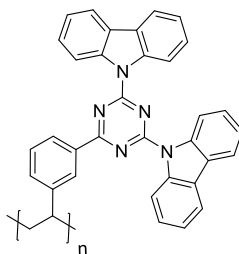
#### 7.2.14 Poly[9,9'-((3-vinylpyridine-2,6-diyl)bis(3,1-phenylene))bis(9H-carbazole)] (P3)



*Polymer P3*, from **10**: The same procedure as for **P1** was employed. After cooling to room temperature and quenching with methanol, the mixture was diluted with tetrahydrofuran. Precipitations were carried out in heptane/ ethyl acetate (1:1) mixtures. Yield: 0.43 g (69%).

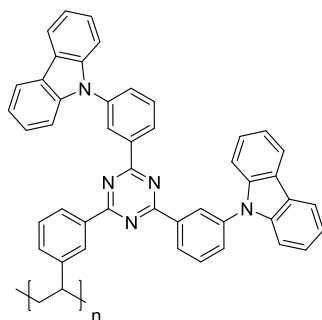
$^1\text{H}$  NMR (500 MHz,  $\text{CDCl}_3$ ,  $\delta$ ): 8.56-7.73 (aromatic), 7.73-5.88 (aromatic), 1.86-0.50 (backbone). Elemental analysis, calculated: C, 87.88; H, 4.97; N, 7.15; found: C, 86.83; H, 5.59; N, 6.53.  $T_g = 244\text{ }^\circ\text{C}$ ;  $M_n = 13.9\text{ kg mol}^{-1}$ ;  $M_w = 30.8\text{ kg mol}^{-1}$ ; PD = 2.21; DP = 23.

#### 7.2.15 Poly[9,9'-(6-(3-vinylphenyl)-1,3,5-triazine-2,4-diyl)bis(9H-carbazole)] (P4)



*Polymer P4*, from **13a**: The same procedure as for **P1** was employed. After cooling to room temperature and quenching with methanol, the mixture was diluted with tetrahydrofuran. Precipitations were carried out in heptane/ethyl acetate (1:1) mixtures. Yield: 0.52 g (80%).

$^1\text{H}$ -NMR (500 MHz,  $\text{THF-}d_6$ ,  $\delta$ ): 9.13-5.54 (aromatic), 2.20-0.57 (backbone). Elemental analysis, calculated: C, 81.85; H, 4.51; N, 13.64; found: C, 81.39; H, 4.67; N, 13.42.  $T_g = 275\text{ }^\circ\text{C}$ ;  $M_n = 11.8\text{ kg mol}^{-1}$ ;  $M_w = 35.0\text{ kg mol}^{-1}$ ; PD = 2.96; DP = 22.

**7.2.16 Poly[9,9'-((6-(3-vinylphenyl)-1,3,5-triazine-2,4-diyl)bis(3,1-phenylene))bis(9H-carbazole)] (P5)**

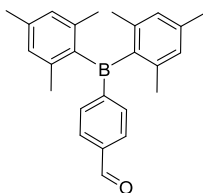
*Polymer P5*, from **13b**: The same procedure as for **P1** was employed. After cooling to room temperature and quenching with methanol, the mixture was diluted with tetrahydrofuran. Precipitations were carried out in heptane/ethyl acetate (1:1) mixtures. Yield: 0.24 g (71%).

$^1\text{H}$  NMR (500 MHz, THF-*d*<sub>6</sub>,  $\delta$ ): 9.16-6.08 (aromatic), 2.03-0.57 (backbone). Elemental analysis, calculated: C, 84.79; H, 4.96; N, 10.52; found: C, 83.51; H, 4.79; N, 9.71.  $T_g = 229\text{ }^\circ\text{C}$ ;  $M_n = 21.2\text{ kg mol}^{-1}$ ;  $M_w = 72.6\text{ kg mol}^{-1}$ ; PD = 3.42; DP = 31.

### Chapter 3

**General:** (4-bromophenyl)triphenylsilane **14a**, bis(4-bromophenyl)diphenylsilane **14b** and tris(4-bromophenyl)-(phenyl)silane **14c** were synthesized according to previously described procedures.<sup>129</sup>

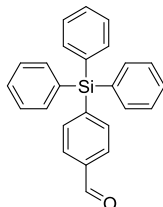
#### 7.2.17 General technique I: 4-(dimesitylboranyl)-benzaldehyde (**19**)



To a solution of (4-bromophenyl)dimesitylborane **18** (2.00 g, 4.93 mmol) in *anhydrous* tetrahydrofuran (50 mL) cooled to  $-78\text{ }^{\circ}\text{C}$ , *n*-butyllithium 1.6 M in hexane was added dropwise (3.24 mL, 5.18 mmol). The mixture was stirred at this temperature for 1.5 hours and then *N,N*-dimethylformamide (720 mg, 9.86 mmol) was added. The reaction was let to warm up to room temperature and stirred for 3 hours until the full consumption of the starting material was observed by TLC analysis. Subsequently, aqueous HCl 1 N (30 mL) was added to the mixture and stirred at room temperature for 0.5 hours. Evaporation of tetrahydrofuran under reduced pressure was followed by extraction of the aqueous phase with dichloromethane. The combined organic phases were dried over  $\text{MgSO}_4$ , filtered and concentrated. The reaction crude was purified by silica gel column chromatography using heptane/ethyl acetate (9:1) as eluent, giving **19** as a white powder. Yield: 1.25 g (71%).<sup>50</sup>

$^1\text{H}$  NMR (500 MHz,  $\text{CDCl}_3$ ,  $\delta$ ): 10.08 (s, 1H), 7.85 (d,  $J = 7.8\text{ Hz}$ , 2H), 7.66 (d,  $J = 7.9\text{ Hz}$ , 2H), 6.85 (s, 4H), 2.33 (s, 6H), 1.99 (s, 12H).  $^{13}\text{C}$  (126 MHz,  $\text{CDCl}_3$ ,  $\delta$ ): 192.83, 152.91, 141.53, 140.95, 139.53, 138.10, 136.07, 129.16, 128.52, 23.57, 21.39.

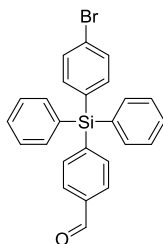
#### 7.2.18 4-(Triphenylsilyl)benzaldehyde (**15**)



According to general technique I, (4-bromophenyl)triphenylsilane **14a** (8.00 g, 19.3 mmol), *n*-butyllithium 1.6 M in hexane (9.24 mL, 23.1 mmol) and *N,N*-dimethylformamide (2.82 g, 38.5 mmol) were used. Recrystallization with ethanol/dichloromethane mixtures gave **15** as a white solid. Yield: 5.69 g (81%).

$^1\text{H}$  NMR (500 MHz,  $\text{CDCl}_3$ ,  $\delta$ ): 10.07 (s, 1H), 7.88 (d,  $J = 7.7$  Hz, 2H), 7.78 (d,  $J = 7.9$  Hz, 2H), 7.64 – 7.53 (m, 10H), 7.52 – 7.32 (m, 15H).  $^{13}\text{C}$  (126 MHz,  $\text{CDCl}_3$ ,  $\delta$ ): 192.72, 143.24, 137.06, 137.02, 136.52, 136.47, 134.32, 133.27, 130.10, 129.72, 128.77, 128.22, 128.00.

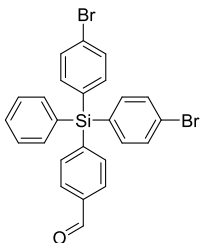
#### 7.2.19 4-((4-Bromophenyl)diphenylsilyl)benzaldehyde (**23a**)



According to general technique I, bis(4-bromophenyl)diphenylsilane **14b** (1.47 g, 2.97 mmol), *n*-butyllithium 1.6 M in hexane (2.04 mL, 3.27 mmol) and *N,N*-dimethylformamide (0.44 g, 6.00 mmol) were used. Yield: 1.17 g (88%).

$^1\text{H}$  NMR (500 MHz,  $\text{CDCl}_3$ ,  $\delta$ ): 10.05 (s, 1H), 7.87 (d,  $J = 7.6$  Hz, 2H), 7.73 (d,  $J = 7.6$  Hz, 2H), 7.61 – 7.48 (m, 10H), 7.47 – 7.33 (m, 12H).  $^{13}\text{C}$  (126 MHz,  $\text{CDCl}_3$ ,  $\delta$ ): 192.63, 142.53, 137.97, 137.19, 136.94, 136.38, 132.68, 132.32, 131.46, 130.31, 128.86, 128.34, 125.28.

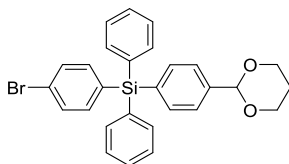
#### 7.2.20 4-(Bis(4-bromophenyl)(phenyl)silyl)benzaldehyde (**23b**)



According to general technique I, tris(4-bromophenyl)(phenyl)silane **14c** (7.22 g, 12.6 mmol), *n*-butyllithium 1.6 M in hexane (8.66 mL, 13.9 mmol), *N,N*-dimethylformamide (1.84 g, 25.2 mmol) were used. Yield: 4.25 g (65%).

$^1\text{H}$  NMR (500 MHz,  $\text{CDCl}_3$ ,  $\delta$ ): 10.06 (s, 1H), 7.88 (d,  $J = 8.1$  Hz, 2H), 7.71 (d,  $J = 8.0$  Hz, 2H), 7.58 – 7.48 (m, 7H), 7.47 – 7.35 (m, 7H).  $^{13}\text{C}$  (126 MHz,  $\text{CDCl}_3$ ,  $\delta$ ): 192.54, 141.82, 137.87, 137.33, 136.87, 136.30, 132.09, 131.72, 131.59, 130.52, 128.94, 128.46, 125.52.

#### 7.2.21 General technique II: (4-(1,3-dioxan-2-yl)phenyl)(4-bromophenyl)diphenylsilane (**24a**)

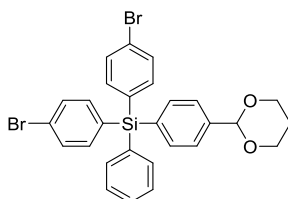


A mixture of 4-((4-bromophenyl)diphenylsilyl)benzaldehyde **23a** (4.00 g, 9.02 mmol), 1,3-propanediol (2.75 g, 36.1 mmol), and *p*-toluenesulfonic acid (0.09 mg, 0.54 mmol) dissolved in *anhydrous* toluene (60 mL) was heated to 150 °C using a *Dean-Stark* apparatus for the removal of water formed during the condensation reaction. The mixture was heated at this temperature for 3 hours. Afterwards, the reaction was cooled to room temperature and the solvent was evaporated. The reaction crude was absorbed on silica gel, and purified by silica gel column chromatography using heptane/ethyl acetate (4:1) as eluent. Recrystallization in methanol/dichloromethane mixture gave **11a** as a white solid. Yield: 2.58 g (57%).

$^1\text{H}$  NMR (500 MHz,  $\text{CDCl}_3$ ,  $\delta$ ): 7.58 – 7.49 (m, 10H), 7.46 – 7.35 (m, 8H), 5.54 (s, 1H), 4.35 – 4.20 (m, 2H), 4.01 (td,  $J = 12.3, 2.1$  Hz, 2H), 2.25 (qt,  $J = 12.5, 4.9$  Hz, 1H), 1.46 (d,  $J = 13.5$  Hz, 1H).  $^{13}\text{C}$

(126 MHz, CDCl<sub>3</sub>, δ): 140.26, 138.05, 136.53, 136.43, 134.50, 133.62, 133.29, 131.20, 129.93, 128.09, 125.70, 124.87, 101.61, 67.57, 25.90.

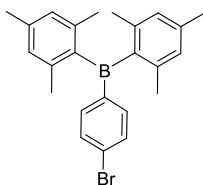
### 7.2.22 (4-(1,3-Dioxan-2-yl)phenyl)bis(4-bromophen-yl)(phenyl)silane (**24b**)



According to general technique II, **23b** (4.25 g, 8.13 mmol), 1,3-propanediol (2.48 g, 32.5 mmol) and *p*-toluenesulfonic acid (0.08 g, 0.49 mmol) were used. Yield: 3.22 g (70%).

<sup>1</sup>H NMR (500 MHz, CDCl<sub>3</sub>, δ): 7.58 – 7.42 (m, 12H), 7.38 (d, *J* = 7.4 Hz, 5H), 5.54 (s, 1H), 4.29 (dd, *J* = 11.5, 4.8 Hz, 2H), 4.01 (t, *J* = 11.6 Hz, 2H), 2.24 (dtd, *J* = 17.7, 12.7, 6.3 Hz, 1H), 1.47 (d, *J* = 13.5 Hz, 1H). <sup>13</sup>C (126 MHz, CDCl<sub>3</sub>, δ): 140.49, 137.94, 136.44, 136.34, 133.87, 133.02, 132.67, 131.32, 130.14, 128.21, 125.83, 125.11, 101.51, 67.58, 25.89.

### 7.2.23 General Technique III: (4-bromophenyl)-dimesitylborane (**18**)

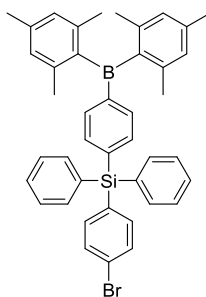


A solution of 1,4-dibromobenzene **17** (4.22 g, 17.9 mmol) in *anhydrous* tetrahydrofuran (100 mL) was cooled to -78 °C before *n*-butyllithium 1.6 M in hexane (11.2 mL, 17.9 mmol) was added dropwise. The reaction mixture was stirred at this temperature for 1.5 hours. In a separated flask, dimesitylboron fluoride (4.00 g, 14.9 mmol) was dissolved in tetrahydrofuran and added dropwise to the previous solution and stirred at -78 °C for 30 minutes. The reaction mixture was let to warm to room temperature before it was heated at 50 °C for 2 hours. Subsequently, the reaction was cooled to room temperature and quenched with methanol (5 mL). After removal of

the solvent under reduced pressure, water was added and the aqueous phase was extracted with dichloromethane. The combined organic fractions were dried over  $\text{MgSO}_4$ , filtered and the solvent was removed under reduced pressure. The crude product was purified by silica gel chromatography using toluene/heptane (1:9) as eluent. Product **5** was recrystallized using ethanol/dichloromethane mixtures. Yield: 3.80 g (63%).<sup>130</sup>

$^1\text{H}$  NMR (500 MHz,  $\text{CDCl}_3$ ,  $\delta$ ): 7.50 (d,  $J = 8.2$  Hz, 2H), 7.38 (d,  $J = 8.2$  Hz, 2H), 6.84 (s, 4H), 2.32 (s, 6H), 2.01 (s, 12H).  $^{13}\text{C}$  (126 MHz,  $\text{CDCl}_3$ ,  $\delta$ ): 144.50, 141.42, 140.86, 139.04, 137.91, 131.44, 128.41, 127.53, 23.58, 21.37.

#### 7.2.24 (4-Bromophenyl)(4-(dimesitylboranyl)phenyl)diphenylsilane (**21**)

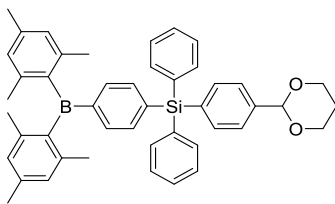


According to general technique III, bis(4-bromophenyl)diphenylsilane **14b** (5.98 g, 12.09 mmol), *n*-butyllithium 1.6 M in hexane (8.3 mL, 13.3 mmol), and dimesitylboron fluoride (3.57 g, 13.3 mmol) were used. Yield: 5.76 g (76%).

$^1\text{H}$  NMR (500 MHz,  $\text{CDCl}_3$ ,  $\delta$ ): 7.59 – 7.47 (m, 10H), 7.45 – 7.36 (m, 8H), 6.81 (s, 4H), 2.30 (s, 6H), 2.01 (s, 12H).  $^{13}\text{C}$  (126 MHz,  $\text{CDCl}_3$ ,  $\delta$ ): 140.90, 138.90, 138.04, 137.94, 136.54, 136.43, 135.88, 135.20, 133.55, 133.24, 131.24, 129.98, 128.31, 128.13, 128.01, 124.92, 23.58, 21.37.

#### 7.2.25 (4-(1,3-Dioxan-2-yl)phenyl)(4-(dimesitylboranyl)phenyl)diphenylsilane (**25a**)

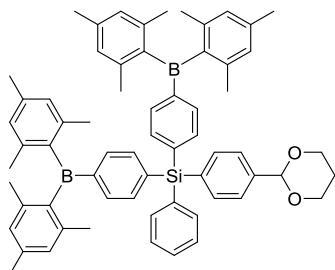




According to general technique III, (4-(1,3-dioxan-2-yl)phenyl)(4-bromophenyl)diphenylsilane **24a** (2.58 g, 5.14 mmol), *n*-butyllithium 1.6 M in hexane (4.81 mL, 7.71 mmol), and dimesitylboron fluoride (2.07 g, 7.71 mmol) were used. Yield: 2.34 g (67%).

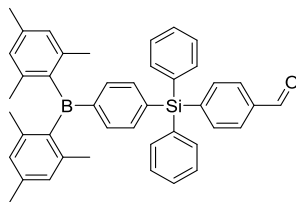
$^1\text{H}$  NMR (500 MHz,  $\text{CDCl}_3$ ,  $\delta$ ): 7.63 – 7.30 (18H, m), 6.81 (4H, s), 5.53 (1H, d,  $J=3.8$  Hz), 4.28 (2H, d,  $J=10.7$  Hz), 4.00 (2H, t,  $J=12.2, 12.2$  Hz), 2.30 (6H, s), 2.28 – 2.15 (1H, m), 2.01 (12H, s), 1.46 (1H, d,  $J=13.4$  Hz).  $^{13}\text{C}$  (126 MHz,  $\text{CDCl}_3$ ,  $\delta$ ): 141.87, 140.91, 140.12, 138.81, 138.33, 136.54, 136.51, 135.97, 135.10, 134.82, 133.82, 129.81, 128.29, 127.99, 127.03, 125.57, 101.59, 67.52, 25.91, 23.57, 21.36.

#### 7.2.26 (4-(1,3-Dioxan-2-yl)phenyl)bis(4-(dimesityl-boranyl)phenyl)(phenyl)silane (**25b**)



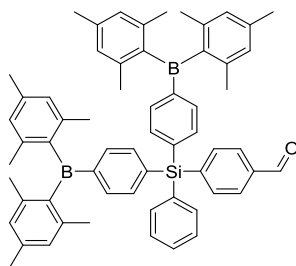
According to general technique III, (4-(1,3-Dioxan-2-yl)phenyl)bis(4-bromophenyl)(phenyl)silane **24b** (3.32 g, 5.72 mmol), *n*-butyllithium 1.6 M in hexane (8.94 mL, 14.3 mmol) and dimesitylboron fluoride (3.84 g, 14.30 mmol) were used. Yield: 4.06 g (77%).

The formation of product **25b** was confirmed by using dinitrophenylhydrazine (DNP) stain solution, which reacts selectively with aldehydes and ketones. In this case aldehyde-protected product showed a higher  $R_f$  (0.5) than **24b** (0.3) and the characteristic orange spot was not observed.

**7.2.27 General Technique IV: 4-((4-(dimesityl-boranyl)phenyl)diphenylsilyl)-benzaldehyde (26a)**

To a solution of (4-(1,3-Dioxan-2-yl)phenyl)(4-(dimesityl-boranyl)phenyl)diphenylsilane **25a** (2.00 g, 2.98 mmol) in tetrahydrofuran (30 mL) and water (10 mL), *p*-toluenesulfonic acid (30 mg, 0.18 mmol) acid was added. The reaction was then heated to 100 °C for 20 hours until the full consumption of the starting material was observed by TLC analysis. Afterwards, the reaction was cooled to room temperature and tetrahydrofuran was removed under reduced pressure. Addition of water was followed by extraction with dichloromethane. The combined organic fractions were dried over MgSO<sub>4</sub>, filtered and concentrated. The reaction crude was purified by silica gel column chromatography using toluene/ heptane (5:95) as eluent. Yield: 1.07 g (60%).

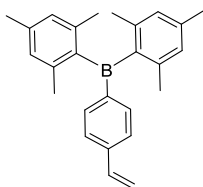
The formation of product **26a** was confirmed by using dinitrophenylhydrazine (DNP) stain solution, which reacts selectively with aldehydes and ketones. In this case, aldehyde **26a** showed a lower R<sub>f</sub> (0.4) than **25a** (0.6) and the characteristic orange spot was observed after revealing.

**7.2.28 4-(Bis(4-(dimesitylboranyl)phenyl)(phenyl)-silyl)benzaldehyde (26b)**

According to general technique IV, (4-(1,3-Dioxan-2-yl)phenyl)bis(4-(dimesitylboranyl)phenyl)(phenyl)silane **25b** (3.70 g, 4.03 mmol) and *p*-toluenesulfonic acid (0.04 g, 0.24 mmol) were used. Yield: 1.95 g (56%).

$^1\text{H}$  NMR (500 MHz,  $\text{CDCl}_3$ ,  $\delta$ ): 10.04 (s, 1H), 7.85 (d,  $J = 7.7$  Hz, 2H), 7.72 (d,  $J = 7.7$  Hz, 2H), 7.56 – 7.35 (m, 13H), 6.81 (s, 8H), 2.30 (s, 12H), 2.01 (s, 24H).  $^{13}\text{C}$  (126 MHz,  $\text{CDCl}_3$ ,  $\delta$ ): 192.70, 147.67, 142.93, 141.79, 140.91, 138.95, 137.22, 137.09, 136.99, 136.43, 135.92, 135.24, 132.92, 130.19, 128.78, 128.33, 128.24, 23.58, 21.37.

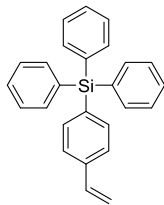
### 7.2.29 General Technique V: dimesityl(4-vinyl-phenyl)borane (**20**)



A mixture of potassium *tert*-butoxide (0.64 g, 5.56 mmol) and methyltriphenylphosphonium bromide (1.84 g, 5.15 mmol) was suspended in *anhydrous* tetrahydrofuran (15 mL). The reaction mixture was cooled to 0 °C and stirred for 0.5 hours under argon atmosphere. 4-(dimesitylboranyl)benzaldehyde **19** (1.21 g, 3.41 mmol) was dissolved in tetrahydrofuran (15 mL), added dropwise to the mixture and stirred for 1.5 hours at 0 °C. After completion of the reaction, the solvent was evaporated; water was added to the crude and then extracted with dichloromethane. The combined organic phase was dried over  $\text{MgSO}_4$ . The crude was purified by silica gel chromatography using heptane as eluent. Recrystallization using methanol/dichloromethane mixtures gave **20** as a white solid. Yield: 0.45 g (37%).<sup>85</sup>

$^1\text{H}$  NMR (500 MHz,  $\text{CDCl}_3$ ,  $\delta$ ): 7.49 (d,  $J = 8.0$  Hz, 2H), 7.39 (d,  $J = 8.0$  Hz, 2H), 6.83 (s, 4H), 6.75 (dd,  $J = 17.6, 10.9$  Hz, 1H), 5.86 (d,  $J = 17.6$  Hz, 1H), 5.33 (d,  $J = 11.0$  Hz, 1H), 2.32 (s, 6H), 2.02 (s, 12H).  $^{13}\text{C}$  (126 MHz,  $\text{CDCl}_3$ ,  $\delta$ ): 145.54, 141.86, 140.94, 138.72, 136.99, 136.97, 128.29, 125.93, 115.63, 23.59, 21.37.

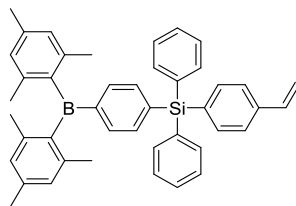
### 7.2.30 Triphenyl(4-vinylphenyl)silane (**16**)



According to general technique V, 4-(Triphenylsilyl)benzaldehyde **15** (4.60 g, 12.6 mmol), potassium *tert*-butoxide (2.31 g, 20.6 mmol) and methyltriphenylphosphonium bromide (6.81 g, 19.1 mmol) were used. Purification by silica gel column chromatography using heptane/toluene (9:1) gave **3** as a white solid. Yield: 2.73 g (60%).

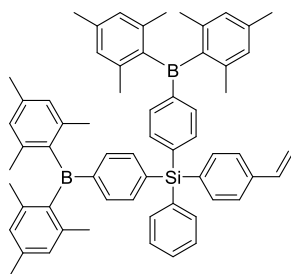
$^1\text{H}$  NMR (500 MHz,  $\text{CDCl}_3$ ,  $\delta$ ): 7.58 (dd,  $J = 17.8, 7.8$  Hz, 8H), 7.49 – 7.32 (m, 11H), 6.76 (dd,  $J = 18.1, 10.4$  Hz, 1H), 5.83 (d,  $J = 17.6$  Hz, 1H), 5.31 (d,  $J = 10.9$  Hz, 1H).  $^{13}\text{C}$  (126 MHz,  $\text{CDCl}_3$ ,  $\delta$ ): 138.79, 136.91, 136.79, 136.51, 134.31, 133.96, 129.75, 128.02, 125.79, 114.83.

### 7.2.31 (4-(Dimesitylboranyl)phenyl)diphenyl(4-vinylphenyl)silane (**27a**)



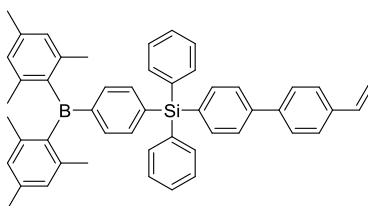
According to general technique V, 4-((4-(dimesityl-boranyl)phenyl)diphenylsilyl)-benzaldehyde **26a** (1.00 g, 1.63 mmol), potassium *tert*-butoxide (0.30 g, 2.66 mmol) and methyltriphenylphosphonium bromide (0.87 g, 2.45 mmol) were used. Purification by silica gel column chromatography using heptane/ ethyl acetate (9:1), followed by recrystallization using ethanol/ dichloromethane mixtures gave **27a** as a white solid. Yield: 0.43 g, 0.71 mmol (71%).

$^1\text{H}$  NMR (500 MHz,  $\text{CDCl}_3$ ,  $\delta$ ): 7.58 – 7.35 (m, 18H), 6.81 (s, 4H), 6.74 (dd,  $J = 17.6, 10.9$  Hz, 1H), 5.81 (d,  $J = 17.6, 0.7$  Hz, 1H), 5.29 (d,  $J = 10.5$ , 1H), 2.30 (s, 6H), 2.02 (s, 12H).  $^{13}\text{C}$  (126 MHz,  $\text{CDCl}_3$ ,  $\delta$ ): 147.20, 141.88, 140.91, 138.83, 138.59, 136.88, 136.77, 136.50, 135.95, 135.15, 134.11, 133.76, 129.80, 128.29, 128.03, 125.80, 114.87, 23.58, 21.37.

7.2.32 Bis(4-(dimesitylboranyl)phenyl)(phenyl)(4-vinylphenyl)silane (**27b**)

According to general technique V, 4-(Bis(4-(dimesitylboranyl)phenyl)(phenyl)silyl)benzaldehyde **26b** (1.93 g, 2.24 mmol), potassium *tert*-butoxide (0.40 g, 3.58 mmol) and methyltriphenylphosphonium bromide (1.20 g, 3.36 mmol) were used. Purification by silica gel column chromatography using heptane/ ethyl acetate (9:1), followed by recrystallization using methanol/ dichloromethane mixtures gave **27b** as a white solid. Yield: 1.47g, 1.71 mmol (88%).

$^1\text{H}$  NMR (500 MHz,  $\text{CDCl}_3$ ,  $\delta$ ): 7.49 – 7.38 (m, 12H), 7.37 – 7.27 (m, 5H), 6.74 (s, 8H), 6.66 (dd,  $J = 17.6, 10.9$  Hz, 1H), 5.73 (d,  $J = 17.6$  Hz, 1H), 5.22 (d,  $J = 10.9$  Hz, 1H), 2.23 (s, 12H), 1.94 (s, 24H).  
 $^{13}\text{C}$  (126 MHz,  $\text{CDCl}_3$ ,  $\delta$ ): 147.26, 141.87, 140.92, 138.84, 138.39, 136.86, 136.74, 136.47, 135.96, 135.14, 133.94, 133.59, 129.84, 128.29, 128.04, 125.81, 114.89, 23.59, 21.37.

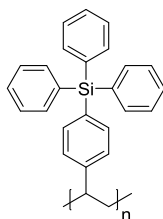
7.2.33 (4-(Dimesitylboranyl)phenyl)diphenyl(4'-vinyl-[1,1'-biphenyl]-4-yl)silane (**22**)

A mixture of (4-Bromophenyl)(4-(dimesitylboranyl)phenyl)diphenylsilane **21** (2.50 g, 3.91 mmol), 4-vinylphenylboronic acid (0.96 g, 6.49 mmol), sodium carbonate (5.30 g, 50 mmol) and tetrakis(triphenylphosphine)palladium(0) (0.23 g, 0.20 mmol) was dissolved in tetrahydrofuran (50 mL) and water (30 mL). The solution was purged from oxygen applying three vacuum-argon cycles before heat to 100 °C for 4 hours. After completion of the reaction, water was added to the mixture. Phase separation was followed by extraction with ethyl

acetate. The combined organic fractions were dried over  $\text{MgSO}_4$ . The crude product was purified by neutral aluminium oxide column chromatography using chloroform/ hexane (1:9) as eluent. Yield: 0.61 g, (22%).<sup>86</sup>

$^1\text{H}$  NMR (500 MHz,  $\text{CDCl}_3$ ,  $\delta$ ): 7.65 – 7.58 (m, 12H), 7.50 (dd,  $J = 8.2, 2.1$  Hz, 4H), 7.47 – 7.42 (m, 2H), 7.39 (dd,  $J = 7.8, 6.5$  Hz, 4H), 6.81 (s, 4H), 6.76 (dd,  $J = 17.6, 10.9$  Hz, 1H), 5.80 (d,  $J = 18.3$  Hz, 1H), 5.28 (d,  $J = 11.6$  Hz, 1H), 2.30 (s, 6H), 2.02 (s, 12H).  $^{13}\text{C}$  (126 MHz,  $\text{CDCl}_3$ ,  $\delta$ ): 147.24, 141.90, 140.91, 140.36, 138.84, 138.59, 137.02, 136.97, 136.53, 135.98, 135.18, 134.12, 133.03, 129.83, 128.29, 128.06, 127.38, 126.82, 126.50, 114.17, 23.59, 21.37., 21.23.

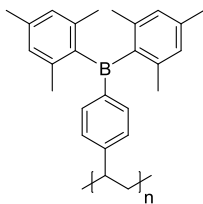
#### 7.2.34 General technique VI: Poly(triphenyl(4-vinylphenyl)silane) (P6)



*Polymer P6*, from **16**: The same procedure as for **P1** was employed. After cooling to room temperature and quenching with methanol, the mixture was diluted with tetrahydrofuran. Precipitations were carried out in methanol/ethyl acetate mixtures. Yield: 0.54 g (63%).

$^1\text{H}$  NMR (500 MHz,  $\text{CDCl}_3$ ,  $\delta$ ): 7.7-6.7 (aromatics), 6.7-6.0 (aromatics), 2.4-1.6 (backbone). Elemental analysis, calculated: C, 86.14; H, 6.12; Si, 7.75; found: C, 86.31; H, 6.26.  $T_g = 200$  °C;  $M_n = 16.3$  kg mol<sup>-1</sup>;  $M_w = 40.2$  kg mol<sup>-1</sup>; PD = 2.47; DP = 44.

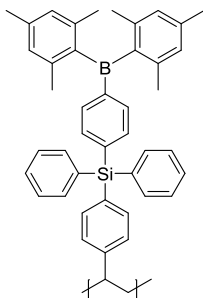
## 7.2.35 Poly(dimesityl(4-vinyl-phenyl)borane) (P7)



*Polymer P2*, from **20**: The same procedure as for **P1** was employed. After cooling to room temperature and quenching with methanol, the mixture was diluted with tetrahydrofuran. Precipitations were carried out in methanol. Yield: 0.38 g (79%).

$^1\text{H}$  NMR (500 MHz,  $\text{CDCl}_3$ ,  $\delta$ ): 7.2-7.0 (aromatics), 6.9-6.1 (aromatics), 2.4-2.0 (backbone), 2.0-1.6 (backbone). Elemental analysis, calculated: C, 88.64; H, 8.30; B, 3.07; found: C, 88.47; H, 8.76.  $T_g = 202\text{ }^\circ\text{C}$ ;  $M_n = 18.7\text{ kg mol}^{-1}$ ;  $M_w = 77.2\text{ kg mol}^{-1}$ ; PD = 4.13; DP = 53.

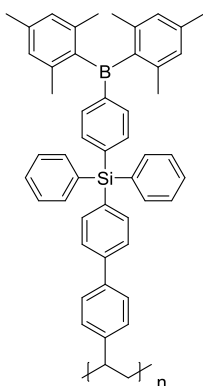
## 7.2.36 Poly[4-(dimesitylboranyl)phenyl)diphenyl(4-vinylphenyl)silane] (P8)



*Polymer P8*, from **27a**: The same procedure as for **P1** was employed. After cooling to room temperature and quenching with methanol, the mixture was diluted with tetrahydrofuran. Precipitations were carried out in methanol/ethyl acetate (2:1) mixtures. Yield: 0.42 g (73%).

$^1\text{H}$  NMR (500 MHz,  $\text{CDCl}_3$ ,  $\delta$ ): 7.6-7.0 (aromatics), 7.0-6.1 (aromatics), 2.3-2.1 (backbone), 2.0-1.6 (backbone). Elemental analysis, calculated: C, 86.53; H, 7.10; B, 1.77; Si, 4.60; found: C, 86.46; H, 7.28.  $T_g = 187\text{ }^\circ\text{C}$ ;  $M_n = 15.6\text{ kg mol}^{-1}$ ;  $M_w = 46.3\text{ kg mol}^{-1}$ ; PD = 2.96; DP = 25.

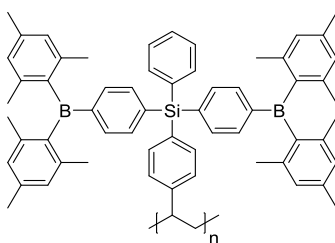
## 7.2.37 Poly[4-(dimesitylboranyl)phenyl)diphenyl(4'-vinyl-[1,1'-biphenyl]-4-yl)silane] (P9)



*Polymer P9*, from **22**: The same procedure as for **P1** was employed. After cooling to room temperature and quenching with methanol, the mixture was diluted with tetrahydrofuran. Precipitations were carried out in methanol/ethyl acetate (2:1) mixtures. Yield: 0.19 g (37%).

$^1\text{H NMR}$  (500 MHz,  $\text{THF-}d_6$ ,  $\delta$ ): 7.6-7.3 (aromatics), 7.3-7.2 (aromatics), 7.2-6.9 (aromatics), 2.2-2.0 (backbone). Elemental analysis, calculated: C, 87.44; H, 6.90; B, 1.57; Si, 4.09; found: C, 87.33; H, 7.00.  $T_g = 214\text{ }^\circ\text{C}$ ;  $M_n = 32.7\text{ kg mol}^{-1}$ ;  $M_w = 60.0\text{ kg mol}^{-1}$ ; PD = 1.84; DP = 47.

## 7.2.38 Poly[bis(4-(dimesitylboranyl)phenyl)(phenyl)(4-vinylphenyl)silane] (P10)



*Polymer P10*, from **27b**: The same procedure as for **P1** was employed. After cooling to room temperature and quenching with methanol, the mixture was diluted with tetrahydrofuran. Precipitations were carried out in methanol/ethyl acetate (2:1) mixtures. Yield: 0.35 g (51%).

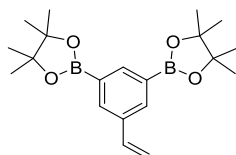


$^1\text{H}$  NMR (500 MHz,  $\text{CDCl}_3$ ,  $\delta$ ): 7.7-7.1 (aromatics), 7.1-6.2 (aromatics), 2.4-2.1 (backbone), 2.0-1.4 (backbone). Elemental analysis, calculated: C, 86.70; H, 7.51; B, 2.52; Si, 3.27; found: C, 84.82; H, 7.70.  $T_g$  = n.d.;  $M_n$  = 13.3 kg mol $^{-1}$ ;  $M_w$  = 20.8 kg mol $^{-1}$ ; PD = 1.56; DP = 15.

## Chapter 4

**General:** 3-(4-bromophenyl)pyridine **c**, 3-(3-bromophenyl)pyridine **d** and 3,3'-(5-bromo-1,3-phenylene)dipyridine **e** were synthesized by Pd-catalyzed cross-coupling reactions according to the literature procedures.<sup>118</sup>

### 7.2.39 2,2'-(5-Vinyl-1,3-phenylene)bis(4,4,5,5-tetramethyl-1,3,2-dioxaborolane) (**28**)

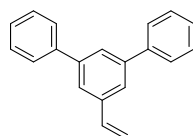


A mixture of bis(pinacolato)diboron (9.88 g, 38.9 mmol), 1,3-dibromo-5-vinylbenzene **2** (4.63 g, 17.7 mmol), 1,1'-bis(diphenylphosphino)-ferrocene dichloropalladium (II) (0.72 g, 0.90 mmol) and potassium acetate (11.8 g, 120 mmol) in *anhydrous* 1,4-dioxane was heated at 80 °C for 24 hours under argon atmosphere. After cooling to room temperature the mixture was filtered through celite, washing the filter with ethyl acetate. The solvents were evaporated; water was added to the crude and then extracted with dichloromethane. The combined organic phase was washed with brine and dried over MgSO<sub>4</sub>. The reaction crude was purified with silica gel chromatography using toluene as eluent. The final white product **28** (3.30 g) was obtained by recrystallization in dichloromethane/methanol mixtures. Yield: 3.34 g (53%).<sup>118</sup>

<sup>1</sup>H NMR (500 MHz, CDCl<sub>3</sub>, δ): 8.10 (d, *J* = 1.3 Hz, 1H), 7.87 (d, *J* = 1.1 Hz, 2H), 6.67 (dd, *J* = 17.6, 10.9 Hz, 1H), 5.77 (dd, *J* = 17.7, 0.9 Hz, 1H), 5.17 (d, *J* = 10.9 Hz, 1H), 1.27 (s, 24H).

<sup>13</sup>C NMR (126 MHz, CDCl<sub>3</sub>): δ 140.82, 136.78, 136.27, 135.54, 114.14, 83.95, 25.01.

### 7.2.40 5'-Vinyl-1,1':3',1''-terphenyl (**29a**)

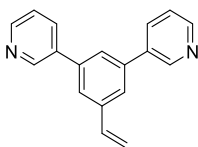


Bromobenzene (4.76 g, 30.3 mmol), 2,2'-(5-Vinyl-1,3-phenylene)bis(4,4,5,5-tetramethyl-1,3,2-dioxaborolane) **28** (1.80 g, 5.1 mmol), potassium carbonate (16.8 g, 121 mmol),

tetrakis(triphenylphosphine)palladium(0) (0.47 g, 0.40 mmol) were dissolved in a mixture of toluene (90 mL), ethanol (30 mL) and water (30 mL) and stirred under reflux for 20 hours under argon atmosphere. After cooling to room temperature, the organic phase was separated and the aqueous phase was extracted using chloroform. The combined organic phase was dried over  $\text{MgSO}_4$  and evaporated to give the crude product, which was purified by column chromatography on silica gel using ethyl acetate/heptane (1:4) as eluent, giving **29a** (1.11 g) as a white solid. Yield: 1.11 g (85%).<sup>86</sup>

$^1\text{H}$  NMR (500 MHz,  $\text{CDCl}_3$ ,  $\delta$ ): 7.73 (t,  $J = 1.8$  Hz, 1H), 7.71 – 7.66 (m, 4H), 7.64 (d,  $J = 1.8$  Hz, 2H), 7.50 (ddd,  $J = 7.9, 6.3, 1.2$  Hz, 4H), 7.45 – 7.36 (m, 2H), 6.88 (dd,  $J = 17.6, 10.8$  Hz, 1H), 5.92 (dd,  $J = 17.6, 0.9$  Hz, 1H), 5.38 (dd,  $J = 10.8, 0.8$  Hz, 1H).  $^{13}\text{C}$  NMR (126 MHz,  $\text{CDCl}_3$ ):  $\delta$  148.97, 148.40, 139.32, 139.21, 136.27, 136.14, 134.62, 125.55, 124.84, 123.72, 115.71.

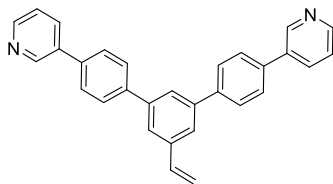
#### 7.2.41 3,3'-(5-Vinyl-1,3-phenylene)dipyridine (29b)



The same procedure as for **29a** was employed. 3-Bromopyridine (5.33 g, 33.7 mmol), **28** (2.00 g, 5.60 mmol), potassium carbonate (18.6 g, 135 mmol), tetrakis(triphenylphosphine)-palladium(0) (0.39 g, 0.34 mmol) were used. The product was purified by silica gel chromatography using chloroform/ethyl acetate (1:1) as eluent. The final white powder **29b** (0.94 g) was obtained after recrystallization with dichloromethane/hexane mixtures. Yield: 0.94 g (65%).

$^1\text{H}$  NMR (500 MHz,  $\text{CDCl}_3$ ,  $\delta$ ): 8.89 (d,  $J = 1.8$  Hz, 2H), 8.63 (dd,  $J = 4.8, 1.5$  Hz, 2H), 7.91 (dt,  $J = 7.9, 2.0$  Hz, 2H), 7.62 (s, 3H), 7.45 – 7.33 (m, 2H), 6.84 (dd,  $J = 17.6, 10.9$  Hz, 1H), 5.90 (d,  $J = 17.6$  Hz, 1H), 5.39 (d,  $J = 10.9$  Hz, 1H).  $^{13}\text{C}$  NMR (126 MHz,  $\text{CDCl}_3$ ):  $\delta$  142.25, 141.21, 138.63, 136.90, 128.94, 127.64, 127.42, 125.92, 124.24, 114.72.

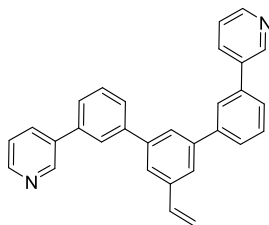
#### 7.2.42 3,3'-(5'-Vinyl-[1,1':3',1''-terphenyl]-4,4''-diyl)dipyridine (29c)



The same procedure as for **29a** was employed. 3-(4-bromophenyl)pyridine (2.03 g, 8.70 mmol), **28** (1.40 g, 3.94 mmol), potassium carbonate (13.1 g, 94.4 mmol), tetrakis(triphenylphosphine)palladium(0) (0.36 g, 0.30 mmol) were used. The product was purified by silica gel chromatography using chloroform/methanol (9:1) as eluent. After evaporation of the solvent **29c** (1.05 g) was obtained as a white solid. Yield: 1.26 g (78%).

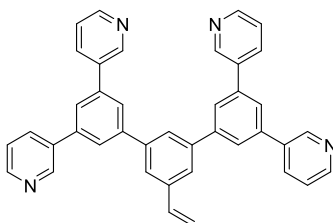
$^1\text{H}$  NMR (500 MHz,  $\text{CDCl}_3$ ,  $\delta$ ): 8.92 (d,  $J = 1.7$  Hz, 2H), 8.62 (dd,  $J = 4.8, 1.6$  Hz, 2H), 7.93 (ddd,  $J = 7.9, 2.3, 1.7$  Hz, 2H), 7.78 (dt,  $J = 7.9, 1.7$  Hz, 5H), 7.74 – 7.66 (m, 6H), 7.39 (ddd,  $J = 7.9, 4.8, 0.7$  Hz, 2H), 6.88 (dd,  $J = 17.6, 10.9$  Hz, 1H), 5.92 (d,  $J = 17.2$  Hz, 1H), 5.39 (d,  $J = 11.1$  Hz, 1H).  $^{13}\text{C}$  NMR (126 MHz,  $\text{CDCl}_3$ ):  $\delta$  148.69, 148.32, 141.52, 140.82, 138.89, 137.13, 136.67, 136.19, 134.36, 128.05, 127.68, 125.58, 124.38, 123.73, 115.08.

#### 7.2.43 3,3'-(5'-Vinyl-[1,1':3,1''-terphenyl]-3,3''-diyl)dipyridine (**29d**)



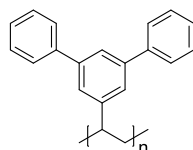
The same procedure as for **29a** was employed. 3-(3-bromophenyl)pyridine (2.17 g, 9.27 mmol), **28** (1.10 g, 3.09 mmol), potassium carbonate (10.3 g, 74.2 mmol), tetrakis(triphenylphosphine)palladium(0) (0.36 g, 0.3 mmol) were used. Yield: 0.76 g (60%).

$^1\text{H}$  NMR (500 MHz,  $\text{CDCl}_3$ ,  $\delta$ ): 8.92 (d,  $J = 2.3$  Hz, 2H), 8.63 (dd,  $J = 4.8, 1.5$  Hz, 2H), 7.95 (dt,  $J = 7.9, 1.8$  Hz, 2H), 7.84 (d,  $J = 1.7$  Hz, 2H), 7.77 (t,  $J = 1.6$  Hz, 1H), 7.73 – 7.66 (m, 4H), 7.64 – 7.57 (m, 4H), 7.40 (dd,  $J = 7.9, 4.8$  Hz, 2H), 6.88 (dd,  $J = 17.6, 10.9$  Hz, 1H), 5.92 (d,  $J = 17.6$  Hz, 1H), 5.39 (d,  $J = 10.9$  Hz, 1H).

7.2.44 3,3',3'',3'''-(5'-Vinyl-[1,1':3',1''-terphenyl]-3,3'',5,5'''-tetrayl)tetrapyrindine (**29e**)

The same procedure as for **29a** was employed. 3,3'-(5-bromo-1,3-phenylene)dipyridine (2.79 g, 8.97 mmol), **28** (1.47 g, 4.08 mmol), potassium carbonate (15.8 g, 114 mmol), tetrakis(triphenylphosphine)palladium(0) (0.36 g, 0.33 mmol) were used. The product was purified by silica gel chromatography using chloroform/methanol (95:5) as eluent. Recrystallization using methanol/dichloromethane mixtures gave **29e** (0.92 g) as a white solid. Yield: 0.92 g (40%).

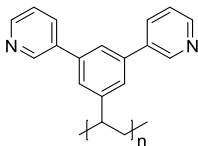
$^1\text{H}$  NMR (500 MHz,  $\text{CDCl}_3$ ,  $\delta$ ): 8.96 (d,  $J = 1.8$  Hz, 4H), 8.65 (dd,  $J = 4.8, 1.5$  Hz, 4H), 7.99 (dt,  $J = 7.9, 1.9$  Hz, 4H), 7.87 (d,  $J = 1.6$  Hz, 4H), 7.83 (s, 1H), 7.81 – 7.72 (m, 4H), 7.42 (dd,  $J = 7.9, 4.8$  Hz, 4H), 6.90 (dd,  $J = 17.6, 10.9$  Hz, 1H), 5.95 (d,  $J = 17.6$  Hz, 1H), 5.42 (d,  $J = 10.9$  Hz, 1H).  $^{13}\text{C}$  NMR (126 MHz,  $\text{CDCl}_3$ ):  $\delta$  149.14, 148.53, 142.92, 141.79, 139.68, 139.24, 136.36, 136.26, 134.75, 126.11, 125.98, 125.50, 124.98, 123.82, 115.64.

7.2.45 Poly(5'-vinyl-1,1':3',1''-terphenyl) (**P11a**)

*Polymer P11a*, from **29a**: The same procedure as for **P1** was employed. After cooling to room temperature and quenching with methanol, the mixture was diluted with chloroform. Precipitations were carried out in methanol. Yield: 0.60 g (83%).

$^1\text{H}$  NMR (500 MHz,  $\text{CDCl}_3$ ,  $\delta$ ): 7.22-6.95 (aromatic), 6.95-6.23 (aromatic), 2.36-1.05 (backbone). Elemental analysis calculated: C 93.71, H 6.29; found: C 93.18, H 6.29.  $T_g = 161$  °C;  $M_n = 36.1$  kg mol $^{-1}$ ;  $M_w = 90.1$  kg mol $^{-1}$ ; PD = 2.50; DP = 140.

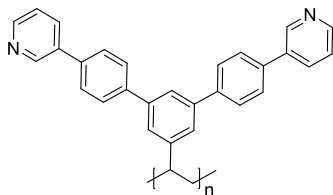
## 7.2.46 Poly(3,3'-(5-vinyl-1,3-phenylene)dipyridine) (P11b)



*Polymer P11b*, from **29b**: The same procedure as for **P1** was employed using N,N-dimethylformamide as solvent. After cooling to room temperature and quenching with methanol, the mixture was diluted with chloroform. Precipitations were carried out in ethyl acetate. Yield: 0.57 g (75%).

$^1\text{H}$  NMR (500 MHz,  $\text{CDCl}_3$ ,  $\delta$ ): 8.53 – 8.22 (aromatic), 8.22 – 7.85 (aromatic), 7.22 – 6.22 (aromatic), 2.55 – 1.41 (backbone). Elemental analysis calculated for: C 83.69, H 5.46, N 10.84; found: C 82.10, H 5.41, N 10.50.  $T_g = 192\text{ }^\circ\text{C}$ ;  $M_n = 21.5\text{ kg mol}^{-1}$ ;  $M_w = 50.8\text{ kg mol}^{-1}$ ; PD = 2.36; DP = 83.

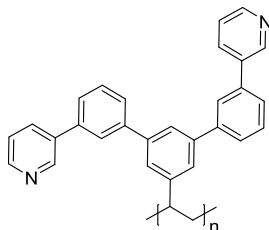
## 7.2.47 Poly(3,3'-(5'-vinyl-[1,1':3,1''-terphenyl]-4,4''-diyl)dipyridine) (P11c)



*Polymer P11c*, from **29c**: The same procedure as for **P1** was employed. After cooling to room temperature and quenching with methanol, the mixture was diluted with chloroform. Precipitations were carried out in methanol. Yield: 0.39 g (70%).

$^1\text{H}$  NMR (500 MHz,  $\text{CDCl}_3$ ,  $\delta$ ): 8.83-8.16 (aromatic), 7.55-6.25 (aromatic), 2.57-1.15 (backbone). Elemental analysis calculated: C 87.77, H 5.40, N 6.82; found: C 86.16, H 5.32, N 6.57.  $T_g = 241\text{ }^\circ\text{C}$ ;  $M_n = 48.8\text{ kg mol}^{-1}$ ;  $M_w = 280.8\text{ kg mol}^{-1}$ ; PD = 5.75; DP = 118.

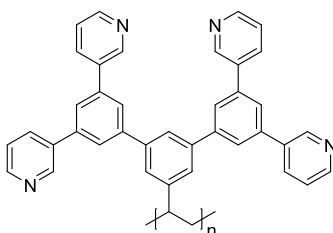
## 7.2.48 Poly(3,3'-(5'-vinyl-[1,1':3',1''-terphenyl]-3,3''-diyl)dipyridine) (P11d)



*Polymer P11d*, from **29d**: The same procedure as for **P1** was employed. After cooling to room temperature and quenching with methanol, the mixture was diluted with chloroform. Precipitations were carried out in methanol. Yield: 0.53 g (69%).

$^1\text{H}$  NMR (500 MHz,  $\text{CDCl}_3$ ,  $\delta$ ): 8.68-8.00 (aromatic), 7.24-6.68 (aromatic), 6.70-5.92 (aromatic), 2.58-1.33 (aromatic). Elemental analysis calculated for: C 87.77, H 5.40, N 6.82; found: C 87.11, H 5.36, N 6.70.  $T_g = 136$  °C;  $M_n = 17.6$  kg mol $^{-1}$ ;  $M_w = 133.7$  kg mol $^{-1}$ ; PD = 7.59; DP = 42.

## 7.2.49 Poly(3,3',3'',3'''-(5'-vinyl-[1,1':3',1''-terphenyl]-3,3'',5,5''-tetrayl)tetrapyridine) (P11e)



*Polymer P11e*, from **29e**: The same procedure as for **P1** was employed, using N,N-dimethylformamide as solvent. After cooling to room temperature and quenching with methanol, the mixture was diluted with chloroform. Precipitation was carried firstly into ethyl acetate/heptane (1:4) mixtures and finally in diethylether. Yield: 0.50 g (55%).

$^1\text{H}$  NMR (500 MHz,  $\text{CDCl}_3$ )  $\delta$  9.04-7.92 (aromatic), 7.92-7.39 (aromatic), 7.39-5.56 (aromatic), 2.90-1.32 (backbone). Elemental analysis calculated for: C 85.08, H 5.00, N 9.92; found: C 83.70, H 4.96, N 9.53.  $T_g = 247$  °C;  $M_n = 48.1$  kg mol $^{-1}$ ;  $M_w = 355.6$  kg mol $^{-1}$ ; PD = 7.39; DP = 85.





## 8. Literature

1. *Light's labour's lost*. (Organisation for Economic Co-operation and Development, 2006).
2. Edison, T. Electric lamp. (1880).
3. Yamae, K., Tsuji, H., Kittichungchit, V., Ide, N. & Komoda, T. Highly efficient white organic light-emitting diodes with over 100 lm/W for next-generation solid-state lighting. *J. Soc. Inf. Disp.* **21**, 529–540 (2013).
4. H. J. Round. A note on Carborundum. *Elect World* **19**, 309 (1907).
5. Heber, J. Nobel Prize 2014: Akasaki, Amano & Nakamura. *Nat. Phys.* **10**, 791–791 (2014).
6. Thejo Kalyani, N. & Dhoble, S. J. Organic light emitting diodes: Energy saving lighting technology – A review. *Renew. Sustain. Energy Rev.* **16**, 2696–2723 (2012).
7. Parashkov, R., Becker, E., Riedl, T., Johannes, H. H. & Kowalsky, W. Large Area Electronics Using Printing Methods. *Proc. IEEE* **93**, 1321–1329 (2005).
8. Krayla, J. Organic Light Emitting Diodes: The Future Display. *Int. J. Comput. Appl.* **137**, 12–14 (2016).
9. Tang, C. W. & VanSlyke, S. A. Organic electroluminescent diodes. *Appl. Phys. Lett.* **51**, 913–915 (1987).
10. Burroughes, J. H. *et al.* Light-emitting diodes based on conjugated polymers. *Nature* **347**, 539–541 (1990).
11. Bochkarev, M. N., Katkova, M. A., Ilichev, V. A. & Konev, A. N. New cathode materials for organic light-emitting diodes: Tm:Yb and Eu:Yb. *Nanotechnologies Russ.* **3**, 470–473 (2008).
12. Malliaras, G. G. & Scott, J. C. The roles of injection and mobility in organic light emitting diodes. *J. Appl. Phys.* **83**, 5399–5403 (1998).

13. Parker, I. D. Carrier tunneling and device characteristics in polymer light-emitting diodes. *J. Appl. Phys.* **75**, 1656–1666 (1994).
14. Kim, H. *et al.* Electrical, optical, and structural properties of indium–tin–oxide thin films for organic light-emitting devices. *J. Appl. Phys.* **86**, 6451–6461 (1999).
15. Kim, J. S. *et al.* Indium–tin oxide treatments for single- and double-layer polymeric light-emitting diodes: The relation between the anode physical, chemical, and morphological properties and the device performance. *J. Appl. Phys.* **84**, 6859–6870 (1998).
16. Groenendaal, L., Jonas, F., Freitag, D., Pielartzik, H. & Reynolds, J. R. Poly(3,4-ethylenedioxythiophene) and Its Derivatives: Past, Present, and Future. *Adv. Mater.* **12**, 481–494 (2000).
17. *Physics of Organic Semiconductors: BRUETTING:ORG.SEMICONDUCT O-BK.* (Wiley-VCH Verlag GmbH & Co. KGaA, 2005).
18. Kador, L. Stochastic theory of inhomogeneous spectroscopic line shapes reinvestigated. *J. Chem. Phys.* **95**, 5574–5581 (1991).
19. Marcus, R. A. On the Theory of Oxidation-Reduction Reactions Involving Electron Transfer. I. *J. Chem. Phys.* **24**, 966–978 (1956).
20. Wohlgenannt, M., Tandon, K., Mazumdar, S., Ramasesha, S. & Vardeny, Z. V. Formation cross-sections of singlet and triplet excitons in  $\pi$ -conjugated polymers. *Nature* **409**, 494–497 (2001).
21. Köhler, A. & Bässler, H. in *Electronic Processes in Organic Semiconductors* 1–86 (Wiley-VCH Verlag GmbH & Co. KGaA, 2015).
22. Alam, M. M. & Jenekhe, S. A. Polybenzobisazoles Are Efficient Electron Transport Materials for Improving the Performance and Stability of Polymer Light-Emitting Diodes. *Chem. Mater.* **14**, 4775–4780 (2002).

23. Qihuang, G., Liu, Z. & Chen, Z. Red Organic Light-Emitting Diode with Non-doping DCM as Emitter. in *Conference on Lasers and Electro-Optics/Quantum Electronics and Laser Science and Photonic Applications Systems Technologies (2005)*, paper CMR6 CMR6 (Optical Society of America, 2005).
24. McDowell, J. J. *et al.* Synthesis and Application of Photolithographically Patternable Deep Blue Emitting Poly(3,6-Dimethoxy-9,9-dialkylsilafuorene)s. *ACS Appl. Mater. Interfaces* **6**, 83–93 (2014).
25. Forrest, S. r., Bradley, D. d. c. & Thompson, M. e. Measuring the Efficiency of Organic Light-Emitting Devices. *Adv. Mater.* **15**, 1043–1048 (2003).
26. Loebel, P. *et al.* White OLEDs for lighting applications. *ResearchGate* **41**, (2009).
27. Baldo, M. A., Lamansky, S., Burrows, P. E., Thompson, M. E. & Forrest, S. R. Very high-efficiency green organic light-emitting devices based on electrophosphorescence. *Appl. Phys. Lett.* **75**, 4–6 (1999).
28. Smith, A. R. G., Burn, P. L. & Powell, B. J. Spin–Orbit Coupling in Phosphorescent Iridium(III) Complexes. *ChemPhysChem* **12**, 2429–2438 (2011).
29. Gildea, L. F. & Williams, J. A. G. in *Organic Light-Emitting Diodes (OLEDs)* 77–113 (Woodhead Publishing, 2013).
30. *Highly Efficient OLEDs with Phosphorescent Materials.* (Wiley-VCH Verlag GmbH & Co. KGaA, 2007).
31. Tao, Y. *et al.* Thermally Activated Delayed Fluorescence Materials Towards the Breakthrough of Organoelectronics. *Adv. Mater.* **26**, 7931–7958 (2014).
32. Grzywacz, J. Difference between Prompt and Delayed Fluorescence Spectra. *Nature* **213**, 385–386 (1967).
33. Valeur, B. *Molecular Fluorescence.* (Wiley-VCH Verlag GmbH, 2001).

34. Endo, A. *et al.* Thermally Activated Delayed Fluorescence from Sn<sup>4+</sup>-Porphyrin Complexes and Their Application to Organic Light Emitting Diodes – A Novel Mechanism for Electroluminescence. *Adv. Mater.* **21**, 4802–4806 (2009).
35. Uoyama, H., Goushi, K., Shizu, K., Nomura, H. & Adachi, C. Highly efficient organic light-emitting diodes from delayed fluorescence. *Nature* **492**, 234–238 (2012).
36. Volz, D. *et al.* Bridging the Efficiency Gap: Fully Bridged Dinuclear Cu(I)-Complexes for Singlet Harvesting in High-Efficiency OLEDs. *Adv. Mater.* **27**, 2538–2543 (2015).
37. Nuyken, O., Jungermann, S., Wiederhorn, V., Bacher, E. & Meerholz, K. Modern Trends in Organic Light-Emitting Devices (OLEDs). *Monatshefte Für Chem. Chem. Mon.* **137**, 811–824 (2006).
38. Adachi, C., Tokito, S., Tsutsui, T. & Saito, S. Electroluminescence in Organic Films with Three-Layer Structure. *Jpn. J. Appl. Phys.* **27**, L269 (1988).
39. Adachi, C., Tokito, S., Tsutsui, T. & Saito, S. Organic Electroluminescent Device with a Three-Layer Structure. *Jpn. J. Appl. Phys.* **27**, L713 (1988).
40. Chen, D., Su, S.-J. & Cao, Y. Nitrogen heterocycle-containing materials for highly efficient phosphorescent OLEDs with low operating voltage. *J. Mater. Chem. C* **2**, 9565–9578 (2014).
41. Yook, K. S. & Lee, J. Y. Organic Materials for Deep Blue Phosphorescent Organic Light-Emitting Diodes. *Adv. Mater.* **24**, 3169–3190 (2012).
42. Tao, Y., Yang, C. & Qin, J. Organic host materials for phosphorescent organic light-emitting diodes. *Chem. Soc. Rev.* **40**, 2943–2970 (2011).
43. Thelakkat, M. Star-Shaped, Dendrimeric and Polymeric Triarylamines as Photoconductors and Hole Transport Materials for Electro-Optical Applications. *Macromol. Mater. Eng.* **287**, 442–461 (2002).

44. Kim, S. H. *et al.* Triplet host engineering for triplet exciton management in phosphorescent organic light-emitting diodes. *J. Appl. Phys.* **103**, 054502 (2008).
45. Lee, J., Lee, J.-I., Lee, J.-W. & Chu, H. Y. Effects of charge balance on device performances in deep blue phosphorescent organic light-emitting diodes. *Org. Electron.* **11**, 1159–1164 (2010).
46. Sasabe, H. *et al.* Wide-Energy-Gap Electron-Transport Materials Containing 3,5-Dipyridylphenyl Moieties for an Ultra High Efficiency Blue Organic Light-Emitting Device. *Chem. Mater.* **20**, 5951–5953 (2008).
47. Kulkarni, A. P., Tonzola, C. J., Babel, A. & Jenekhe, S. A. Electron Transport Materials for Organic Light-Emitting Diodes. *Chem. Mater.* **16**, 4556–4573 (2004).
48. Xiao, L. *et al.* Recent Progresses on Materials for Electrophosphorescent Organic Light-Emitting Devices. *Adv. Mater.* **23**, 926–952 (2011).
49. Sasabe, H. & Kido, J. Development of high performance OLEDs for general lighting. *J. Mater. Chem. C* **1**, 1699–1707 (2013).
50. Debeaux, M. *et al.* Charge-Transporting Polymers based on Phenylbenzoimidazole Moieties. *Adv. Funct. Mater.* **20**, 399–408 (2010).
51. Tanaka, D., Takeda, T., Chiba, T., Watanabe, S. & Kido, J. Novel Electron-transport Material Containing Boron Atom with a High Triplet Excited Energy Level. *Chem. Lett.* **36**, 262–263 (2007).
52. Sasabe, H. *et al.* Influence of Substituted Pyridine Rings on Physical Properties and Electron Mobilities of 2-Methylpyrimidine Skeleton-Based Electron Transporters. *Adv. Funct. Mater.* **21**, 336–342 (2011).

53. Masui, K., Nakanotani, H. & Adachi, C. Analysis of exciton annihilation in high-efficiency sky-blue organic light-emitting diodes with thermally activated delayed fluorescence. *Org. Electron.* **14**, 2721–2726 (2013).
54. Luo, Y. & Aziz, H. Correlation Between Triplet-Triplet Annihilation and Electroluminescence Efficiency in Doped Fluorescent Organic Light-Emitting Devices. *Adv. Funct. Mater.* **20**, 1285–1293 (2010).
55. Yang, X. & Neher, D. in *Organic Light Emitting Devices* (eds. Müllen, K. & Scherf, U.) 333–367 (Wiley-VCH Verlag GmbH & Co. KGaA, 2005).
56. Strohriegel, P. *et al.* Novel host materials for blue phosphorescent OLEDs. in **8829**, 882906–882906–12 (2013).
57. Holmes, R. J. *et al.* Efficient, deep-blue organic electrophosphorescence by guest charge trapping. *Appl. Phys. Lett.* **83**, 3818–3820 (2003).
58. Ren, X. *et al.* Ultrahigh Energy Gap Hosts in Deep Blue Organic Electrophosphorescent Devices. *Chem. Mater.* **16**, 4743–4747 (2004).
59. Chen, H.-F. *et al.* 1,3,5-Triazine derivatives as new electron transport-type host materials for highly efficient green phosphorescent OLEDs. *J. Mater. Chem.* **19**, 8112–8118 (2009).
60. Holmes, R. J. *et al.* Blue organic electrophosphorescence using exothermic host-guest energy transfer. *Appl. Phys. Lett.* **82**, 2422–2424 (2003).
61. Chaskar, A., Chen, H.-F. & Wong, K.-T. Bipolar Host Materials: A Chemical Approach for Highly Efficient Electrophosphorescent Devices. *Adv. Mater.* **23**, 3876–3895 (2011).
62. Zuniga, C. A. Solution-processable charge transport layers for phosphorescent OLEDs. (2011).
63. Jou, J.-H., Kumar, S., Agrawal, A., Li, T.-H. & Sahoo, S. Approaches for fabricating high efficiency organic light emitting diodes. *J. Mater. Chem. C* **3**, 2974–3002 (2015).

64. Biswas, S., Shalev, O. & Shtein, M. Thin-Film Growth and Patterning Techniques for Small Molecular Organic Compounds Used in Optoelectronic Device Applications. *Annu. Rev. Chem. Biomol. Eng.* **4**, 289–317 (2013).
65. Kim, H., Byun, Y., Das, R. R., Choi, B.-K. & Ahn, P.-S. Small molecule based and solution processed highly efficient red electrophosphorescent organic light emitting devices. *Appl. Phys. Lett.* **91**, 093512 (2007).
66. Hast, J. *et al.* 18.1: Invited Paper: Roll-to-Roll Manufacturing of Printed OLEDs. *SID Symp. Dig. Tech. Pap.* **44**, 192–195 (2013).
67. Pardo, D. A., Jabbour, G. E. & Peyghambarian, N. Application of Screen Printing in the Fabrication of Organic Light-Emitting Devices. *Adv. Mater.* **12**, 1249–1252 (2000).
68. Pschenitzka, F. & Sturm, J. C. Three-color organic light-emitting diodes patterned by masked dye diffusion. *Appl. Phys. Lett.* **74**, 1913–1915 (1999).
69. Kim, E., Xia, Y. & Whitesides, G. M. Micromolding in Capillaries: Applications in Materials Science. *J. Am. Chem. Soc.* **118**, 5722–5731 (1996).
70. Villani, F. *et al.* Inkjet Printed Polymer Layer on Flexible Substrate for OLED Applications. *J. Phys. Chem. C* **113**, 13398–13402 (2009).
71. Zuniga, C. A., Barlow, S. & Marder, S. R. Approaches to Solution-Processed Multilayer Organic Light-Emitting Diodes Based on Cross-Linking. *Chem. Mater.* **23**, 658–681 (2011).
72. Zuniga, C. A. *et al.* Crosslinking Using Rapid Thermal Processing for the Fabrication of Efficient Solution-Processed Phosphorescent Organic Light-Emitting Diodes. *Adv. Mater.* **25**, 1739–1744 (2013).
73. Zhang, Y.-D. *et al.* Photo-crosslinkable polymers as hole-transport materials for organic light-emitting diodes. *J. Mater. Chem.* **12**, 1703–1708 (2002).

74. So, F., Kido, J. & Burrows, P. Organic Light-Emitting Devices for Solid-State Lighting. *MRS Bull.* **33**, 663–669 (2008).
75. Ma, W. *et al.* Water/Methanol-Soluble Conjugated Copolymer as an Electron-Transport Layer in Polymer Light-Emitting Diodes. *Adv. Mater.* **17**, 274–277 (2005).
76. Scherf, U. Counterion Pinning in Conjugated Polyelectrolytes for Applications in Organic Electronics. *Angew. Chem. Int. Ed.* **50**, 5016–5017 (2011).
77. Earmme, T., Ahmed, E. & Jenekhe, S. A. Solution-Processed Highly Efficient Blue Phosphorescent Polymer Light-Emitting Diodes Enabled by a New Electron Transport Material. *Adv. Mater.* **22**, 4744–4748 (2010).
78. Zhang, Y., Lee, J. & Forrest, S. R. Tenfold increase in the lifetime of blue phosphorescent organic light-emitting diodes. *Nat. Commun.* **5**, 5008 (2014).
79. Fukagawa, H. *et al.* Highly efficient and stable organic light-emitting diodes with a greatly reduced amount of phosphorescent emitter. *Sci. Rep.* **5**, 9855 (2015).
80. Kim, S. Y., Kim, K. Y., Tak, Y.-H. & Lee, J.-L. Dark spot formation mechanism in organic light emitting diodes. *Appl. Phys. Lett.* **89**, 132108 (2006).
81. Duan, L. *et al.* Solution processable small molecules for organic light-emitting diodes. *J. Mater. Chem.* **20**, 6392–6407 (2010).
82. Suzuki, M. *et al.* Highly efficient polymer light-emitting devices using ambipolar phosphorescent polymers. *Appl. Phys. Lett.* **86**, 103507 (2005).
83. Aizawa, N. *et al.* Solution-processed multilayer small-molecule light-emitting devices with high-efficiency white-light emission. *Nat. Commun.* **5**, (2014).
84. McKeown, N. B., Badriya, S., Helliwell, M. & Shkunov, M. The synthesis of robust, polymeric hole-transport materials from oligoarylamine substituted styrenes. *J. Mater. Chem.* **17**, 2088–2094 (2007).



- 
85. Thesen, M. W. *et al.* Hole-transporting host-polymer series consisting of triphenylamine basic structures for phosphorescent polymer light-emitting diodes. *J. Polym. Sci. Part Polym. Chem.* **48**, 3417–3430 (2010).
86. Salert, B. C. D. *et al.* Polystyrene Backbone Polymers Consisting of Alkyl-Substituted Triazine Side Groups for Phosphorescent OLEDs. *Adv. Mater. Sci. Eng.* **2012**, e385178 (2012).
87. Thesen, M. W., Krueger, H., Janietz, S., Wedel, A. & Graf, M. Investigation of spacer influences in phosphorescent-emitting nonconjugated PLED systems. *J. Polym. Sci. Part Polym. Chem.* **48**, 389–402 (2010).
88. Limberg, F. R. P. *et al.* Hole-transporting side-chain polystyrenes based on TCTA with tuned glass transition and optimized electronic properties. *RSC Adv.* **5**, 83122–83128 (2015).
89. Limberg, F. R. P. *et al.* 1- Ethynyl Ethers as Efficient Thermal Crosslinking System for Hole Transport Materials in OLEDs. *Adv. Funct. Mater.* (2016). doi:10.1002/adfm.201603862
90. Adachi, C., Baldo, M. A., Thompson, M. E. & Forrest, S. R. Nearly 100% internal phosphorescence efficiency in an organic light-emitting device. *J. Appl. Phys.* **90**, 5048–5051 (2001).
91. Gong, X., Ostrowski, J. c., Moses, D., Bazan, G. c. & Heeger, A. j. Electrophosphorescence from a Polymer Guest-Host System with an Iridium Complex as Guest: Förster Energy Transfer and Charge Trapping. *Adv. Funct. Mater.* **13**, 439–444 (2003).
92. Noriega, R. *et al.* A general relationship between disorder, aggregation and charge transport in conjugated polymers. *Nat. Mater.* **12**, 1038–1044 (2013).
93. Fan, C., Wei, Y., Ding, D. & Xu, H. Linkage engineering in hosts for dramatic efficiency enhancement of blue phosphorescent organic light-emitting diodes. *Opt. Express* **23**, 12887 (2015).

94. Su, S.-J., Chiba, T., Takeda, T. & Kido, J. Pyridine-Containing Triphenylbenzene Derivatives with High Electron Mobility for Highly Efficient Phosphorescent OLEDs. *Adv. Mater.* **20**, 2125–2130 (2008).
95. Tang, C. *et al.* A versatile efficient one-step approach for carbazole-pyridine hybrid molecules: highly efficient host materials for blue phosphorescent OLEDs. *Chem. Commun.* **51**, 1650–1653 (2015).
96. Williams, E. L., Haavisto, K., Li, J. & Jabbour, G. E. Excimer-Based White Phosphorescent Organic Light-Emitting Diodes with Nearly 100 % Internal Quantum Efficiency. *Adv. Mater.* **19**, 197–202 (2007).
97. An, Z.-F. *et al.* Conjugated Asymmetric Donor-Substituted 1,3,5-Triazines: New Host Materials for Blue Phosphorescent Organic Light-Emitting Diodes. *Chem. – Eur. J.* **17**, 10871–10878 (2011).
98. Su, S.-J., Cai, C., Takamatsu, J. & Kido, J. A host material with a small singlet-triplet exchange energy for phosphorescent organic light-emitting diodes: Guest, host, and exciplex emission. *Org. Electron.* **13**, 1937–1947 (2012).
99. Kim, D., Coropceanu, V. & Brédas, J.-L. Design of Efficient Ambipolar Host Materials for Organic Blue Electrophosphorescence: Theoretical Characterization of Hosts Based on Carbazole Derivatives. *J. Am. Chem. Soc.* **133**, 17895–17900 (2011).
100. Su, S.-J., Cai, C. & Kido, J. RGB Phosphorescent Organic Light-Emitting Diodes by Using Host Materials with Heterocyclic Cores: Effect of Nitrogen Atom Orientations. *Chem. Mater.* **23**, 274–284 (2011).
101. Liu, X.-K. *et al.* Novel bipolar host materials based on 1,3,5-triazine derivatives for highly efficient phosphorescent OLEDs with extremely low efficiency roll-off. *Phys. Chem. Chem. Phys.* **14**, 14255–14261 (2012).

102. Son, K. S., Yahiro, M., Imai, T., Yoshizaki, H. & Adachi, C. Blue Organic Electrophosphorescence Diodes using Diarylamino-substituted Heterocyclic Compounds as Host Material. *J. Photopolym. Sci. Technol.* **20**, 47–51 (2007).
103. Rehmann, N., Hertel, D., Meerholz, K., Becker, H. & Heun, S. Highly efficient solution-processed phosphorescent multilayer organic light-emitting diodes based on small-molecule hosts. *Appl. Phys. Lett.* **91**, 103507 (2007).
104. Son, K. S., Yahiro, M., Imai, T., Yoshizaki, H. & Adachi, C. Analyzing Bipolar Carrier Transport Characteristics of Diarylamino-Substituted Heterocyclic Compounds in Organic Light-Emitting Diodes by Probing Electroluminescence Spectra. *Chem. Mater.* **20**, 4439–4446 (2008).
105. Liu, H. *et al.* A Highly Efficient, Blue-Phosphorescent Device Based on a Wide-Bandgap Host/Flrpic: Rational Design of the Carbazole and Phosphine Oxide Moieties on Tetraphenylsilane. *Adv. Funct. Mater.* **22**, 2830–2836 (2012).
106. Yamaguchi, S. & Wakamiya, A. Boron as a key component for new  $\pi$ -electron materials. *Pure Appl. Chem.* **78**, 1413–1424 (2009).
107. Mou, X. *et al.* A class of fascinating optoelectronic materials: Triarylboron compounds. *Sci. China Chem.* **53**, 1235–1245 (2010).
108. Chan, L.-H., Yeh, H.-C. & Chen, C.-T. Blue Light-Emitting Devices Based on Molecular Glass Materials of Tetraphenylsilane Compounds. *Adv. Mater.* **13**, 1637–1641 (2001).
109. Lee, C. W. & Lee, J. Y. Comparison of Tetraphenylmethane and Tetraphenylsilane as Core Structures of High-Triplet-Energy Hole- and Electron-Transport Materials. *Chem. – Eur. J.* **18**, 6457–6461 (2012).
110. Ren, X. *et al.* Ultrahigh Energy Gap Hosts in Deep Blue Organic Electrophosphorescent Devices. *Chem. Mater.* **16**, 4743–4747 (2004).

- 
111. Köhnen, A. *et al.* The Simple Way to Solution-Processed Multilayer OLEDs – Layered Block-Copolymer Networks by Living Cationic Polymerization. *Adv. Mater.* **21**, 879–884 (2009).
112. Liaptsis, G., Hertel, D. & Meerholz, K. Solution Processed Organic Double Light-Emitting Layer Diode Based on Cross-Linkable Small Molecular Systems. *Angew. Chem. Int. Ed.* **52**, 9563–9567 (2013).
113. Chiba, T., Pu, Y.-J. & Kido, J. Solution-processable electron injection materials for organic light-emitting devices. *J Mater Chem C* (2015). doi:10.1039/C5TC02421H
114. Sax, S. *et al.* Efficient Blue-Light-Emitting Polymer Heterostructure Devices: The Fabrication of Multilayer Structures from Orthogonal Solvents. *Adv. Mater.* **22**, 2087–2091 (2010).
115. Chiba, T. *et al.* Solution-processed inorganic-organic hybrid electron injection layer for polymer light-emitting devices. *ACS Appl. Mater. Interfaces* **4**, 6104–6108 (2012).
116. Chiba, T., Pu, Y.-J., Takahashi, S., Sasabe, H. & Kido, J. Lithium Phenolate Complexes with a Pyridine-Containing Polymer for Solution-Processable Electron Injection Layers in PLEDs. *Adv. Funct. Mater.* **24**, 6038–6045 (2014).
117. Su, S.-J., Sasabe, H., Takeda, T. & Kido, J. Pyridine-Containing Bipolar Host Materials for Highly Efficient Blue Phosphorescent OLEDs. *Chem. Mater.* **20**, 1691–1693 (2008).
118. Su, S.-J. *et al.* Novel Four-Pyridylbenzene-Armed Biphenyls as Electron-Transport Materials for Phosphorescent OLEDs. *Org. Lett.* **10**, 941–944 (2008).
119. Sasabe, H. *et al.* Influence of Substituted Pyridine Rings on Physical Properties and Electron Mobilities of 2-Methylpyrimidine Skeleton-Based Electron Transporters. *Adv. Funct. Mater.* **21**, 336–342 (2011).

- 
120. Kira, A. & Thomas, J. K. Equilibriums between triplet states of aromatic hydrocarbons. *J. Phys. Chem.* **78**, 196–199 (1974).
121. Su, S.-J., Sasabe, H., Pu, Y.-J., Nakayama, K. & Kido, J. Tuning Energy Levels of Electron-Transport Materials by Nitrogen Orientation for Electrophosphorescent Devices with an ‘Ideal’ Operating Voltage. *Adv. Mater.* **22**, 3311–3316 (2010).
122. Kamata, T. *et al.* A series of fluorinated phenylpyridine-based electron-transporters for blue phosphorescent OLEDs. *J. Mater. Chem. C* **4**, 1104–1110 (2016).
123. Lorente, A., Pingel, P., Liaptsis, G., Krüger, H. & Janietz, S. Modulation of ambipolar charge transport characteristics in side-chain polystyrenes as host materials for solution processed OLEDs. *Org. Electron.* **41**, 91–99 (2017).
124. Xiao, L., Su, S.-J., Agata, Y., Lan, H. & Kido, J. Nearly 100% Internal Quantum Efficiency in an Organic Blue-Light Electrophosphorescent Device Using a Weak Electron Transporting Material with a Wide Energy Gap. *Adv. Mater.* **21**, 1271–1274 (2009).
125. Pommerehne, J. *et al.* Efficient two layer leds on a polymer blend basis. *Adv. Mater.* **7**, 551–554 (1995).
126. Thelakkat, M. & Schmidt, H.-W. Synthesis and Properties of Novel Derivatives of 1,3,5-Tris(diarylamino)benzenes for Electroluminescent Devices. *Adv. Mater.* **10**, 219–223 (1998).
127. Admassie, S., Inganäs, O., Mammo, W., Perzon, E. & Andersson, M. R. Electrochemical and optical studies of the band gaps of alternating polyfluorene copolymers. *Synth. Met.* **156**, 614–623 (2006).
128. Deng, L. *et al.* Living Radical Polymerization of Bipolar Transport Materials for Highly Efficient Light Emitting Diodes. *Chem. Mater.* **18**, 386–395 (2006).

129. Liu, H. *et al.* Solution-Processable Hosts Constructed by Carbazole/PO Substituted Tetraphenylsilanes for Efficient Blue Electrophosphorescent Devices. *Adv. Funct. Mater.* **24**, 5881–5888 (2014).
130. Sun, C., Hudson, Z. M., Helander, M. G., Lu, Z.-H. & Wang, S. A Polyboryl-Functionalized Triazine as an Electron Transport Material for OLEDs. *Organometallics* **30**, 5552–5555 (2011).

---

## List of publications

### Peer-reviewed articles

*Modulation of ambipolar charge transport characteristics in side-chain polystyrenes as host materials for solution processed OLEDs*

Lorente, A., Pingel, P., Liaptsis, G., Krüger, H. & Janietz, S.

Org. Electron. 41, 91–99 (2017).

*Orthogonal solution processable electron transport layers based on phenylpyridine side-chain polystyrenes*

Lorente, A., Pingel, P., Miasojedovas, A., Krüger, H. & Janietz, S.

ACS Appl. Mater. Interfaces, Article ASAP. DOI: 10.1021/acsami.7b06701

*High triplet energy electron transport side-chain polystyrenes containing dimesitylboron and tetraphenylsilane for solution processed OLEDs*

Lorente, A., Pingel, P., Miasojedovas, A., Krüger, H. & Janietz, S.

RSC Journal of Materials Chemistry C (submitted)

### Posters

Polydays 2014, 30<sup>th</sup> September – 2<sup>nd</sup> October, Berlin, Germany

*New Solution-Processable Electron Transport Polymers for Cu(I)-Based OLEDs*

A. Lorente-Sanchez, P. Pingel, F. Limberg, H. Krüger, S. Janietz

ECME 2015, 1<sup>st</sup> -5<sup>th</sup> September, Strasbourg, France

*Polymeric tetraphenylsilanes with dimesitylboron units for electron transport in solution processed OLEDs*

A. Lorente-Sanchez, P. Pingel, F. Limberg, H. Krüger, S. Janietz





---

# Curriculum vitae

## Personal information

Name: Alejandro Jose

Surname: Lorente Sanchez

Date of birth: 19.06.1989

Place of birth: Valencia, Spain

## Work experience

**Since 08/2013** PhD student in materials science and polymer chemistry at University Potsdam

**01/2013 - 07/2013** Trainee student taking part in the "Leonardo da Vinci" EU-Mobility Program at Fraunhofer IAP under supervision of Priv.-Doz. Dr. habil. Silvia Janietz Topic: "Synthesis of p-dopants and hole-transport polymers with cross-linking properties".

**09/2011-09/2012** Master student taking part in ERASMUS exchange program at Freie Universität Berlin under supervision of Prof. Dr. Constantin Czekelius. Topic: "Porphyrin-functionalized polyacetylenes via cyclopolymerization of 1,6-heptadiynes".

**07/2010-09/2010** Trainee student at Universitat de Valencia under supervision of Ana M. Costero. Topic: "Synthesis and characterization of anion sensors in the NIR based on borondipyrrromethene units".

## Studies

**09/2007-09-2012** Five-years degree in chemistry (Licenciatura) awarded by Universitat de Valencia.